GEOLOGY OF HUDSPETH COUNTY, TEXAS

GUIDEBOOK OF AIPG-TEXAS

SPRING FIELD TRIP

APRIL 21 – 23, 2023

Version 1 (Draft), 2025

TABLE OF CONTENTS

COVER PAGE – DAY ONE ROAD LOG

COVER PAGE – FIGURES 1.01 – 1.32

COVER PAGE – SUPPLEMENTAL MATERIAL, UTEP

COVER PAGE – DAY TWO ROAD LOG

COVER PAGE – FIGURES 2.01 – 2.32

COVER PAGE – DAY THREE ROAD LOG

OVERVIEW OF ROAD LOG – DAY THREE

COVER PAGE – FIGURES 3.01 – 3.23

COVER PAGE – SUPPLEMENTAL MATERIAL

Ugurhan, M. and Kyle, J.R., 2023, Geology of the Cave Peak porphyry Mo deposit, TransPecos Texas: University of Texas at Austin – Bureau of Economic Geology paper prepared for AIPG-Texas 2023 Spring field trip guidebook.

PREFACE

This field guide is a revision of the guide prepared for the April 2023 field trip. I have added more detail, along with photos shot by field trip participants. I caution against following the field guide without first obtaining permission to gain access to sites described in the road logs. With few exceptions, land in Hudspeth County is privately owned and accessible only by permission of landowners.

I recommend purchasing maps listed below from The University of Texas at Austin, Bureau of Economic Geology Bookstore (https://store.beg.utexas.edu) to accompany this field guide. Copies of the maps were distributed along with the original field guide, but AIPG-Texas does not own copyrights. The maps are:

Dietrich, J.W., Owen, D.E., Shelby, C.A., and Barnes, V.E., 1973, Geologic Atlas of Texas, Van Horn – El Paso Sheet, scale 1:250,000: University of Texas at Austin, Bureau of Economic Geology,

Jones, B.R. and Reaser, D.F., 1970, Geology of the Southern Quitman Mountains, Hudspeth County, Texas: University of Texas at Austin, Bureau of Economic Geology, Geologic Quadrangle No. 39.

Twiss, P.C., 1979, Geologic Atlas of Texas, Marfa Sheet: University of Texas at Austin, Bureau of Economic Geology, scale 1:250,000.

Underwood, J.R.,Jr,, 1963, Geologic Map of the Eagle Mountains and Vicinity, Hudspeth County, Texas: University of Texas at Austin, Bureau of Economic Geology, Quadrangle Map No. 26.

Hudspeth County is one of the largest and most scenic counties in the State of Texas. Located in the mountainous and high desert Trans-Pecos region of the state, Hudspeth is the locus of some of the most complex geology in the southwestern United States. William R. Muehlberger, a faculty member for many years in the Jackson School of Geological Sciences of The University of Texas at Austin, commented to me on a field trip to the Big Bend Region of Texas (way back in 1985) that Trans-Pecos is much like the "solar plexus of North America". By that comment, he meant that the many orogenic episodes that overlapped within the region over a period of 1.4 billion years created a geological jig-saw puzzle unexcelled by that of any other region of the continent. Plate collisions, thrust-faulting, metamorphism of rocks of Precambrian age, wrench-faulting, Laramide compression, millions of years of volcanic eruptions, followed by regional uplift and the formation of rift basins created a complicated geological mosaic. Hudspeth County was, very much, at the center of that activity.

I have had the privilege and the pleasure of spending much of my time as a geological consultant working in this region of Texas over a career that has spanned more than four decades. I fell in love with the starkness, ruggedness, arid climate, complex geology, topography, and the people of Trans-Pecos during my undergraduate geology field camp in the late 1970s. When I returned from my six-week geo-bootcamp, I knew that I would gravitate back to Trans-Pecos over the course of

my graduate work and career. Over the many years since field camp, I have spent so much time there that My wife regards Trans-Pecos as my "happy place".

While working with the University of Texas at Austin – Bureau of Economic Geology (UT-BEG), I was offered the opportunity to take a significant role as a hydrogeologist on a multi-year project to assess the suitability of the Eagle Flat Basin of Hudspeth County to be the location of a site for processing and disposal of low-level radioactive waste. I did not hesitate to accept the offer.

Beginning in May 1991 and ending in June 1994, I spent many months on the ground in the county (and in the Best Western Inn of Van Horn), selecting locations for monitoring wells in the Eagle Flat Basin, and measuring water depths every quarter in nearly every accessible well between the southern margin of the Diablo Plateau and the Rio Grande; and we conducted lengthy pumping tests at the Eagle Flat monitoring wells drilled for the project. I also collected samples periodically of groundwater in many wells to build a geochemical database for analysis of major and minor dissolved solids, along with important stable and unstable isotopes needed to build a comprehensive model of the aquifer systems of southern Hudspeth County. My colleagues and I submitted a final report (Darling and others, 1994, see references at end of Day One road log) to the Texas Low-Level Radioactive Waste Disposal Authority in 1994; and I left UT-BEG to pursue other career opportunities in hydrogeology and geochemistry. Over the next three years, I revised and expanded the report to address elements of my dissertation research proposal; and in December 1997, I submitted the extensive revision as my Ph.D. dissertation to the UT-Austin Department of Geological Sciences (Darling, B.K., 1997, see references at end of Day One road log). I've returned to Hudspeth County for other projects, but none as intensive and as long-lasting as the regional hydrogeological investigation described above.

When officers of AIPG-Texas sought recommendations for a field trip to be scheduled for Spring 2022, I nominated Hudspeth County because I know the area and many of the landowners very well. I was confident that I would be able to negotiate access to sites that might be off-limits to others, and I wanted to showcase the complex geology of the county for AIPG members and other geologists who would be able to set aside three days to study this area. We delayed the field trip to Spring 2023, thanks to a virus that led to questionable government-mandated shutdowns throughout the economy in 2022; but we continued to make preparations and were ready to schedule reservations by early 2023.

I worked closely with Michael Jacobs to compile and drive road logs for days one through three. Michael earned his M.S. in geology at UT-El Paso (UTEP). His thesis research dealt with the geology and the formation of fluorspar deposits of the northeast Eagle Mountains. I also sought agreements with Philip C. Goodell, Professor of Geology, Department of Earth, Environmental and Resource Sciences, UTEP, and with J. Richard "Rich" Kyle, Professor Emeritus, University of Texas at Austin, Jackson School of Geosciences, to be field guides. Their assistance was invaluable.

Over a span of three days in April 2023, the field trip covered a lot of ground in Hudspeth County. Attendees examined the results of much of the tectonic activity that created the geological framework of Trans-Pecos. A highlight of the field trip was an excursion on Day Two to Eagle

Peak, the highest point of the Eagle Mountains (7484 ft (2281 m)), along Radar Road, the highest paved road in Texas. The Federal Aviation Administration (FAA) built the road in 1996 to provide access to a radar station at Eagle Peak to track military and civilian aircraft movements within a 200-mile radius and to provide air-ground radio communication with aircraft. We covered a lot of ground and geological history in a short period of time, but the field trip leaders were excited to guide attendees through this maze … one that we … after many years … are still deciphering.

Bruce K Darling
Bastrop, Texas
November 2025

FIELD TRIP LEADERS

Bruce Darling earned a Master of Science in Geology from the University of Louisiana at Lafayette; a Master of Arts in Energy & Mineral Resources (Mineral Economics) from the University of Texas at Austin; and the Ph.D. in Geology, also from UT-Austin (1997). He specializes in the integration of low-temperature aqueous geochemistry, isotope geochemistry, and physical hydrogeology to resolve problems related to the delineation of flow systems, the effects of groundwater-surface water interaction, the effects of rock-water interaction on hydrochemistry, the transport and fate of naturally occurring and anthropogenic contaminants, and geochemical age-dating of groundwater. ,His doctoral research covered nearly all of southern Hudspeth County. He has 40 years of experience in the energy and groundwater consulting industries, and he has compiled more than 30 years of experience conducting geological investigations in Hudspeth County.

Michael Jacobs is a graduate of Eastern New Mexico University with a Bachelor's degree in Geology. He also earned a Master of Science degree in Geological Sciences from the University of Texas at El Paso. He began his geological career working as a minerals exploration geologist searching for volcanogenic and stratigraphic roll-front uranium and precious metal deposits with Noranda Exploration US in Reno, Nevada and with Tenneco Minerals Inc., Corpus Christi, Texas and Carson City, Nevada. He has over 40 years of experience as a professional geologist in mining, petroleum, and environmental consulting.

Philip C Goodell earned a Bachelor of Science in Solid State Physics from Yale University (1964) and his Master of Science and PhD in Geology from Harvard University (1968 and 1971). He has been a Geological Sciences faculty member at the University of Texas at El Paso since 1975. Prof. Goodell and his students have extensive experience conducting research programs in Hudspeth County, especially in the Sierra Blanca and Quitman Mountains areas.

Rich Kyle is Emeritus Professor in the Jackson School of Geological Sciences, The University of Texas at Austin. His diverse research interests center on mineral resource formation as an integral aspect of the development of the host geologic environment. Rich's major interests are in "strata-controlled" metal and industrial mineral deposits ranging from low-temperature sedimentary basins to volcanic and plutonic environments. He has long recognized the importance of field experience to complement the traditional classroom education and offers students the opportunity to participate in international field work in mineral resources geology. He earned a Bachelor of Science degree in Earth Sciences from Tennessee Technological University, a Master of Science degree in Geology from the University of Tennessee (Knoxville), and the PhD in Geology in 1977 from the University of Western Ontario.

GEOLOGY OF HUDSPETH COUNTY, TEXAS

GUIDEBOOK OF AIPG-TEXAS
SPRING FIELD TRIP
APRIL 21 – 23, 2023

Introductory Material

LOCATION, PHYSIOGRAPHY, REGIONAL TECTONICS, STRUCTURAL GEOLOGY AND MINERAL RESOURCES

The location of this three-day field trip is the Trans-Pecos Subprovince of the Basin and Range Physiographic Province (Figure 0.01) – a series of Late Tertiary basins bounded by mountainous highlands, a broad plateau along the north, and the Rio Grande along the south. Rocks exposed in the area range in age from Precambrian to Quaternary (Figures 0.02a and 0.02b; also refer to the accompanying Van Horn – El Paso and Marfa Geological Atlas of Texas Quadrangles: Dietrich *et al.*, 1983; Twiss, 1979). The structural geology is complicated by the intersection of four orogenic episodes over more than 1 billion years (Ga). Figure 0.03 encompasses the area of the subprovince covered by this field trip. The figure delineates highlands, basins, and aquifers of El Paso, Hudspeth, and western Culberson counties.

The complex geology of the region is the result of:

1. Thrust faulting and metamorphism in Late Precambrian time;

2. Thrust faulting from Late Cretaceous through Early Tertiary time;

3. Intrusions of magma and volcanic eruptions over Middle to Late Tertiary time; and

4. Regional uplift and extensional faulting during Late Tertiary Basin-and-Range tectonism.

Precambrian Tectonics and Structural Domains

Precambrian rocks are exposed in the Streeruwitz, Bean, and Millican Hills, the Carrizo Mountains, and in isolated occurrences on the northeast flank of the Eagle Mountains, the Van Horn Mountains, and on the Diablo Plateau (Dietrich et al., 1983; Twiss, 1979). The rocks date to 1.4 to 1.0 billion years bp (Muehlberger, et al, 1966) and are separated into northern and southern domains (the Carrizo Mountain Group and the Allamoore and Hazel formations) by the Streeruwitz thrust fault (Figures 0.04 and 0.05; and King and Flawn, 1953). The Carrizo Mountains Group forms the hanging wall of the thrust (Fig. 0.4), cropping out mainly in the Carrizo Mountains (Figures 0.06 – 0.08) and less extensively in the Van Horn Mountains and along the northern edge of the Eagle Mountains (Collins and Raney, 1993). Rocks of the footwall are exposed north of I-10, specifically in the area mined for talc at Allamoore (0.09 and 0.10).

Ewing (2016) describes the division of Precambrian rocks into northern and southern domains by the Streeruwitz thrust fault:

> … a major low long-angle fault that places the southern domain (Carrizo Mountain Group) over the northern domain (Millican Hills: Allamoore, Tumbledown, and Hazel). The northern domain is thrusted and folded. The faults and folds mostly have a west-northwest strike and show north-northeast movement. All of the rocks are also cut by high-angle west-northwest trending faults. The folding becomes gentler northward away from the thrust. Near the thrust, the Allamoore Formation is metamorphosed into greenschist facies with

commercial occurrences of talc, but rocks farther north show little evidence of metamorphism.

The southern domain shows much higher metamorphic grade and complex deformation. The rocks are deformed into tight northeast-trending synclines and anticlines. They contain mylonite zones (where fault movement has pervasively sheared the rocks) and small-scale ductile features in multiple phases, indicating movement under high temperatures (over 500ºC). Transport of the rocks was to the northwest, judging from the overturned structures. Regional metamorphism is of greenschist to upper amphibolite facies, increasing to the southeast, with peak temperatures up to 640ºC at depths of 6-12 miles (10-20 km). The southern domain was buried much more deeply than the northern domain and was moved into its present location with the formation of the Streeruwitz Thrust.

The thrusting occurred between $1,057 \pm 6$ Ma and 982 ± 2 Ma according to argon isotopic studies.

Mesozoic Basin Formation and Sedimentation

Ewing (2016) describes the formation of sedimentary basins during the Mesozoic Era as follows:

During the Jurassic Period, a series of deep sedimentary basins formed in what is northern Mexico. More than 15,000 ft (4,600 m) of limestone, shale, sandstone, and evaporites were deposited in the basin from Late Jurassic to Late Cretaceous time (Haenggi, 2002). The basins subsided through the Early Cretaceous. Prominent among the basins is the Chihuahua Trough in West Texas and adjacent Chihuahua, Mexico (Figure 0.11, from Ewing (2016), based on Haenggi (2002)).

The Chihuahua Trough (Figure 0.12, from Ewing (2016)) is 120 miles (193 km) wide and extends over 200 miles (322 km) from southwestern New Mexico to south of the Big Bend region of Texas. The eastern boundary of the basin is sharply defined along the Rio Grande corridor between El Paso and Presidio. The trough passes through the gap at El Paso, then runs southeastward to the Malone Mountains and Sierra Blanca, then south of Van Horn at the southern tip of Culberson County.

Laramide Tectonism

During Late Cretaceous through Early Cenozoic time, sediments of the Chihuahua Trough were thrust more than 50 miles (80 km) northeastward against the Diablo Platform (Figure 0.13, from Ewing (2016), modified from Haenngi (2002) and Figure 0.14, Ewing (2016), modified from Henry and Price (1985). In Texas, these rocks are exposed in the Malone Mountains, the southern Quitman Mountains, the Eagle Mountains, the Indio Mountains,

and the Devil Ridge Thrust (see accompanying GAT sheets by Dietrich et al. (1983) and Twiss, 1979)

Cenozoic Igneous Activity

Igneous activity was widespread throughout much of Trans-Pecos during Early to Middle Cenozoic (Paleogene to Oligocene) time. Volcanic flows and tuffs erupted from small cones and dikes to large calderas and central-vent volcanoes (Figures 0.15 and 0.16, from Ewing (2016), modified from Henry and Price (1985)). Most of the activity was spread over a broad region to the southeast of the area covered by this field trip, where extensive flows extend over much of eastern Culberson County, central and southern Jeff Davis County, northern and central Presidio County and western and southern Brewster County. The major centers of eruptive activity in Hudspeth County and western Culberson County are (from oldest to youngest, based on radiometric age dates (Figures 0.15 and 0.16) are the calderas of the Van Horn Mountains, the Wylie Mountains, the Eagle Mountains, and the Quitman Mountains. The Sierra Blanca laccoliths were emplaced either before or were coterminous with the formation of the calderas of the Eagle and Quitman mountains.

Henry and McDowell (1986) offer a concise summary of Cenozoic igneous activity in Trans-Pecos Texas:

> Magmatism in the Trans-Pecos volcanic field was limited to about 48 to 17 m.y. (million years) ago. During this period, magmatism was nearly continuous, but it varied considerably in location, style, composition, volume, and tectonic setting.

> Earliest activity occurred dominantly in southern and northwestern Trans-Pecos Texas and consisted of abundant, small, mafic to silicic intrusions and mafic lavas. Ash-flow volcanism and caldera formation began 38 and 32 m.y. ago, numerous intrusions and lava flows unrelated to calderas occurred widely over the Trans-Pecos region. About 35 m.y. ago, both caldera and noncaldera activity shifted markedly from northern and central to southern Trans-Pecos Texas. The last calderas formed about 32 m.y. ago.

> After a fundamental change in tectonic setting from compression to tension about 31 m.y. ago, caldera formation was limited to two overlapping structures that formed in adjacent Chihuahua about 30 and 28 m.y. ago. Nearby in Texas, an alkalic, mafic to intermediate stratovolcano erupted; minor peralkaline rhyolites and silica-undersaturated mafic intrusions were emplaced. The last volcanism in Texas occurred between and 24 and 17 m.y. ago, during Basin and Range faulting, when widespread but volumetrically minor alkalic basalts were emplaced as dikes, lava flows, small stocks, and rarely as sills.

Basin-and-Range Uplift, Rifting and Basin Formation

About 25 Ma, regional uplift led to extension of the crust and to the formation of basins and horsts, generally trending toward the northwest (Collins and Raney (1993); Ewing (2016); Figure 0.17 from Ewing (2016), modified from Henry and Price (1985). The uplifts and basins occur over a wide area of Trans-Pecos Texas and adjoining areas of northern Mexico. Summarizing the work of Henry and Price (1985), Ewing (2016) notes the following with respect to the system of Neogene structures:

> In Trans-Pecos Texas, the Neogene structures fall into three general areas. In the northern and southern areas, large, mainly north-south grabens and uplifts are similar to those in southern New Mexico. In a broad central area, by contrast, the structures trend southeasterly and show some evidence of strike slip in addition to extension. East-trending transfer faults with strike-slip movement are also present here.

Figure 0.17 (Ewing, 2016) illustrates the division of uplifts and basins into northern, central and southern areas. Although we will drive the length of the Hueco Bolson on Day One, the trip will focus primarily on the structures in the central area of Figure 0.17, as it is within this area where we will see the effects of the intersection of four orogenic episodes on the geology of Trans-Pecos Texas.

Regional Structure Map

Figure 0.18 illustrates the dominant northwest orientation of major structural features of western Trans-Pecos Texas. The Diablo Plateau forms the northern buttress against which basins and faults south and east of the plateau are aligned. The Chichuahua Trough stands out as the primary negative feature south of the Plateau, with the leading edge of the Laramide thrust forming the boundary between the trough and the Plateau. The Hueco Bolson, and the Eagle Flat and Red Light basins are located within the trough, where compressive forces related to Late Cretaceous and Early Tertiary Laramide tectonism shoved thousands of feet of sediments of the Chihuahua Trough toward the north-northeast against the stable North American Craton. The northwest orientation of the basins and faults is also evident in key features on the Diable Plateau. The Victorio and Babb monoclinal flexures are two such structures. Both are describes in the Day Three roadlog.

Mineral Resources of Trans-Pecos Texas and Border Regions

This section of text is abstracted from a technical report on the deveopment of a geospatial database on the occurrence and distribution of metallic and industrial mineral resources of Trans-Pecos Texas and adjoining areas of southern New Mexico and northern Mexico (Becker and Kyle, 2011):

> Despite favorable geology and the widespread and diverse occurrences of metal and industrial mineral prospects in Trans-Pecos Texas, this 30,000+ mi^2 (7770 km^2) area remains underexplored relative to similar geologic terranes of the western United

States. The reasons for this situation are complex, including the paucity of public land available for mineral entry, but another reason is the lack of a geospatial database of known mineral deposits that would facilitate exploration activity.

The Trans-Pecos region is arguably the most complex geologic province of Texas, reflecting more than a billion years of Earth history recorded by the rocks in west Texas and contiguous Mexico and New Mexico. The major tectonic, magmatic, and sedimentation events range in age from the Meso-Proterozoic to the present, including the 1.3–0.9 Ga Grenville orogenic belt; Paleozoic continental shelf sedimentation, the late Paleozoic Marathon tectonic belt and resultant development of Permian foreland basins; Laramide compressional deformation and local magmatism; Paleogene caldera-related volcanism and related intrusive activity, and Neogene extensional deformation that is responsible for the current Basin and Range topography and that continues today. The major structural features have been reactivated in each Phanerozoic tectonic episode, an inheritance from the Late Proterozoic orogenic event (Muehlberger and Dickerson, 1989a,b).

Each of these events resulted in favorable conditions for the formation of diverse metal and industrial mineral resources. Historic production in the region is dominated by silver and lead from the Shafter district (Ross, 1943; Head, 2002; Rambaud, 2005), silver and copper from the Van Horn district (Price et al., 1985), mercury from the Terlingua district (Yates and Thompson, 1959), sulfur from Culberson and Pecos Counties (Crawford, 1990; Hentz et al., 1989), talc from the Allamoore district (Davis, 2007), and fluorspar from the Eagle and Christmas Mountains (Gillerman, 1953; McAnulty, 1974; Daugherty, 1982). A few of these concentrations have been significant producers, but a much larger number of occurrences and "prospects" have been documented. Price et al. (1983) provided a valuable compilation of the Trans-Pecos Texas mineral occurrences. Additional information on industrial mineral resources of the region is available in Austin (1978) and Kyle (1990).

Becker and Kyle (2011) compiled mineral location data from sources cited in the above paragraph. They built an Excel spreadsheet that was imported into Google Earth to create a regional map (Figure 0.19) showing the locations of metallic minerals and nonmetallic industrial minerals in Trans-Pecos Texas and adjacent lands. Because the map predates the latest exploratory work on beryllium and rare earth elements at Sierra Blanca, those minerals are not shown on the map. Nonetheless, there is marked clustering of many mineral deposits in the area covered by this field trip.

Mesoproterozoic Basement Architecture and Mineralization

Kyle (2023), drawing from Kyle and Elliott (2021), comments on the association between Mesoproterozoic basement architecture and mineralization in Trans-Pecos Texas:

> The basement exposures in the Van Horn and other smaller areas of western Texas provide key information toward geologic interpretation of buried basement provinces known solely from sparsely distributed and volumetrically insignificant samples provided by deep drilling. The Van Horn region includes exposures of the Mesoproterozoic deformation front, with commercial talc concentrations developed along the thrust zone. Cu-Ag concentrations along brittle structures within basement rocks have been interpreted to represent Cenozoic mineralization systems (Price and others, 1985). Some Van Horn basement-hosted mineral concentrations were emplaced during younger events along what likely represent reactivated structures (Grimes, 2014).

Citing Davis (2007) and Davis and Mosher (2015), Kyle (2023) also observes that Mesoproterozoic basement rocks represent a complete section of the Grenville (Llano) orogenic front, "from the metamorphic core in the Carrizo Mountains to the foreland deformation front to the north in the Van Horn area":

> The Carrizo Mountain Group represents the oldest rocks exposed in the Van Horn area (~1.3–1.4 Ga [Bickford and others, 2000]) and is composed of metaigneous and metasedimentary rocks that represent the metamorphic core of the Grenville Orogen. Metarhyolites and metadiabase sills occur along the Streeruwitz Thrust, the major decollement that crops out in the southern portions of the area (Fig. 1). The Streeruwitz Thrust defines the boundary between the high-grade Carrizo Mountain Group to the south and the weakly metamorphosed to unmetamorphosed footwall strata of the Allamoore, Tumbledown, and Hazel formations to the north. The Allamoore, Tumbledown, and Hazel formations are preorogenic and synorogenic sedimentary and volcanic rocks that form the foreland fold-and-thrust belt of the Grenville orogeny (King and Flawn, 1953; Soegaard and Callahan, 1994; Bickford and others, 2000; Davis and Mosher, 2015).

> Additional narrow belts of Proterozoic basement are exposed on the upthrown side of north–northwest-trending fault blocks due to late Cenozoic Basin and Range extension in Trans-Pecos Texas and contiguous Mexico (Henry and Price, 1986).

In the Van Horn region, exposures of Mesoproterozoic rocks include "talc and other mineral concentrations developed along the Streeruwitz Thrust Zone, as well as Cu-Ag vein mineralization in basement and younger rocks interpreted to be a product of Cenozoic events (Kyle, 2023), citing King and Flawn, 1953 and Price and others, 1985)." Kyle (2023) also notes that small copper and associated metal occurrences in the Carrizo Mountains (Loidolt, 1970) are less well defined, but

Price and others (1985) suggest that the deposits are of probable metamorphic origin and thus represent Mesoproterozoic fluid systems.

Also from Kyle (2023):

Over the past few decades, the only significant mineral resource production from the basement in the Van Horn region has been ceramic- and paint-grade talc from the Allamoore district (Bourbon, 1981, 1982; Edwards, 1980, 1984; Kyle and Clark, 1990). The commercial talc deposits occur within a narrow fold-and-thrust belt that represents the northernmost extent of a Grenville-age collisional belt (Grenville Front) that records a complex history of deformation and associated fluid flow (Davis, 2007; Davis and Mosher, 2015).

Historically, the Van Horn area is known as the largest copper-producing and second largest silver-producing region in Texas. The major Hazel vein outcrop in the Proterozoic basement (*see also the Day Three road log of this guideook*) was discovered in 1856 but was not developed until the 1880's. Records of early production are incomplete, but typical ores appear to have had several percent Cu with variable amounts of Ag ranging up to 30 ounces of Ag per ton (King and Flawn, 1953; Evans, 1975). Vein (Hazel)-type mineralization has high Ag concentrations, whereas stratabound (Blackshaft) ores of similar Cu grades have minor Ag values. Although ore tonnages appear modest by modern global standards, production of these high-grade ores encouraged additional mineral assessment in Trans-Pecos Texas. Intermittent minor Cu-Ag production from the Hazel and other mineralized zones took place until the late 1940's, with exploration activities as recently as the early 1980's seeking larger-tonnage deposits.

The Cu-Ag sulfide concentrations occur along steeply dipping, brittle structures, as well as local stratabound zones within Proterozoic, Permian, and Cretaceous red bed sequences (King and Flawn, 1953; Price et al., 1985). Among other features, the ores are anomalous in Pb, Zn, As, Cd, and Mo and are not enriched in gold, an elemental assemblage that led Price et al. (1985) to conclude that these mineralizing systems were not associated with Cenozoic magmatism. Fluid inclusion studies confirm that mineralization was from relatively low-temperature (120°C to 170°C), intermediate-salinity (9–19 wt% NaCl equivalent) fluids, further suggesting metals were supplied by formation waters focused along Basin and Range extensional structures, with mineral precipitation in response to mixing with shallow groundwater (Price et al., 1985).

Although the main ore zones in the Van Horn area are hosted by Proterozoic basement, veins locally extend into Phanerozoic cover (King and Flawn, 1953). This relationship and detailed kinematic studies of fractures by Price et al. (1985) indicate that the mineralization took place in the late Cenozoic. However, the Hazel ore zone consists of an en echelon series of steeply dipping, east–west veins (King and Flawn, 1953) that are not typical of those resulting from the northeast–southwest Basin and Range

extension (Henry and Price, 1986). This relationship suggests that vein orientation could be influenced by ancient east–west basement structures, as have been suggested to influence the orientation of Cenozoic mineralized zones elsewhere in Trans-Pecos Texas (e.g., Dickerson, 1981).

Kyle (2023) concludes with the following:

The detailed character of the Mesoproterozoic basement in western Texas is not well known, but studies of limited exposures in the Van Horn region suggest sedimentary brines and other fluids traversed through basement lithologies, particularly along structures of various ages. Fluid-related processes created talc concentrations along the Streeruwitz Thrust during the Grenville orogeny. Cenozoic extensional tectonics created fault zones in basement and younger units in the Van Horn area that were mineralized by metal-bearing formation waters. Some of these structures may represent reactivated older tectonic features. The collective results of these deformational and fluid events have the potential to create modern zones within the Texas basement under Phanerozoic cover that are susceptible to natural or induced tectonic movements.

REFERENCES

Ashworth, J. B., 1995, Ground-water resources of the Bone Spring-Victorio Peak aquifer in the Dell Valley Area, Texas: Texas Water Development Board Report 344, 42 p.

Austin, G. S., ed., 1978, Geology and mineral deposits of Ochoan rocks in Delaware Basin and adjacent areas: New Mexico Bur. Mines Min. Res., Circ. 159, 87 p

Ashworth, J. B., 1995, Ground-water resources of the Bone Spring-Victorio Peak aquifer in the Dell Valley Area, Texas: Texas Water Development Board Report 344, 42 p.

Becker, G.R., and Kyle, J.R., 2011, Geographic distribution of metal and industrial minerals occurrences in Trans-Pecos Texas and border regions: A Google Earth® database and compilation: University of Texas at Austin, Bureau of Economic Geology www.beg.utexas. edu/transpecos/index.htm

Bickford, M.E., Soegaard, K., Nielsen, K.C., and McLelland, J.M., 2000, Geology and geochronology of Grenville-aged rocks in the Van Horn and Franklin Mountains area, west Texas—implications for the tectonic evolution of Laurentia during the Grenville: Geological Society of America Bulletin, v. 112, p. 1134–1148. doi.org/10.1130/0016-7606(2000)112<1134:GAGOGR>2.0.CO;2

Bourbon, W.B., 1981, The origin and occurrence of talc in the Allamoore district, Culberson and Hudspeth counties, Texas: West Texas State University, Canyon, Master's thesis [unpublished], 65 p.

Bourbon, W.B., 1982, The origin of talc in the Allamoore district, Texas: New Mexico Bureau of Mines and Mineral Resources, Circular 182, p. 77-84.

Chapin, C.E., 1971, The Rio Grande Rift, Part 1: Modifications and additions: New Mexico Geological Society 22nd Annual Field Conference Guidebook, p. 191–202.

Collins, E. W., and Raney, J. A. 1991, Tertiary and Quaternary structure and paleotectonics of the Hueco basin, Trans-Pecos Texas and Chihuahua, Mexico: The University of Texas at Austin, Bureau of Economic Geology Geological Circular 91-2, 44 p.

Collins, E.W., and Raney, J.A., 1993, Late Cenozoic faults of the region surrounding the Eagle Flat study area, northwestern Trans-Pecos Texas: Univ. of Texas at Austin, Bureau of Economic Geology final contract report prepared for Texas Low-Level Radioactive Waste Disposal Authority, 74 p.

Crawford, J. E., 1990, Geology and Frasch-mining operations of the Culberson sulfur mine, Culberson County, west Texas, *in* Kyle, J. R., ed., Industrial Mineral Resources of the Delaware Basin, Texas and New Mexico: Soc. Econ. Geol., Guidebook 8, p. 141-162.

Daugherty, F. W., 1982, Fluorspar deposits of the Christmas Mountains district, Brewster County, Texas, *in* Austin, G. S., ed., Industrial rocks and mineral of the Southwest: New Mexico Bur. Mines Min. Res., Circ. 182, p. 85-88.

Davis, B. R., 2007, Complex structural and fluid flow evolution along the Grenville Front, Trans-Pecos Texas: Unpublished M.S. thesis, University of Texas at Austin, 213 p.

Davis, B.R., and Mosher, S., 2015, Complex structural and fluid flow evolution along the Grenville Front, west Texas: Geosphere, v. 11, p. 868–898. doi:10.1130/GES01098.1

Dickerson, P.W., 1981, Evidence for basement control of structural zones transecting the southern Rio Grande rift – Shafter zone: Proceedings, 4th International Basement Tectonics Conference, Oslo, Norway, p. 103–114.

Dietrich, J. W., Owen, D. E., Shelby, C. A., and Barnes, V. E., 1983, Geologic Atlas of Texas, Van Horn-El Paso Sheet: The University of Texas at Austin, Bureau of Economic Geology, Geologic Atlas of Texas, map scale 1:250,000.

Edwards, G., 1980, Tumbledown Mountain talc deposit, Allamoore District, Culberson County, Texas: New Mexico Geological Society, Guidebook, 31st Field Conference, p. 245=250

Edwards, G., 1984, Petrography and geochemistry of the Allamoore Formation, Culberson and Hudspeth counties, Texas: University of Texas, El Paso, PhD dissertation [unpublished], 287 p.

Evans, T.J., 1975, Gold and silver in Texas: University of Texas at Austin, Bureau of Economic Geology Mineral Resource Circular No. 56, 36 p.

Ewing, T.E., 2016, Texas Through Time: Univ. of Texas at Austin, Bureau of Economic Geology, 431 p.

Ewing, T.E., Budnik, R.T., Ames, J.T., Ridner, D.M., and Dillon, R.L., Tectonic Map of Texas: University of Texas at Austin, Bureau of Economic Geology, 1:750,000

Gillerman, E., 1953, Fluorspar deposits of the Eagle Mountains, Trans-Pecos Texas: U. S. Geol. Surv., Bull. 987, 98 p.

Grimes, S., 2014, Precambrian basement structure of the Diablo Platform and its influences throughout the Phanerozoic: American Association of Petroleum Geologists Search ad Discovery, article no. 30338, 29 p.

Haenggi, W.T., 2002, Tectonic history of the Chihuahua trough, Mexico and adjacent USA, Part II: Mesozoic and Cenozoic: Boletin de la Sociedad Geologica Mexicana, v. 55, p. 38-94.

Head, J. A., 2002, Stratigraphic and structural controls of Permian carbonate-hosted silver (Pb-Zn) mineralization, Shafter Presidio County, Texas: Unpublished M.S. thesis, University of Texas at Austin, 214 p.

Henry, C.D., and McDowell, F.W., 1986, Geochronology of magmatism in the Tertiary volcanic field, Trans-Pecos Texas. In Bureau of Economic Geology Guidebook; University of Texas at Austin, v. 23, p 99-122.

Henry, C.D., and Price, J.G., 1985, Variations in caldera development in the Tertiary volcanic field of Trans-Pecos Texas. J Geophys Res, 89, 8765-8786.

Henry, C.D., and Price, J.G. 1986, Early Basin and Range development in Trans-Pecos Texas and adjacent Chihuahua—magmatism and orientation, timing, and style of extension: Journal of Geophysical Research, v. 91, p. 6213–6224. doi.org/10.1029/JB091iB06p06213

Hentz, T. F., Price, J. G., and Gutierrez, G. N., 1989, Geologic occurrence and regional assessment of evaporite-hosted native sulfur, Trans-Pecos Texas: Univ. Texas, Austin, Bur. Econ. Geol., Rept. Invest. 184, 70 p.

King, P.B., and Flawn, P.T., 1953, Geology and mineral deposits of Precambrian rocks of the Van Horn area, Texas: Univ. of Texas at Austin, Bureau of Economic Geology Publication 5301, 218 p.

Kyle, J. R., ed., 1990, Industrial mineral resources of the Delaware Basin, Texas and New Mexico: Soc. Econ. Geol., Guidebook Series, v. 8, 203 p.

Kyle, J.R, 2023, Trans-Pecos Texas mineralization affected by Proterozoic basement architecture: Univ. of Texas at Austin Bureau of Economic Geology unpublished paper, 7 p.

Kyle, J.R., and Clark, K. F., 1990, Geology of the Allamoore talc district, west Texas: Soc. Econ. Geol., Guidebook Series, v. 8, p. 181-190.

Kyle, J.R., and Elliott, B.A., 2021, Texas mineral resources within or affected by Proterozoic basement architecture, *in* Callahan, O.A, and Eichhubl, P., eds., The geologic basement of Texas: A volume in honor of Peter Flawn: Bureau of Economic Geology, University of Texas at Austin, Report of Investigations 286, ch. 4. doi:10.23867/RI0286C4

Langford, R.P., 1993, Landscape evolution of Eagle Flat and Red Light basins, Chihuahuan Desert, South-Central Trans-Pecos Texas: The University of Texas at Austin, Bureau of Economic Geology, contract report, prepared for Texas Low-Level Radioactive Waste Disposal Authority, under Interagency Contract IAC (92-93)-0910.

Langford, R. P., Jackson, M. L. W., and Whitelaw, M. J., 1999, The Miocene to Pleistocene filling of a mature extensional basin in Trans-Pecos Texas–Geomorphic and hydrologic controls on deposition: Sedimentary Geology, v. 128, p. 131-153.

Loidolt, L.H., 1970, Quartz-feldspar-carbonate bodies of the Carrizo Mountains, Texas: University of Arizona, Tucson, Master's thesis [unpublished], 126 p.

McAnulty, W. N., Sr., 1974, Fluorspar in Texas: Univ. Texas, Austin, Bur. Econ. Geol., Handbook 3, 31 p.

Muehlberger, W. R., and Dickerson, P. W., eds., 1989a, Structure and stratigraphy of Trans- Pecos Texas: 28th Int. Geol. Cong., Field trip guidebook T317, Am. Geophy. Union, Washington, D. C., 197 p.

Muehlberger, W. R., and Dickerson, P. W., 1989b, A tectonic history of Trans-Pecos Texas, *in* Muehlberger, W. R., and Dickerson, P. W., eds., Structure and stratigraphy of Trans- Pecos Texas: 28th Int. Geol. Cong., Field trip guidebook T317, Am. Geophy. Union, p. 35-53.

Muehlberger, W.R., Hedge, C.E., Denison, R.E., and Marvin, R.F., 1966, Geochronology of the midcontinent region, United States: 3, southern area: Journal of Geophysical Research, v. 71, p. 5409-5426.

Price, J. G. Henry, C. D., and Standen, A. R., 1983, Annotated bibliography of mineral deposits in Trans-Pecos Texas: Univ. Texas, Austin, Bur. Econ. Geol., Mineral Res. Cir. 73, 108 p.

Price, J. G., Henry, C. D., Standen, A. R., and Posey, J. S., 1985, Origin of silver-copper-lead deposits in red-bed sequences of Trans-Pecos Texas: Tertiary mineralization in Precambrian, Permian, and Cretaceous sandstones: Univ. Texas, Austin, Bur. Econ. Geol., Rept. Inv. 145, 65 p.

Rambaud, F., 2005, Nature and source of the mineralizing fluids at the Presidio mine, Shafter district, Presidio County, Texas: Unpublished M.S. thesis, University of Texas at Austin, 113 p.

Ross, C. P., 1943, Geology and ore deposits of the Shafter mining district, Presidio County, Texas: U. S. Geol. Surv., Bull. 928B, p. 45-125.

Soegaard, K., and Callahan, D.M., 1994, Late Middle Proterozoic Hazel Formation near Van Horn, Trans-Pecos Texas—evidence for transpressive deformation in Grenvillian basement: Geological Society of America Bulletin, v. 106, p. 413–423. doi.org/10.1130/0016-7606(1994)106<0413:LMPHFN>2.3.CO;2

Twiss, P.C., 1979, Geologic Atlas of Texas, Marfa Sheet: The University of Texas at Austin, Bureau of Economic Geologic, Geologic Atlas of Texas, map scale 1:250,000.

Yates, R. G., and Thompson, G. A., 1959, Geology and quick-silver deposits of the Terlingua District, Texas: U.S. Geol. Surv. Prof. Paper 312, 114 p.

GEOLOGY OF HUDSPETH COUNTY, TEXAS

GUIDEBOOK OF AIPG-TEXAS
SPRING FIELD TRIP
APRIL 21 – 23, 2023

Figures 0.01 - 0.19

Figure 0.01 – Basin and Range Physiographic Province of North America and location of Trans-Pecos Subprovince. Source: Bedient and others (1985).

Figure 0.02a – Geological Map of Hudspeth County, based on digital data from the US Geological Survey.
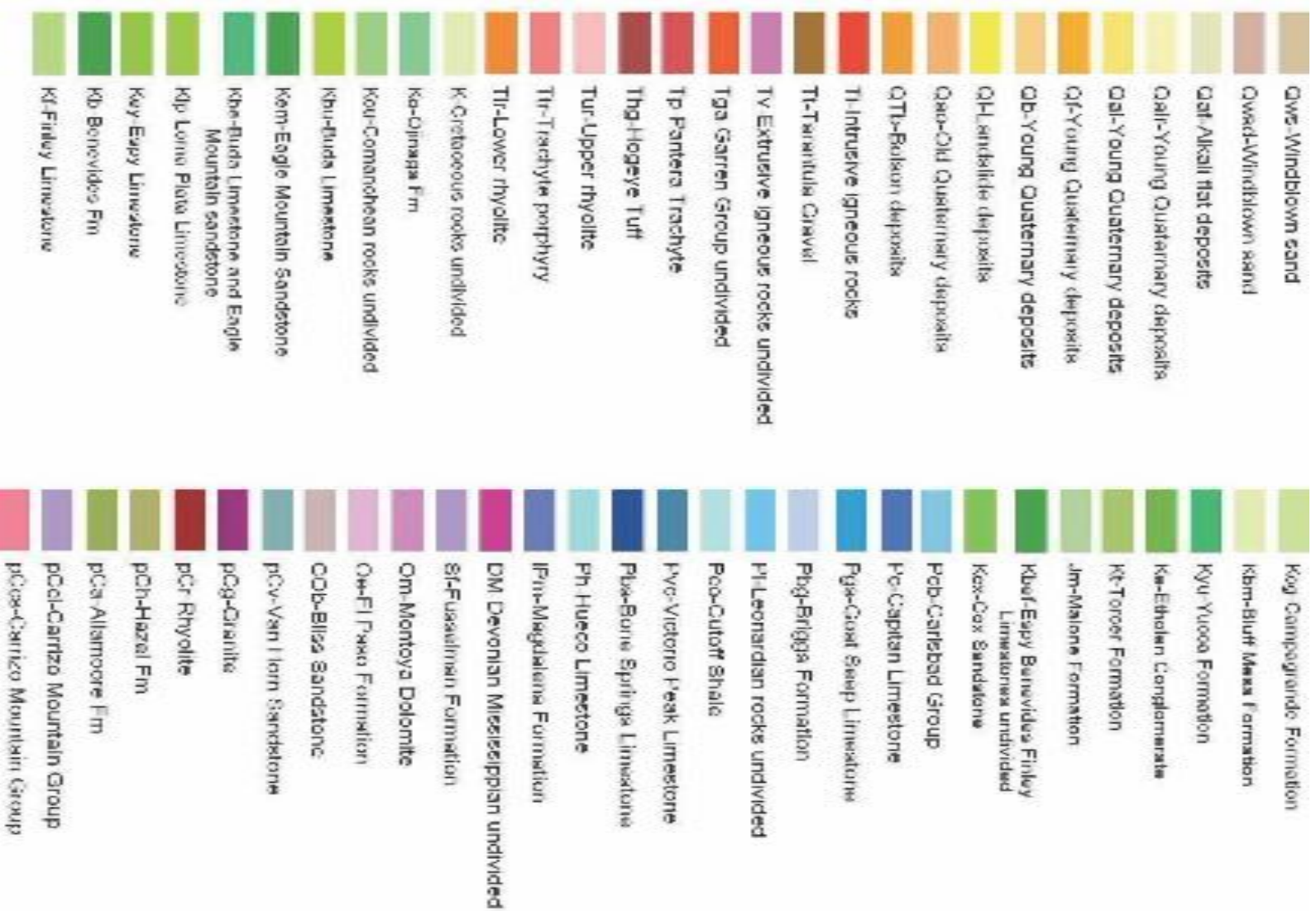
Figure 0.02b – Legend to accompany geological map Figure 0.2a.

Qws-Windblown sand
Qwsd-Windblown sand
Qaf-Alkali flat deposits
Qal-Young Quaternary deposits
Qal-Young Quaternary deposits
Qf-Young Quaternary deposits
Qf-Young Quaternary deposits
Qb-Young Quaternary deposits
QI-Landslide deposits
Qao-Old Quaternary deposits
QTb-Felson deposits
TI-Intrusive igneous rocks
Tt-Terentula Gravel
Tv-Extrusive igneous rocks undivided
Tga-Garren Group undivided
Tp-Pantera Trachyte
Thg-Hogeye Tuff
Tur-Upper rhyolite
Ttr-Trachyte porphyry
Ttr-Lower rhyolite
K-Cretaceous rocks undivided
Ka-Ojinaga Fm
Kou-Comanchean rocks undivided
Kbu-Buda Limestone
Kem-Eagle Mountain Sandstone
Kbe-Buda Limestone and Eagle Mountain sandstone
Klp-Loma Plata Limestone
Key-Espy Limestone
Kb-Benevides Fm
Kf-Finlay Limestone

Kcg-Campagrande Formation
Kbm-Bluff Mesa Formation
Kyu-Yucca Formation
Ke-Etholen Conglomerate
Kt-Torcer Formation
Jm-Malone Formation
Kbef-Espy Benevides Finlay Limestone undivided
Kex-Cox Sandstone
Pcb-Carlsbad Group
Pc-Goat Seep Limestone
Pgs-Goat Seep Limestone
Pbg-Briggs Formation
H-Leonardian rocks undivided
Pco-Cutoff Shale
Pvc-Victorio Peak Limestone
Pbs-Bone Springs Limestone
Ph-Hueco Limestone
IPm-Magdalena Formation
DM-Devonian Mississippian undivided
Sf-Fusselman Formation
Om-Montoya Dolomite
Oe-Fl-Paso Formation
COb-Bliss Sandstone
pCv-Van Horn Sandstone
pCg-Granite
pCr-Rhyolite
pCh-Hazel Fm
pCa-Allamoore Fm
pCcl-Carrizo Mountain Group
pCcs-Carrizo Mountain Group

17

Figure 0.03. Major physiographic features of western Trans-Pecos Texas.
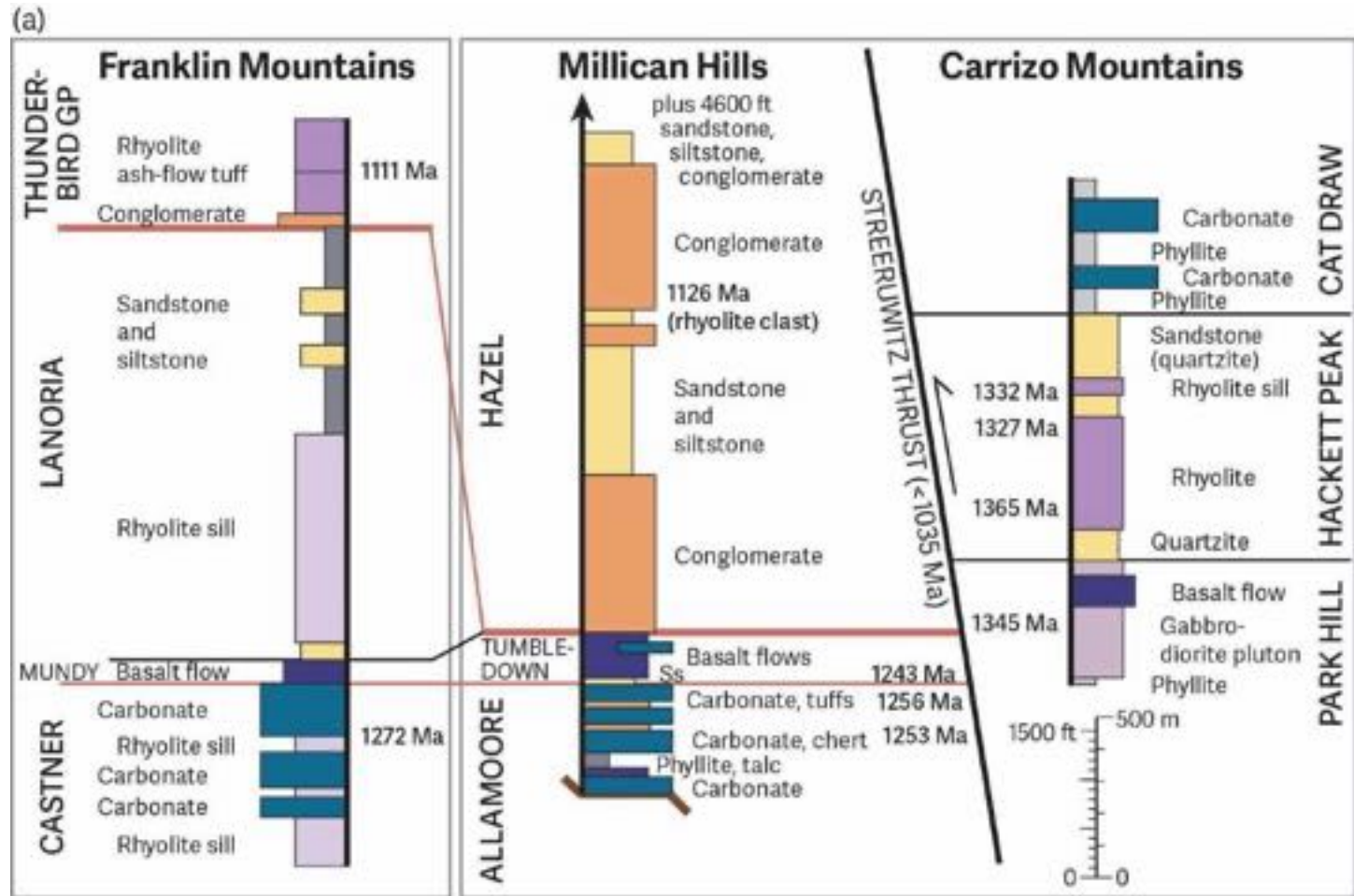
Figure 0.04 - Streeruwitz Thrust Fault and dvision of Precambrian rocks into Northern and Southern Domains, Trans-Pecos Texas. Source: Ewing (2016)

Figure 0.05 – Google Earth image showing northern and southern domains of Precambrian rocks separated by the Streeruwitz thrust fault.

Figure 0.06 – Carrizo Mountains as seen from eastbound I-10 ramp at Allamoore. Photo by BK Darling

Figure 0.07 –Roadcut exposures of southern domain metamorphosed rocks along westbound I-10 lanes b0etween Van Horn and Allamoore. Photo by BK Darling

Figure 0.08 –Roadcut exposures of southern domain metamorphosed rocks along westbound I-10 lanes between Van Horn and Allamoore. Photo by BK Darling

Figure 0.09 – Allamoore Formation (northern domain),
Natural Minerals talc mine, Allamoore, TX. Photo
by BK Darling

Figure 0.10 – Exposures of Allamoore and Hazel formations, Natural Minerals talc mine.
All talc production is from Allamoore Formation. Hazel overburden must be removed before
 talc can be mined. Photo by BK Darling
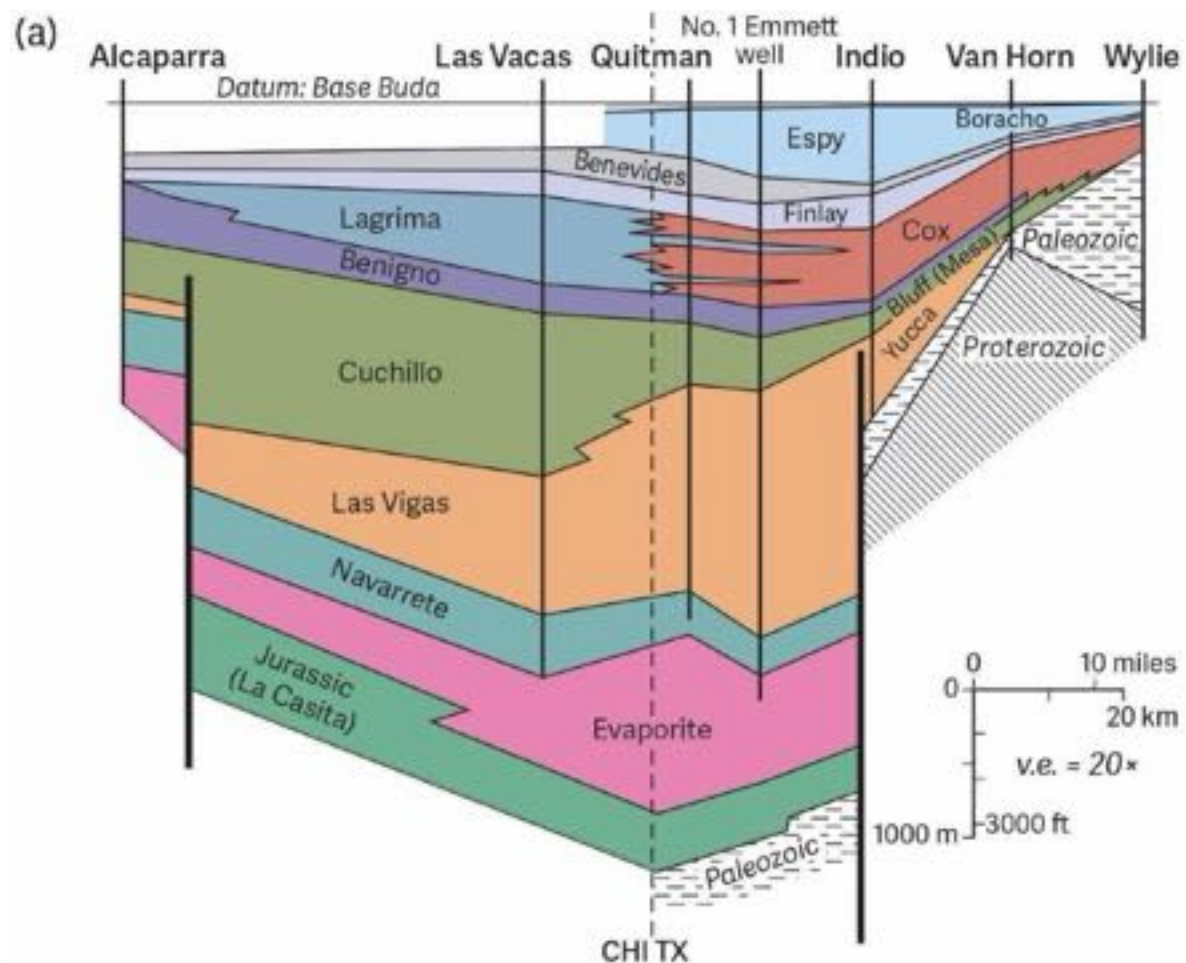
Figure 0.11 – Jurassic and Cretaceous Formations of the Chihuahua Trough.
Source: Ewing (2016), from Haenggi (2002)
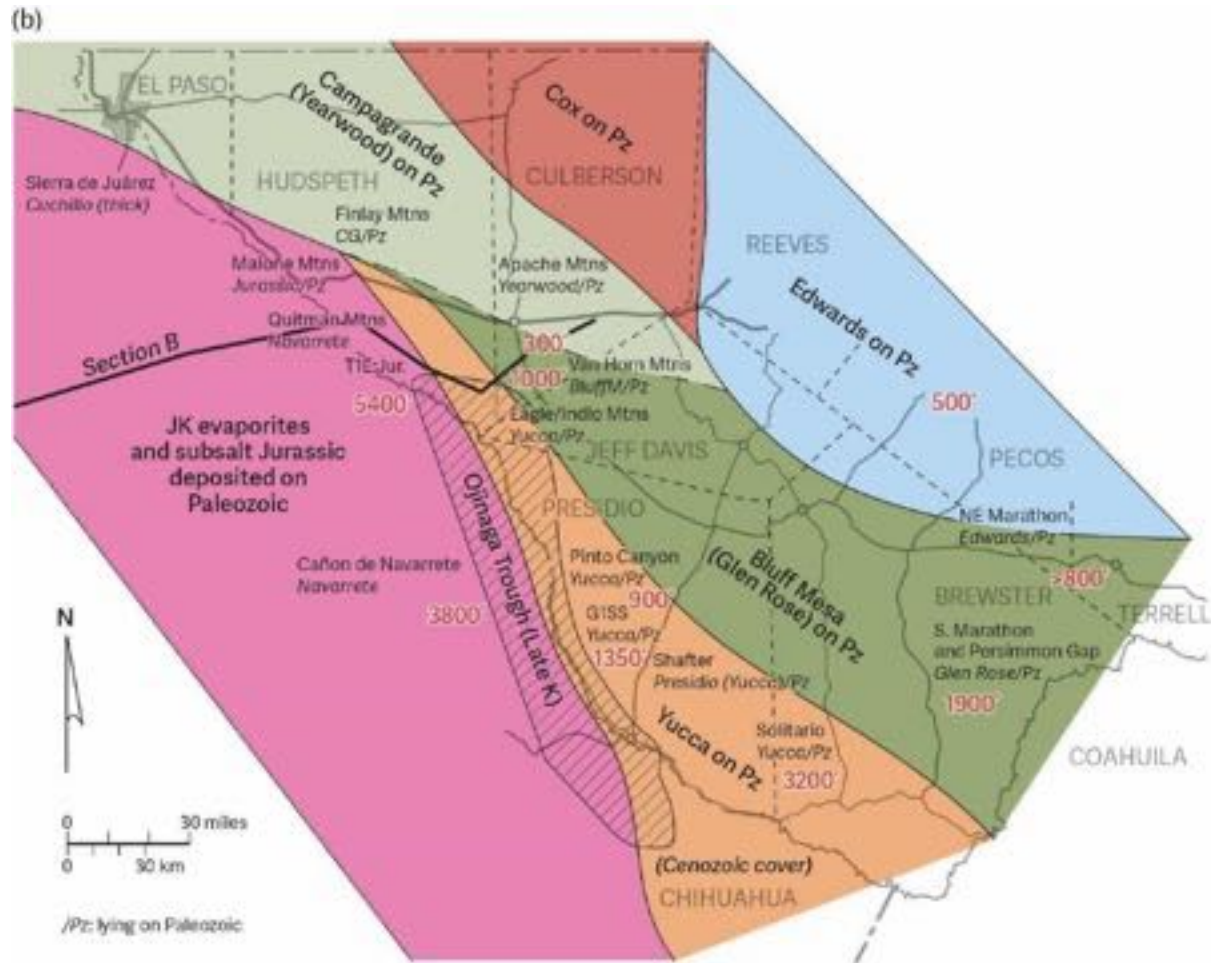
Figure 0.12 – Chihuahua Trough margin in westernmost Texas. Red numbers indicate thickness of Lower Cretaceous formations overlying rocks of the Paleozoic Era. Source: Ewing (2016)

27
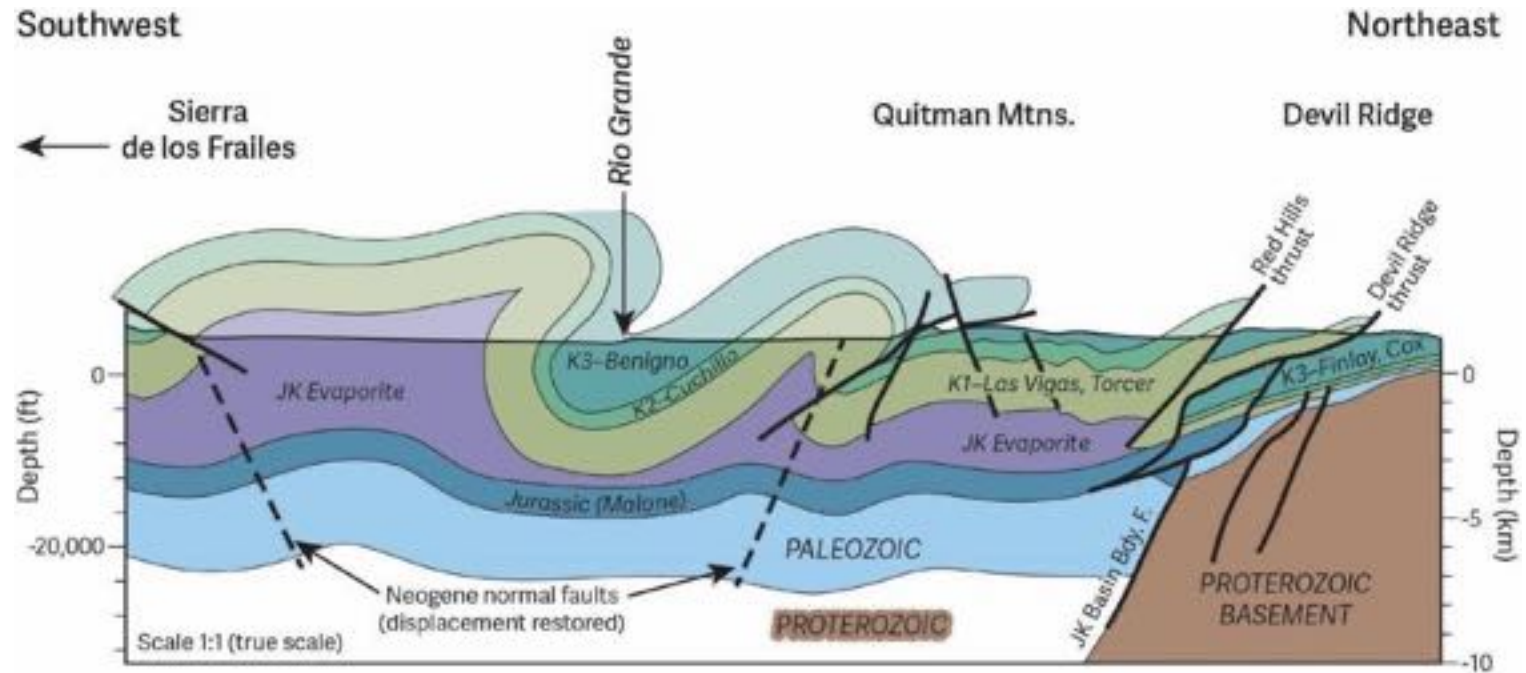
Figure 0.13 –Structure cross section, Quitman Mountains area southwest of Sierra Blanca. Cretaceous rocks are folded above Jurassic and Cretaceous halite and gypsum beds. Source: Ewing (2016), modified from Haenggi (2002)

Figure 0.14 – Laramide structures in Trans-Pecos Texas . Source: Ewing (2016), modified from Henry and Price (1985)
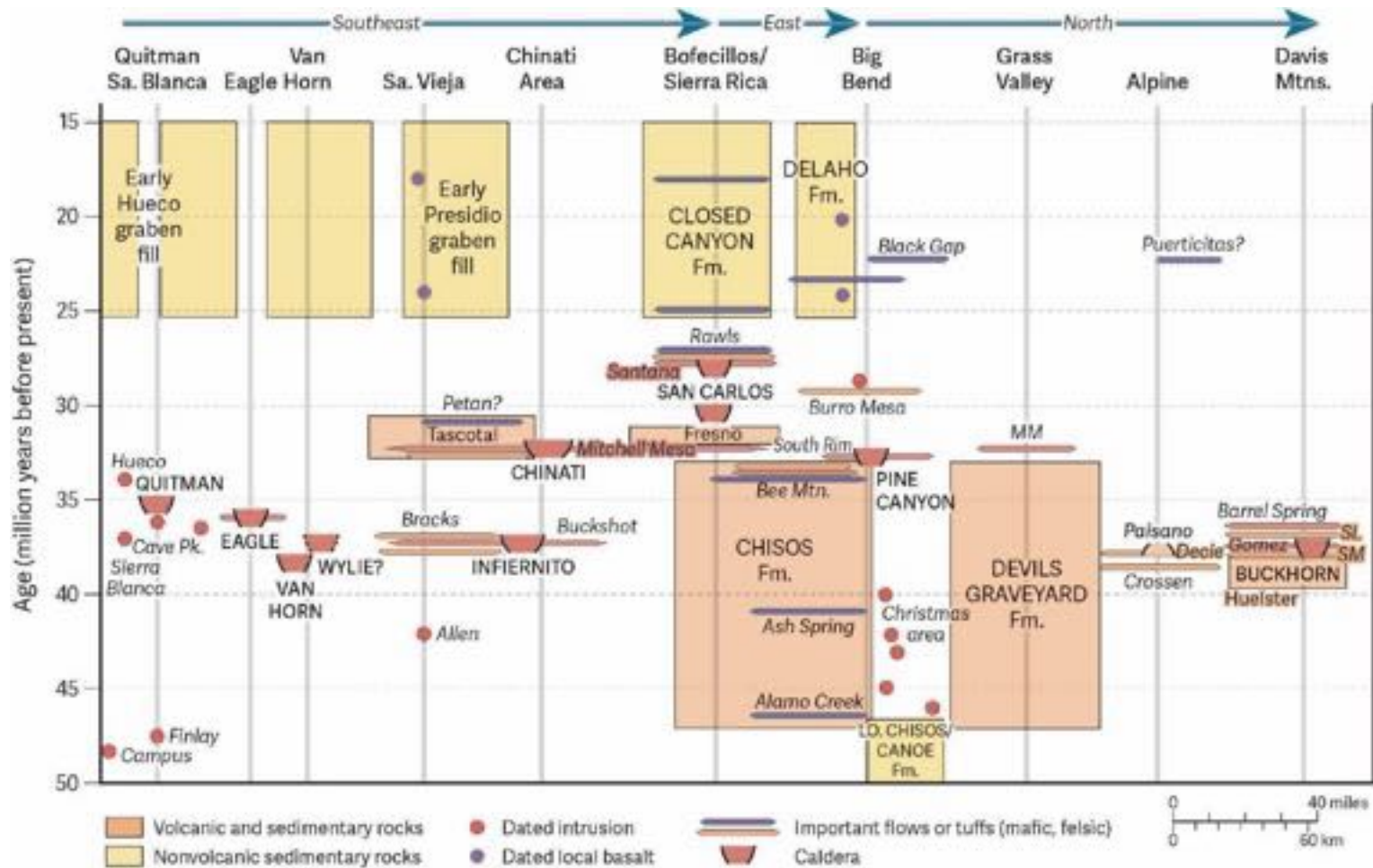
Figure 0.15– Time section of volcanic activity and formation of bolsons. Source: Ewing (2016)
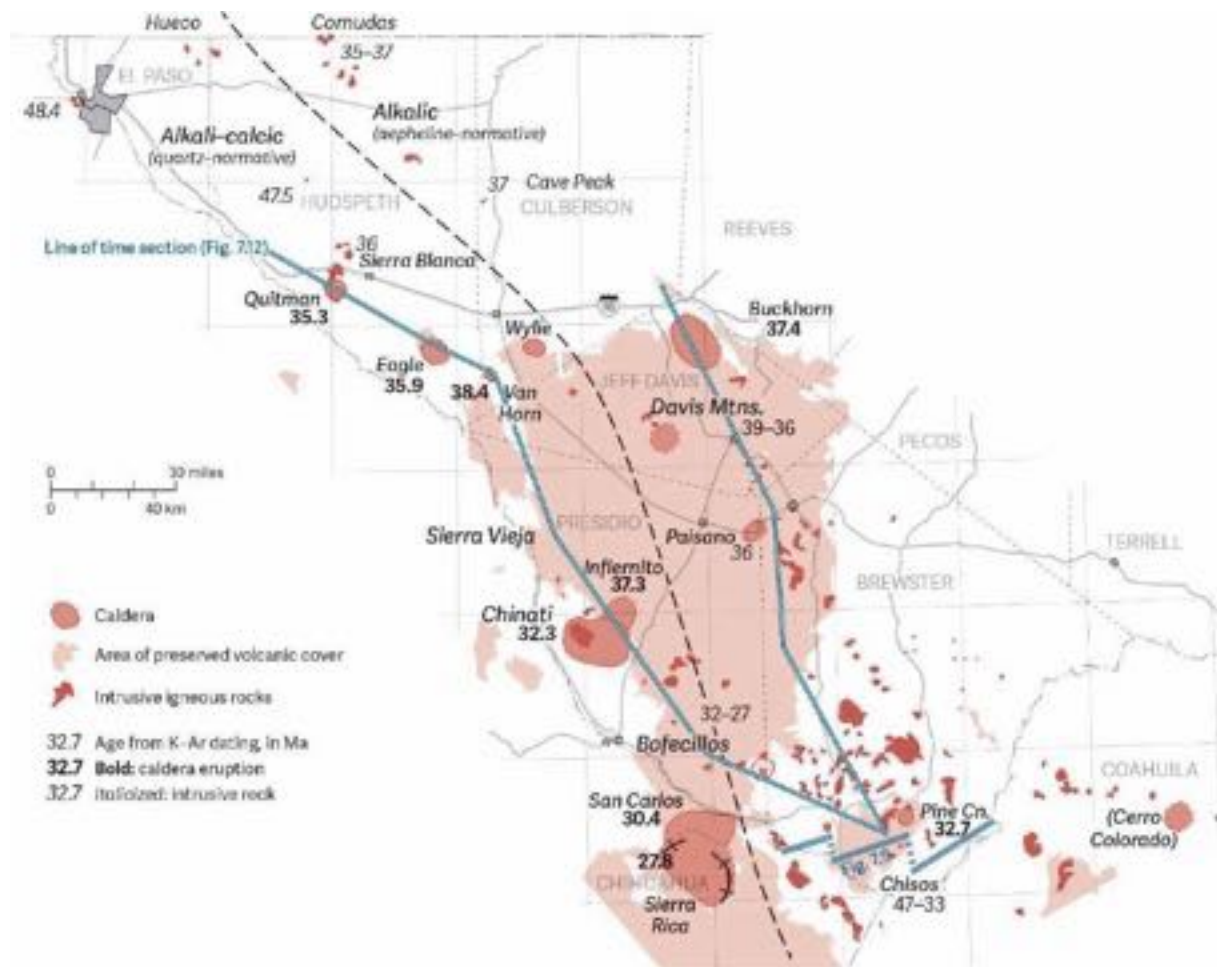
Figure 0.16 - Eruptive centers and extent of volcanic fields in Trans-Pecos Texas, with radiometric dates. Source: Ewing (2016), modified from Henry and Price (1985)
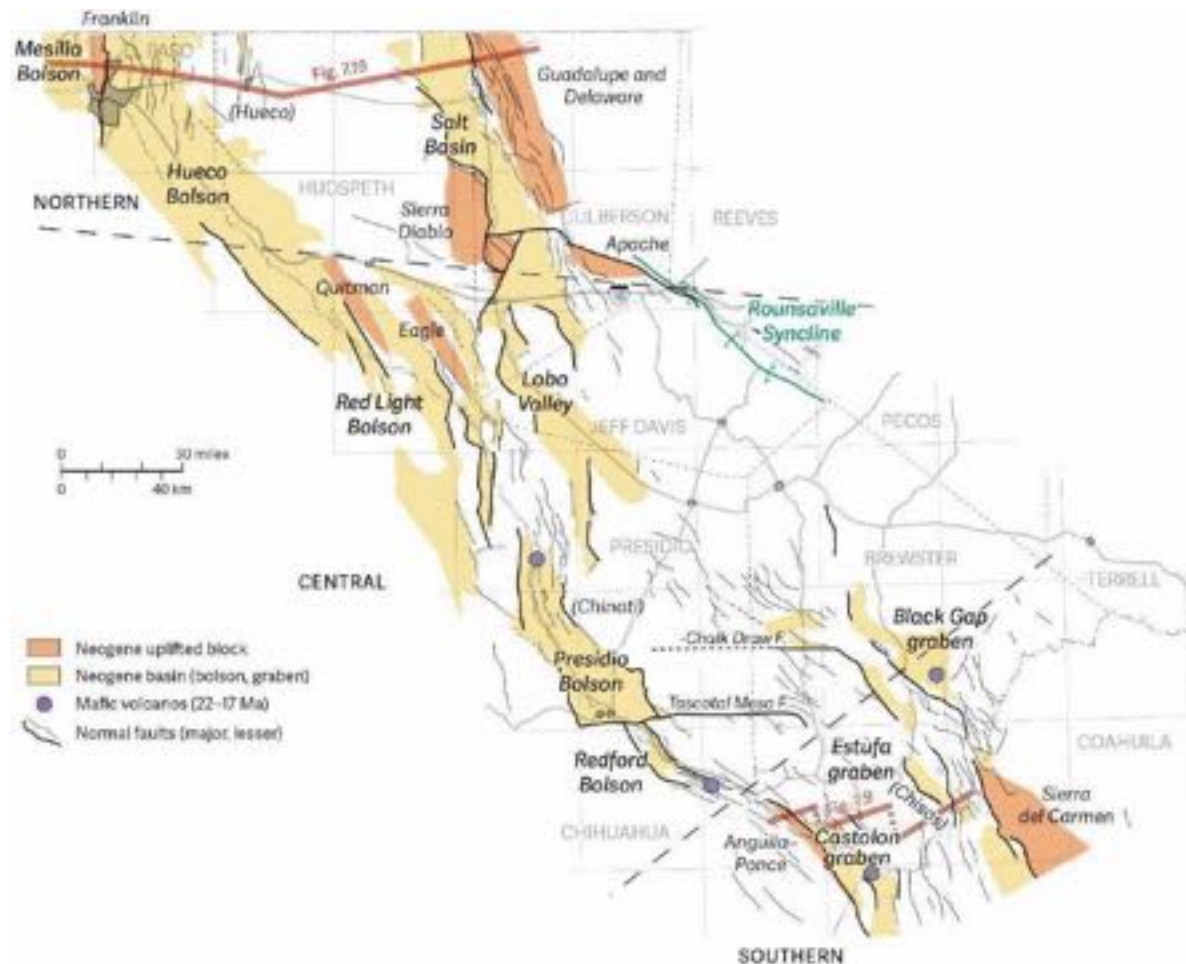
Figure 0.17 – Neogene rift basins of Trans-Pecos Texas. Source: Ewing (2016),   modified from Henry and Price (1985)
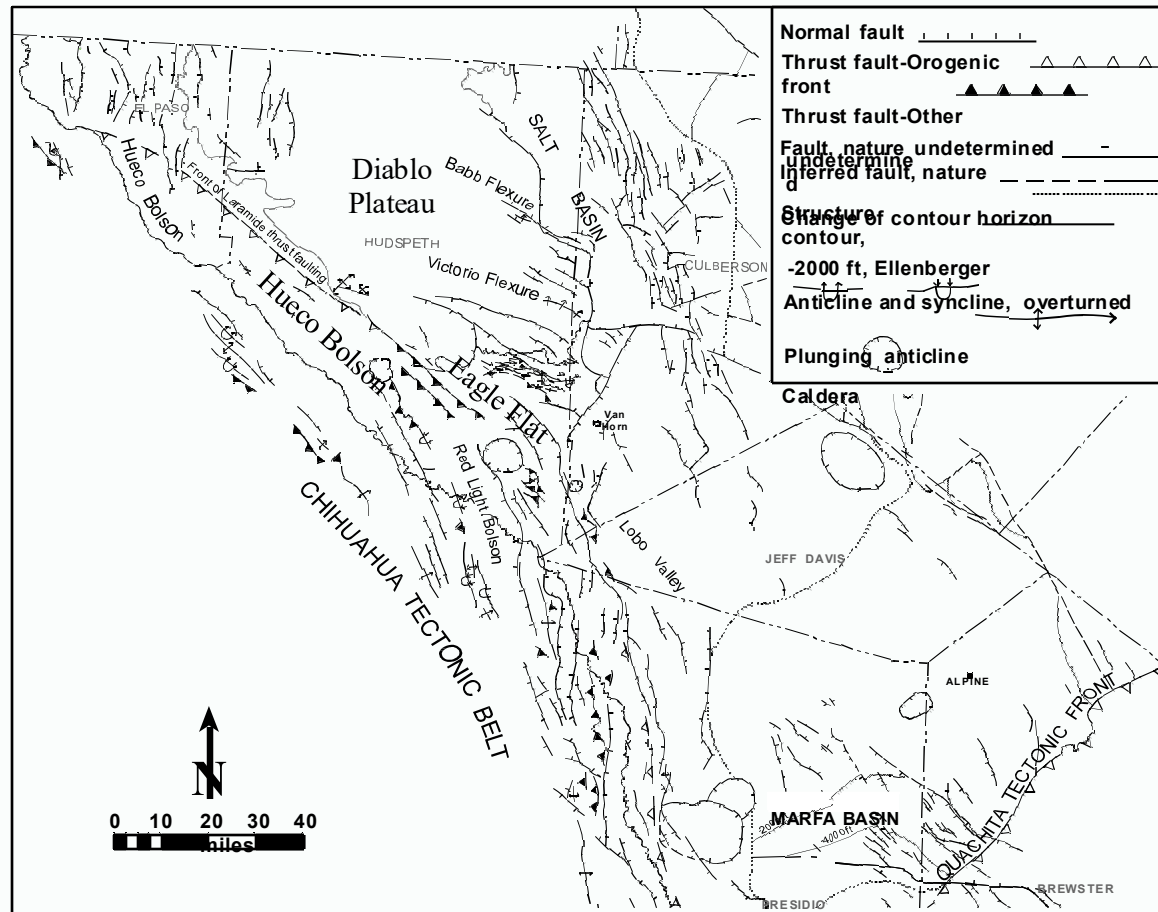
Figure 0.18 – Regional structure map of northwestern Trans-Pecos Texas.
Source: Tectonic Map of Texas (modified from Ewing and others, 1990).

33
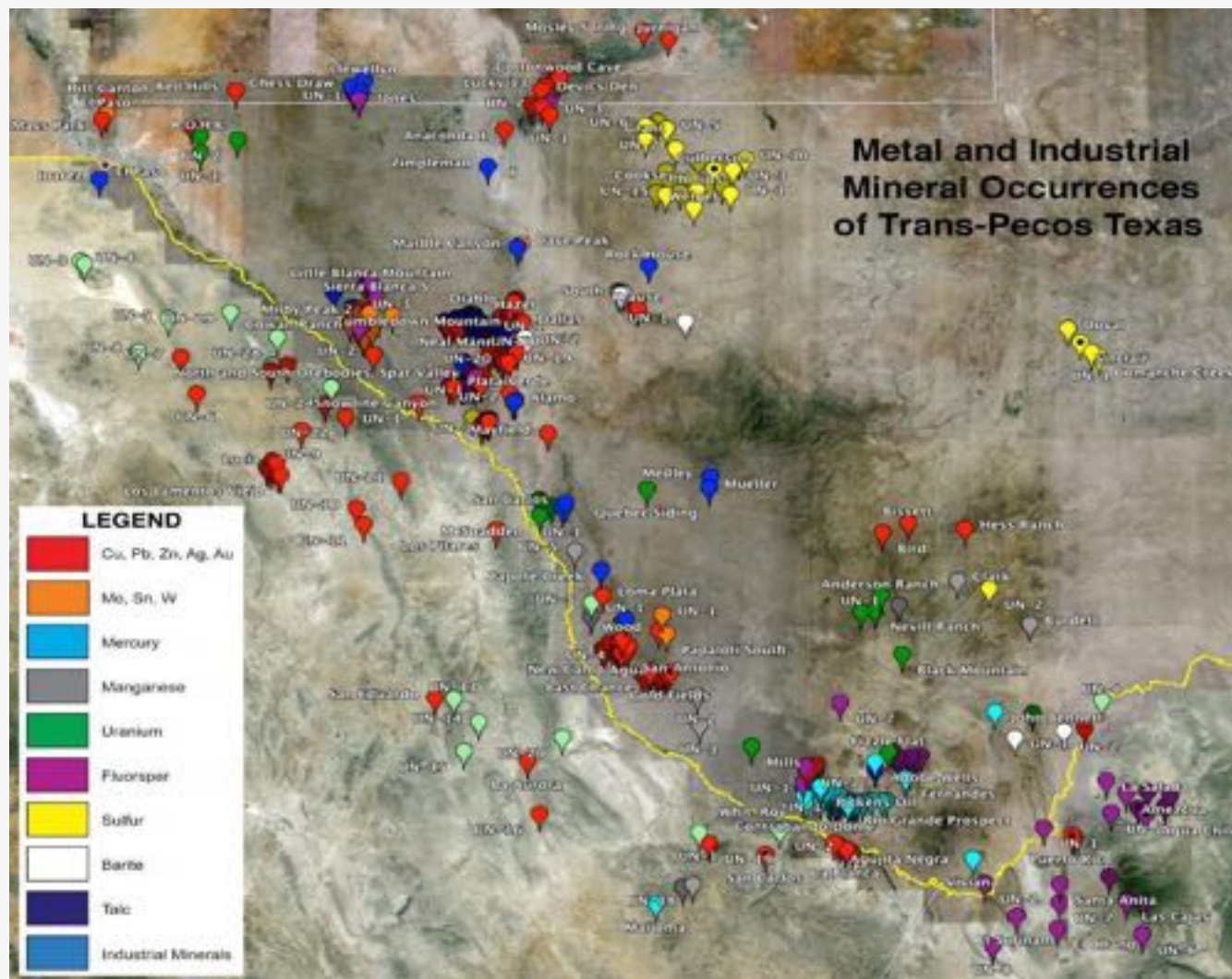
Figure 0.19 – Metallic and industrial minerals of Trans-Pecos Texas. Source: Becker and Kyle (2011)

34

GEOLOGY OF HUDSPETH COUNTY, TEXAS

GUIDEBOOK OF AIPG-TEXAS
SPRING FIELD TRIP
APRIL 21 – 23, 2023

ROAD LOG – DAY ONE

OVERVIEW OF ROAD LOG - DAY ONE

Day One begins in El Paso (El Paso County) and ends in Van Horn (Culberson County). The first 75 miles of the road log are taken from Price and Henry (1986). At Stop 1.1, the narrative changes to reflect the topics of interest to this field trip. The emphasis on Day One is on the tectonic setting and structural geology of the broad region covered by the road logs of Days One through Three, along with the potential of the Sierra Blanca laccoliths to be sources of rare earth elements (REEs) and other minerals essential to a nation that needs a secure source of supply of minerals deemed critical to an economy dependent on materials needed to support advanced technology. The road log of Day One also includes comments on the formation of the Eagle Flat and Red Light basins, along with the hydrogeology of the basins.

Road log by: Bruce K Darling and Michael Jacobs

Begin road log

Begin at El Paso Airport and drive south to Airway Blvd. The Franklin Mountains on the west (right) contain Precambrian sedimentary and igneous rocks, including basalts, rhyolite ash-flow tuffs, and granites which are overlain by Paleozoic sedimentary rocks (Harbour, 1972). South of the Franklin Mountains is the Campus Andesite (Hoffer, 1970). The andesite is the oldest of the Tertiary intrusive rocks of the Trans-Pecos region. Hoffer (1970) reported a K-Ar date of 48 m.y., based on biotite samples. Rocks of similar age are found in the Finlay Mountains 62 mi (100 km) to the southeast (Henry and McDowell, 1986) and in the Christmas Mountains of the Big Bend 248 mi (400 km) to the southeast. South of the Franklin Mountains and south of the Rio Grande is the Sierra de Juarez, a range consisting of Lower Cretaceous limestones that were folded and thrust northward during Laramide tectonism.

Drive under I-10 overpass, turn left and merge with I-10 eastbound.

4.0 mi (6.4 km)

The mountains to the south are Laramide-deformed Cretaceous rocks in Mexico. These mountains are the Sierra de Guadalupe and the Sierra del Presidio.

8.0 (12.8 km)

Mile marker 32 on I-10. We are driving in the Hueco Bolson, the westernmost Basin-and-Range graben in the Trans-Pecos region. Quaternary faulting has been recognized within this and other grabens (Eagle Flat, Red Light, Green River, Lobo Valley, and Salt basin) covered by this field trip (Muehlberger and others, 1978; Seager 1980).

8.3 mi (13.4 km)

The Rio Grande to the south (right) has dissected the Hueco Bolson, along with the Red Light, Green River and Presidio basins. The Presidio basin, the southernmost in the Texas System of Bolsons, is south of the area covered by this field trip.

29.5 mi (13.4 km)

The northern Quitman Mountains are straight ahead (that is, at 12:00). North of the Quitman Mountains (at 11:00) are five Tertiary rhyolitic intrusive bodies that form the prominent Sierra Blanca laccoliths (Figure 1.04a), the largest of which is Sierra Blanca Mountain.

60.6 mi (97.5 km)

The highway curves to the left near mile-marker 84. At this point, we are moving away from the Rio Grande, climbing out of the Hueco Bolson and will drive over a broad inter-basin pass that will take us into the Eagle Flat Bolson. In the El Paso to Van Horn road log of the 1986 field trip guidebook, Price and Henry (1986) include the following extensive description:

> The Quitman Mountains are straight ahead. Caldera-filling volcanics are exposed in the central part of the range, and a large quartz monzonite intrusion, which may be part of a ring dike, crops out in the northern part of the range. The southern Quitman Mountains, mapped by Jones and Reaser (1970), are Cretaceous rocks folded and thrust-faulted during Laramide deformation. The Finlay Mountains, to the north of the road at 9:30, are cored by Permian sedimentary rocks overlain by Cretaceous sedimentary rocks (Albritton and Smith, 1965). Numerous 47-m.y.-old sills and dikes (Henry and McDowell, 1986), intrude this sedimentary sequence. These intrusions are unusual for the Trans-Pecos region in having abundant titaniferous hornblende phenocrysts and megacrysts. The Malone Mountains at 10:30 are south of the Finlay Mountains (Figure 1.01 of this guidebook); Sierra Blanca Mountain is in the background behind the Malone Mountains. The Malone Mountains contain Permian evaporites deposited in a basin more or less coincident with the Hueco Bolson. The only outcrops of Jurassic sedimentary rocks were deposited in the Chihuahua trough, a depositional basin centered to the southwest in Chihuahua, Mexico, and active at least through Early Cretaceous time.

64.8 mi (104.2 km)

Dissected basin fill of Hueco Bolson on south side of I-10.

66.6 mi (107.2 km)

The low hill at 2:00 is basalt surrounded by basin fill. This was originally mapped as Quaternary by Albritton and Smith (1965); but McDowell (1979) reported K-Ar ages ranging from 31 to 34 m.y.

70.0 mi (112.6 km)

Straight ahead is quartz monzonite of the northern Quitman pluton (Figure 1.01).

71.9 mi (115.7 km)

Five laccoliths of aphanitic rhyolite occur north of the Quitman Mountains (Figure 1.01 and 1.04a): Sierra Blanca (the largest of the five), Little Blanca Mountain, Round Top, Little Round Top, and Triple Hill. Beryllium- and uranium-rich fluorite deposits occur along the contacts between the first four intrusions and Cretaceous limestone rocks (McAnulty, 1974). The fluorine, beryllium and uranium are probably derived from igneous rocks. Other elements that are enriched in Tertiary alkaline (alkalic and alkalic-calcic) rocks of Trans-Pecos Texas that are known to be concentrated in igneous hydrothermal ore deposits include zinc, yttrium, zirconium, niobium, molybdenum, cadmium, tin, rare-earth elements, tungsten, thorium, silver and mercury (Price and others, 1983).

Take the exit immediately after I-10 mile-marker 95 and stay on access road.

75.2 mi (121 km)

Stop 1.1 - Scenic overlook at northern Quitman Mountains and eastbound I-10

After three miles (4.8 km), turn right at the gravel road and park at the rest stop. We will remain here for 60 minutes or more for a discussion of the geological setting and an overview of regional geology. There is much to see at **Stop 1.1** (Figure 1.01)**.** (Philip C. Goodell and his crew of UTEP geologists (Figures 1.2a,b) led the discussion of geology as seen from **Stop 1.1**.) This point is at the northernmost extent of thrust-faulting and igneous activity associated with the Chihuahua trough. **Stop 1.1** is also at the boundary between the Chihuahua Trough and the North American Craton. It is in this area of Trans-Pecos Texas where the thrust sheets of the trough form prominent northwest-trending structures that terminate south of the Diablo Plateau, a stable geological feature composed of rocks of Precambrian age overlain primarily by rocks of Permian age and rocks of Cretaceous age. Geological features identifiable from **Stop 1.1** are identified in Figure 1.01. More detailed text related to the geology of this area is deferred to **Stop 1.2**.

After **Stop 1.1**, drive 0.75 mi (1.2 km) on access road and then turn left at Lasca Road. Drive under the overpass and then turn right on the access road. Stay on the paved road for 5.1 mi (8.2 km) and turn left at the gate. At this point, note the abandoned buildings (Figures1.03a,b). These buildings were constructed in the early 1970s as part of a land scam that was promoted to attract people who wanted to live in a desert resort community. The project (Mile High Resort) collapsed

in the late 1970s. The buildings were used as offices and check points for vehicles entering and leaving the planned development.

80.8 mi (130 km)

Before driving through the gate, observe Bluff Mesa on right (south of I-10). Bluff Mesa (Figure 1.01 and El Paso - Van Horn GAT sheet (Dietrich and others, 1983)) consists of Cretaceous sedimentary rocks folded and thrust-faulted toward the northeast along the Devil Ridge thrust sheet during Laramide tectonism. North of the highway and west-northwest of the gate are two prominent hills known as the Etholen Knobs (Figures 1.04a,b). Originally part of the Devil Ridge thrust sheet, the Etholen Knobs are erosional remnants (klippen) of the thrust sheet between Bluff Mesa and Sierra Blanca Mountain to the north.

The paved road follows a stream-cut valley between Sierra Blanca Mountain on the west and Triple Hill on the east (Figure 1.04a). Sierra Blanca quarry is on the northeast side of Sierra Blanca Mountain.

Drive 6.4 mi (10.3 km) on the paved road, and then stop at the office of Sierra Blanca Quarry.

87.15 mi (140 km)

Stop 1.2 - Sierra Blanca quarry and view of Sierra Blanca Complex

Sierra Blanca Quarry supplies ballast for Union Pacific Railroad. Average annual shipments are 300,000 to 400,000 tons (Dennis Walker, owner of Sierra Blanca Quarry, LLC). The quarry and processing operations are illustrated in Figures 1.05a,b – 1.012a,b.

The Sierra Blanca Complex (SBC) consists of five topographically prominent, uncovered rhyolite laccoliths (Figures 1.01 and 1.04a) clustered in a structurally complex zone of the Trans-Pecos Magmatic Province (TPMP) (Elliott, 2018). More specifically the SBC is located on the northern margin of the Chihuahua Tectonic Belt, at the southern boundary of the Diablo Platform, astride the projection of the Texas Lineament, and near the northern edge of the Quitman Mountains caldera (Kyger, 2013; Elliott, 2018).

The laccoliths are not symmetrical, mushroom-shaped masses with flat discordant floors. Except for Triple Hill, all are floored above the Cox Sandstone (Cretaceous). Steeply dipping strata on the flanks of the peaks indicate that Washita and younger formations were domed or partially domed over the laccoliths (Kyger, 2013).

Sierra Blanca Mountain (Figure 1.04a and 1.13a), the highest of the laccoliths, stands at an elevation of 6896 ft (2102 m) and about 1968 ft (600 m) above the surrounding flats. Listed in order of decreasing size, the other peaks are Little Blanca Mountain, Round Top (Figure 1.13b), Triple Hill, and Little Round Top (Kyger, 2013).

Igneous intrusions of the TPMP can be divided into two geochemical districts: alkalic-calcic toward the west and alkalic compositions toward the east (Barker,1977 and 1987; Henry and Price, 1984). Elliott (2018) summarizes magmatic activity in the region as follows:

Magmatism in the region occurred between 100 and 40 Ma ago, related with the subduction of the Farallon plate under the North American continent. Bimodal volcanism extended east from the West Coast subduction zone (Price and others, 1990; Henry and others., 1991). Trans-Pecos magmatism occurred between 48–17 Ma and is separated into early and later phases (Henry and McDowell, 1986; Henry and others, 1989; Henry and others. 1991; Price and others, 1990; Rubin and others, 1993). The early phase (48–38 Ma) is characterized by voluminous silicic to mafic igneous intrusions, lava flows and caldera eruptions (Henry and McDowell, 1986; Price and others, 1990). The late phase (38 – 32 Ma) was compositionally variable, ranging from alkalic-calcic to alkalic, and represents the most active magmatism in the region (Barker, 1977; Henry and Price, 1984; Henry and McDowell, 1986; Price and others, 1990). The Sierra Blanca laccolith, adjacent to and associated with Round Top, was emplaced during the main phase of bimodal TPMP activity at 36.2 ± 0.6 Ma (K/Ar in biotite (Shelley, 1992)). Volcanism during this period is characterized by silicic to mafic intrusions, and large-volume caldera eruptions associated with voluminous ash-flow tuffs (Barker, 1977; Henry and McDowell. 1986; Price and others, 1990). Basin and Range extension was initiated by a change in the region's stress around 31 Ma, and extensive normal faulting initiated around 24 Ma (Price and others, 1990). Mafic volcanism in the early stages of rifting has been dated at 17 Ma (Price and others, 1990).

Elliott (2018) describes the SBC as five rhyolite and rhyolite porphyry laccoliths. The largest laccolith (Sierra Blanca, Figure 1.13) was emplaced 36.2 ± 0.6 Ma (Henry and McDowell, 1986). He adds the following with regard to emplacement ages of the laccoliths:

Emplacement ages of the other laccoliths have not been measured, but a relative emplacement sequence can be interpreted through major- and trace-element differentiation. The increasing enrichment of REEs, especially in the increasing ratio of HREES to LREEs (Heavy to Light Rare Earth Elements) between laccoliths, suggests that Triple Hill was emplaced first, followed by Sierra Blanca, Round Top, Little Sierra Blanca, and Little Round Top (Price et al, 1990; Shannon, 1986; Shannon and Goodell, 1986; Dietrich and others, 1983). The slight differences in compositions and rapid cooling textures suggest the timing between emplacement and duration of emplacement was relatively short.

Sierra Blanca Mountain is the largest of the laccoliths (Figures 1.04a and 1.13). The laccolith is pink to gray in color (Figures 1.05a,b), chemically and texturally homogeneous and composed of quartz rhyolite porphyry. Alteration of the rhyolite is not pervasive compared to Round Top, but hematitic and manganese oxide staining is

evident throughout jointed and faulted portions of the laccolith. Round Top is the most westerly of the SBC (Figure 1.04a, 1.13b)) and comprises four variations of rhyolite that differ slightly by color, mineralogy and texture. The rhyolite is fragmented, heavily jointed, blocky, and locally cemented by multiple generations of fluorite, calcite, and quartz.

The mineralogical composition of the laccoliths is interpreted from more than 350 samples collected from outcrops, roadcuts and drill cuttings obtained during exploratory drilling by Texas Mineral Resources Corporation (Elliott, 2018).

The Round Top laccolith is relatively homogenous, high silica, non-topaz bearing rhyolite with low MgO and CaO, high Na_2O and K_2O (Elliott, 2018), and relatively high Zr (960–1100 ppm), Rb (1660–1930 ppm), Th (160–190 ppm), and U (28–58 ppm). Felsic rocks from the Round Top and Sierra Blanca suite of rocks show predominantly Within-Plate Group (WPG) tectonomagmatic affinity (Elliott, 2018). The rocks are F-rich (up to 2.4 wt %), peraluminous with Al:Si ratios (Aluminum Saturation Index) around 1.2, but not peralkaline as is typical of many REE enriched systems (Elliott, 2018). Initial Sr^{87}/Sr^{86} ratios for the mafic constituents of the magmatic suite are around 0.702 (Matthews and Adams, 1986), where values of felsic members are around 0.728 (Shannon and Goodell, 1986). These contrasting ratios imply a more crustal source for the felsic rocks. The Rb/Sr system appears to be affected by late- to post-magmatic processes increasing Rb relative to Sr (Elliott, 2018). The post-magmatic process makes it difficult to rely on Sr in determining crustal contribution to the source of these magmas (Elliott, 2018).

Elliott (2018) comments that the laccoliths of the SBC and other regional magmatic rocks have distinct geochemical characteristics that help to discriminate them from each other (Matthews and Adams, 1986; Shannon, 1986; Shannon and Goodell, 1986). Elliott (2018) lists the following examples: The Finlay Mountains represent nearby mafic to intermediate compositions (40–65 wt % SiO_2), conforming temporally and compositionally to early gabbro/diorite dikes in the immediate SBC area. The Texan Mountain rhyolite represents the lowest silica content from felsic rocks in the magmatic series (64–70 wt % SiO_2), followed by Triple Hill and Sierra Blanca with Round Top, Little Blanca and Little Round Top representing extremely evolved rhyolitic compositions (70–76 wt % SiO_2). These evolved compositions show an increase in Na_2O relative to K_2O, decreasing Al_2O_3 and very low MgO and P_2O_5 (Elliott, 2018).

Mineral endowment and economic potential of the Sierra Blanca laccoliths

The mineral endowment and the economic potential of the SBC have been investigated by researchers with The University of Texas at El Paso and The University of Texas at Austin. (Kyger, 2013). The economic potential of the Sierra Blanca laccoliths was evaluated by McAnulty (1974)

during his study of fluorspar deposits. Murry (1980) examined the economic potential of the area, focusing on the Quitman caldera and its associated hydrothermal veins and contact metasomatic skarn deposits. The potential Be and REE (Rare Earth Element) deposits of the Sierra Blanca laccoliths have been discussed by Shannon (1986), Shannon and Goodell (1986), Rubin and others (1987a,b; Price and others (990), Kyger (2013). In conjunction with this field trip, Goodell and others (2023) and Mahar and Goodell (2023) prepared papers on critical minerals of Trans-Pecos Texas and magmatism within the southern Rio Grande Rift in the vicinity of Sierra Blanca. The papers by Goodell and others (2023) and Mahar and Goodell (2023) are attached as Supplements 1 and 2, respectively, to the text of the Day One road log.

Geology and mineral resources of the SBC – significant observations

Significant observations regarding the geology and mineral resources of the laccoliths are summarized by Kyger (2013):

1. The Sierra Blanca laccoliths represent unusual enrichment in HREE (Heavy Rare Earth Elements).

2. The regional tectonic setting, associated with the Texas Lineament, the Rio Grande Rift, and the associated magmatism are postulated to be factors in the emplacement of the REE-enriched rhyolites. **The emplacement of the Sierra Blanca rhyolites takes place in the stable block near the mobile belt boundary. Hence, the laccoliths are located on the southwest margin of the stable block, just northeast of the Chihuahua Tectonic Belt.** (Emphasis added by BK Darling.)

3. REE enrichment of the rhyolites is consistent throughout the laccoliths at levels well above the crustal average.

4. Enrichment in the HREE and incompatible trace elements Be, F, Rb, Y, Zr, Nb, Sn, and U, indicates economic potential beyond that of a REE deposit.

5. The laccoliths show zoning of the REE, from enrichment of LREE on Little Blanca to HREE on Little Round Top and Round Top.

6. Internal zonation of each laccolith has not been documented.

7. Late-stage enrichment along fractured zones through the action of F-rich liquids is indicated by the higher concentration of F and associated REE.

8. REEs are found in association with Y and F throughout the laccoliths. Yttrocerite and yttrofluorite are the main REE minerals. Geochemical data support their distribution throughout the laccoliths, whereas xenotime and bastnäsite are minor REE-bearing mineral components, with xenotime only in Round Top.

9. Round Top exhibits the least amount of geochemical differentiation in comparison to the other laccoliths.

Exploration history

Texas Mineral Resources (TMR) posts the following on the company's website (https://tmrcorp.com/projects/rare_earths/history/):

> Initial mineral exploration in the area surrounding Round Top commenced in 1969 and continued through the late 1970s. Work in the area included prospecting trenches as well as approximately 22 drill holes within fluorite outcrops in the area. Although a downturn in the fluorite market inhibited further project development, this early work led to the identification of beryllium mineralization in the area. During the 1980s, Cabot Corporation conducted further beryllium exploration at Round Top consisting of mapping, sampling, and reverse circulation rotary drilling.
>
> In 1987, Cabot entered into a joint venture agreement with Cyprus Metals Company to continue beryllium exploration focused on Round Top resulting in a feasibility study completed in 1988. Ultimately, Cyprus decided to exit the beryllium business and chose to refocus its efforts on copper mining, eventually merging with Phelps Dodge in 1999. Throughout the 1990s, the Round Top project lay dormant, eventually falling back under control of the Texas General Land Office. The project was subsequently acquired by Standard Silver Corporation, which changed its name to Texas Mineral Resources Corp. (TMR) in September 2010 to more appropriately reflect the current focus on Heavy Rare Earth Elements (HREEs).

TMR eventually entered into a joint venture agreement with USA Rare Earths, and in 2019, USA Rare Earths announced that the company had taken an 80 percent stake in the Round Top Project (https://www.mining.com/usa-rare-earth-takes-80-stake-in-round-top-project-in-texas/):

> We've got a very unique deposit in a number of respects – we have 16 of the 17 rare earths, with many in the rare earths categories that speak to a number of defense applications, and manufacturing. It is probably the largest heavy rare earths deposit in the world outside of China," Pini Althaus, CEO of USA Rare Earth told MINING.COM last year.

Project economics

The mining and mineral economics consulting firm Gustavson Associates (2014) reported project economics as follows:

- Mining Rate: 20,000 tonnes per day (TPD).

- All mineral processing at site: Deployment of conventional ion exchange and ion chromatography (CIX/CIC) technology to generate high purity individual rare earth oxides (REO) at the site as well as technology metals and industrial minerals.

- REO Production: Averaging 2,313 tonnes per year (TPY) total, including approximately 180 TPY of Neodymium (Nd) and 67 TPY of Praseodymium (Pr).

- New Lithium Resource: Estimated 9,800 TPY lithium carbonate production.

- Heap Leach Processing Technology: Proven conventional technology utilizing leach pads built to Texas Environmental Standards.

- Economic Mine Life: 20 years, based on mining only 14% of the existing Mineral Resource Estimate, implying overall potential mine life of 140 years.

- Net Present Value (NPV): $1.56 Billion at a 10% discount rate, pretax.

- Internal Rate of Return (IRR): 70%.

- Payback Period: 1.4 years.

- Capital Cost: $350.4 Million, including a complete on-site rare REO and mineral separation plant, and a 25% contingency provision of $65.7 Million.

- Mid- 2019 Spot Market Pricing Assumptions: Yields 70% IRR.

[*Round Top was off limits for this field trip. The site was in the early stages of development by USA Rare Earths and access to onsite operations was not allowed because the company's insurance restrictions did not permit visits to the site by anyone not associated with the project.*]

After **STOP 1.2**, Retrace steps 6.4 miles (10.3 km) to I-10 access road.

93.5 mi (154.7 km).

Turn left on the access road and travel 2.6 mi (4.3 km) to Sierra Blanca exit.

96.15 mi (155.0 km) Veer left at exit and drive 1.15 mi (1.8 km) to intersection with RM 1111.

97.30 mi (156.6 km). Stop at the intersection and turn right on RM 1111, then pull into the parking lot at Delfina's Café for lunch (Figures 1.14a,b).

After lunch, drive south 0.8 mi (1.3 km) on RM 1111 to **LANDFILL 3** sign.

98.10 mi (157.9)

Stop 1.3 - Overview of Eagle Flat Basin, surrounding highlands and hydrogeology

Turn right and drive to the top of the hill (Figure 1.15). Stop here for an overview of the geology of Eagle Flat basin and surrounding highlands, the hydrogeology of Eagle Flat, and a discussion of regional groundwater flow.

Eagle Flat is a northwest-trending basin bounded on the north by the Diablo Platform and rocks of the Allamoore and Hazel formations (Precambrian); on the west and southwest by the Sierra Blanca laccoliths and the Devil Ridge thrust sheet; on the south and southeast by the Eagle Mountains; and on the east by the Carrizo Mountains and the Van Horn Mountains (Figure 1.15 and Van Horn - El Paso GAT sheet [Dietrich and others (1983)]). The basin extends 35 mi (56.3 km) from the northwestern boundary at the Diablo Plateau to the southeasternmost extent at the Scott's Crossing water gap between the southern end of the Carrizo Mountains and the northern end of the Van Horn Mountains. Accounting for variations in local topography within the basin, the floor of Eagle Flat is relatively flat, with an average elevation in the center of the basin of approximately 4,500 ft (1,370 m)

Although Eagle Flat is one structural basin, it is divided into two topographic sub-basins: Northwest Eagle Flat and Southeast Eagle Flat (Raney and Collins, 1993; Collins and Raney, 1993; Darling and others, 1994; Darling, 1997). The topographic division is formed by a surface-water divide, the location of which is marked on Figure 1.15. Northwest of the divide, all surface drainage terminates at the Grayton Lake playa. Southeast of the divide, surface flow is along Eagle Flat Draw, an ephemeral stream that exits the basin at the Scott's Crossing water gap.

The geology, geomorphology, and groundwater resources of Eagle Flat and surrounding area were extensively investigated in the 1990s by researchers with The University of Texas at Austin Bureau of Economic Geology as part of a multi-year effort to assess the suitability of the basin to be the location of a processing and disposal facility for low-level radioactive waste (Raney, 1991; Raney and others , 1991; Raney and others, 1992; Seni and Raney, 1992; Wermund and Raney, 1992; Raney and Collins, 1993; Collins and Raney, 1993; Langford, 1993; Darling and others, 1994; Scanlon and others, 1994.

Prior to the above-cited investigations, researchers with the United States Geological Survey (USGS), in conjunction with the Texas Department of Water Resources, conducted assessments of the availability of groundwater resources in Eagle Flat and other basins (Gates and White, 1976; Gates and others, 1980; White and others, 1980). The above-cited studies produced a substantial body of data, much of which supported the research cited above and a Ph.D. dissertation on the

aquifers of the Eagle Flat, Red Light, and Green River basins, as well as local, intermediate, and interbasin flow of groundwater, and age-dating of groundwater (Darling, 1997).

The thickness of the basin fill of Northwest Eagle Flat varies from less than 200 ft (61 m) along the margins of the basin to as much as 500 ft (162 m) in the vicinity of Grayton Lake (Raney and Collins (1993); Collins and Raney 1993; Darling and others, 1994). Southeast of the topographic divide, the thickness of the basin fill expands to more than 2,100 ft (640 m) as measured by cuttings from a 2,200-ft (671 m) borehole drilled by the USGS (Gates and White, 1976) west of the Scott's Crossing water gap and between the southern end of the Carrizo Mountains and the Eagle Mountains.

Four peculiar aspects of Northwest Eagle Flat are:

- There is no area where groundwater discharges within the lower elevations of the basin.

- Everywhere in Northwest Eagle Flat, the basin fill is unsaturated.

- Groundwater occurs under confined conditions in Cretaceous carbonates and sandstones beneath the basin fill.

- The depth to groundwater increases with distance from recharge areas along the boundaries of the basin (Figure 1.16; Darling and others, 1994; Darling, 1997), with the greatest depths in the center of Northwest Eagle Flat. A contour map of the potentiometric surface (Darling, 1997) does not show evidence of lateral flow from Northwest Eagle Flat (Figure 1.17).

In Southeast Eagle Flat, with the exception of intermittent springs in the Eagle Mountains and the Carrizo Mountains:

- Groundwater does not discharge to the surface anywhere along the floor of the basin;

- Groundwater occurs in unconfined to semi-confined/confined conditions everywhere in Southeast Eagle Flat; and

- Groundwater flows toward the east-southeast, discharging from the basin through porous and permeable rocks of Permian age and of Cretaceous age beneath the Scott's Crossing water gap (Figure 1.17; Darling and others, 1994; and Darling, 1997).

The closed potentiometric contours beneath Northwest Eagle Flat (Figure 1.17) are interpreted to indicate downward flow of groundwater to rocks of greater permeability that allow for vertical flow of groundwater (Darling, 1997). The direction of flow from Northwest Eagle Flat is not apparent as there are no wells deep enough to capture information on hydraulic head and flow directions. Wells drilled as part of the low-level radioactive waste site-assessment study were complicated by lost circulation, typically in Cretaceous carbonate rocks. All such problems were handled by the injection of lost-circulation materials (Darling and others, 1994).

The Red Light Draw and Green River Valley groundwater systems, both located south of the Eagle Flat basin (Figure 1.17) are not demonstrably connected with Eagle Flat. The Red Light system, bounded along the northeast by Devil Ridge, the Eagle Mountains and the Indio Mountains, and along the southeast by the Southern Quitman Mountains, drains toward the south and discharges along the Rio Grande. The Green River system, bounded on the east by the Van Horn Mountains and on the west by the Indio Mountains, drains toward the south and also discharges along the Rio Grande.

Darling (1997) describes one Eagle Flat test well that appears to offer support for the occurrence of higher permeability in rocks beneath the Cretaceous bedrock of the Eagle Flat basin:

> In 1965, Texaco, Inc. drilled a 1,633-ft (498-m) core test (Capitan Drilling Co., No. 1 Espy Range) in the Eagle Flat basin. White and others, (1980) listed the well as 48-63-602, but did not report a static-water level. The surface elevation at the wellhead was reported to be 4,368 ft (1,331 m) above msl (White and others, 1980). The drilling record on file with the TWDB shows that the well penetrated 240 ft (104 m) of basin fill before encountering carbonate rocks. The record also reports lost circulation in carbonate rocks between depths of 1,590 ft (485 m) and 1,700 ft (585 m), with inability to regain circulation. The borehole was plugged and abandoned at 1,633 ft (498 m).

> This core test was one of the deepest penetrations of bedrock in the Eagle Flat Basin. The lost circulation reported for this test occurred at an elevation of 2,778 ft (878 m) above msl – or between 900 and 1,000 ft (274 and 305 m) below the potentiometric surface in this part of the Sierra Blanca system. The loss of circulation suggests that a higher-permeability pathway might lie beneath the uppermost part of the zone of regional saturation to provide an avenue for flow beneath local ground-water divides. In this case, ground water in the less permeable rocks beneath the basins fill might drain to deeper and more transmissive rocks. This type of communication was suggested by Winograd (1962) and Winograd and Thodarson (1975) in studies of the regional flow systems of Yucca Flat and Frenchman Flat in the Great Basin of Nevada.

Darling (1997) offers a second line of evidence for the flow of groundwater beyond the boundaries of Eagle Flat. A plot of land-surface elevations versus static water levels reveals two distinct groups with respect to the Eagle Flat, Red Light, and Green River groundwater systems (Figure 1.18).

Beginning with the assumption that groundwater elevation mimics local topography in gravity-driven systems, Darling (1997) observes that the data points in Figure 1.18 can be divided into two groups: Group 1, which manifests a high degree of correlation between topography and groundwater elevation, and Group 2, which displays no apparent correlation between the variables. Using least squares regression, Darling (1997) calculated lines of best fit for each group (Figure 1.18). Pearson's correlation coefficient (r) for Group 1 is 0.98, and the coefficient of determination (r^2) is 0.97. For Group 1, the r^2 coefficient indicates that 97 percent of the variability of groundwater

elevation is correlated with topography. For Group 2, r and r^2 are 0.26 and 0.06, respectively. Based on the low value of r^2 for Group 2.

Darling (1997) interprets the markedly different least squares equations and correlation coefficients between Group 1 and Group 2 to denote two hydrogeologic regimes:

> The first, represented by Group 1 wells, consists of shallow to relatively shallow ground water for which the configuration of the potentiometric surface mimics local topography. The second, represented by wells belonging to Group 2, consists of ground waters of sufficient depth that the potentiometric surface does not reflect variations in local topography.

Group 1 comprises dominantly local flow systems, all driven by gravity and all reflective of overlying topography. Wells that represent this group are located in alluvial fans and in higher elevations surrounding the Eagle Flat, Red Light, and Green River basins; that is, in areas where groundwater occurs under unconfined conditions. Group 2 is represented by deeper basin-center wells that produce groundwater under confined to semi-confined conditions. Darling (1997) infers that groundwater of Group 2 is in communication with deeper, more porous and permeable Cretaceous and Permian formations (primarily carbonate rocks) that transport groundwater beyond local basin boundaries.

Figure 1.19 is a conceptual model of regional groundwater flow paths in the Eagle Flat, Red Light, Green River, Salt, Lobo, Antelope Valley, Lobo Valley, and Wild Horse Flat basins. The inferred paths are based on the work of Darling (1997), Sharp (2001), Uliana (2000), Uliana and Sharp (2001), and Uliana and others (2007). The models incorporate a great many measurements of water levels from wells throughout the region, along with inorganic geochemical and isotopic data. The model shows downward flow of groundwater in Northwest Eagle Flat, upward flow and discharge to the surface in the Salt Basin bolson, and dominantly lateral flow in Southeast Eagle Flat, the Red Light Basin, and Green River Valley, and in Antelope Valley, Lobo Valley and Wild Horse Flat. Southeast Eagle Flat groundwater is inferred to move eastward through porous and permeable rocks beneath Scott's Crossing and to merge with Lobo Valley groundwater flowing northward toward Wild Horse Flat. There is no discharge of groundwater to the surface anywhere along the floors of Antelope Valley, Lobo Valley, and Wild Horse Flat. The nearest point of groundwater discharge is the Salt Flat Basin and the springs of Balmorhea, located 70 miles (113 km) east of Van Horn. The hydrogeology of the Salt Basin is discussed in greater detail in the Day 3 road log of this guidebook.

Sharp (2001) observes that faulting, folding, and dissolution of carbonates and evaporites in Trans-Pecos have created the controlling framework for regional flow systems, with three discharge areas: 1) the Rio Grande, 2) the northern and middle sections of the Salt Basin, and 3) the Pecos River. He adds that the feature common to all Trans-Pecos regional flow systems is the presence

of Cretaceous carbonate rocks in close proximity to Permian carbonate rocks. The formations have been fractured by a variety of tectonic episodes: 1) the Laramide orogeny, 2) Basin-and-Range extension, and 3) subsidence caused by dissolution of underlying evaporite deposits.

Age-dating of groundwater and description of recharge areas

Figure 1.20 is a regional map on which are posted ^{3}H (as Tritium Units, half-life 12.43 yrs) ^{14}C (as percent of modern carbon, or PMC; half-life 5730 yrs), and apparent (unadjusted) ^{14}C ages of groundwater in the Eagle Flat and Red Light Basins. Average values are shown for wells having multiple samples. The data on which the figure is based were compiled by Darling and others (1994) during their three-year investigation of the aquifers of the Eagle Flat, Red Light, and Green River basins in conjunction with the low-level radioactive waste siting study described above. The estimated ages are maximum values and are not based on adjustments for the effects of factors that are known to lower ^{14}C in groundwater. Darling and others (1994) do not regard ^{14}C as a reliable indicator of absolute age, but of relative age. The highest ^{3}H and ^{14}C values are found in groundwater along the mountain fronts and where bedrock is exposed or covered by a thin layer of basin-fill.

The lowest values of ^{14}C and ^{3}H are found in the deepest groundwaters of the Eagle Flat and Red Light basins. In the Southeast Eagle Flat Basin, ^{14}C ranges from 107 PMC to 2 PMC, and ^{3}H from 8 to 0 TU. The highest PMC occurs in groundwaters of the Bean and Millican Hills and the Carrizo and Eagle Mountains. Along the margins of the basins, especially in the Allamoore area of Southeast Eagle Flat, the depth to the potentiometric surface is generally less than 200 ft (<61 m), in areas where bedrock is either exposed or covered by a thin layer of Tertiary basin fill and unconsolidated Quaternary sediments.

The lowest ^{14}C measurements are consistent with apparent ages that range from 23,000 to 31,000 years (Darling and others, 1994; and Darling, 1997). That age range is in line with estimates of ages of groundwater in the Hueco Bolson, as reported by Fisher and Mullican (1990). In northwest Eagle Flat, ^{14}C ranges from 80.5 to 1.3 PMC, and ^{3}H from 2.0 to 0 TU. The largest PMCs occur in groundwater near the margins of the basin, where bedrock of Precambrian or Cretaceous age is exposed. Measurements of 0 TU are characteristic of deep groundwater near the central area of the flow system.

Darling and others (1994) and Darling (1997) comment that the use of ^{14}C in groundwater dating studies is complicated by geochemical processes that render the isotope unreliable as an estimator of absolute age. Such processes include dilution of ^{14}C by interaction with carbonate rocks, and mixing in dual-porosity systems. Darling and others (1994) and Darling (1997) propose an indirect approach to the problem of differentiating between Late Pleistocene and Post-Pleistocene groundwater ages based on the integration of ^{14}C with oxygen-18 (^{18}O) – a stable isotope of the water cycle, with a known temperature-fractionation gradient.

Confined groundwaters of southeast New Mexico and the Southern High Plains have been documented to be more depleted in ^{18}O than unconfined waters (Dutton, 1995). Darling and others (1994) and Darling (1997) offer the hypothesis that the range of δ^{18}O and δ^2H ratios (that is, the abundance of ^{18}O and ^{2}H in groundwater as measured by comparisons with Vienna-Standard Mean Ocean Water (V-SMOW) of confined groundwaters can be attributed to the effects of depletion from heavier precipitation and lower temperatures of the Late-Wisconsinan glacial period. In the Eagle Flat and Red Light basins, groundwater is increasingly depleted in ^{18}O and ^{2}H along flow paths between basin margins and basin centers. The depletion with respect to ^{18}O and ^{2}H along flow paths corresponds well with decreasing ^{14}C, with depletion in both stable isotopes increasing sharply at 15 PMC and lower (Figures 1.21a,b).

Darling and others (1994) and Darling (1997) postulate that the association between ^{14}C, ^{18}O and ^{2}H might constitute a semi-quantitative basis for differentiation of Pleistocene and Holocene dates, with the apparent breakpoint at approximately 15 PMC on plots of PMC v δ18O and δ^2H (Figures 1.21a,b). Darling and others (1994) and Darling (1997) also hypothesize that, over the range of ^{14}C measurements greater than 15 PMC, the trend toward younger groundwater increasingly enriched in ^{18}O and ^{2}H reflects the evolution of a warmer/arid regional climate over the last 11,000 years. Furthermore, based on the range of lightest to heaviest δ^{18}O ratios in groundwater and a fractionation gradient of 0.55o/oo/°C, Darling (1997) estimates a temperature difference of 5.5-7.5°C between Late Pleistocene and modern climates.

The stable isotope ratios and PMC measurements reported by Darling and others (1994) and Darling (1997) indicate that groundwater of the Eagle Flat and Red Light basins ranges in age from modern to Late Pleistocene, with the youngest ages associated with highlands surrounding the basins, and the greatest ages along flow paths beneath basin floors.

After Stop 3, return to vehicles and drive south on FM 1111 for 4.1 mi (6.6 km).

102.2 mi (165.5 km)

Stop 1.4 Entrance to Red Light Basin at FM 1111 and Yucca Mesa

Yucca Mesa is on the left of 1111 (Figure 1.22a,b) and Bluff Mesa is on the right. Yucca Mesa and Bluff Mesa are thrust-faulted Cretaceous rocks of the northwest-trending Devil Ridge thrust sheet. Continue driving south 1 mi (1.6 km) on 1111.

On the left are several down-to-the-north normal faults that offset beds of the Cox and Yucca formations. The road veers back toward the left as it descends into the Red Light basin (Figure 1.23).

Upon entering Red Light basin, observe the Quitman Mountains on the right, the eastern limit of the basin (Figure 1.23). The Quitman Mountains are divided into the Northern and Southern Quitman Mountains. The Northern Quitmans consist of Tertiary igneous rocks that intruded Cretaceous formations. extending northward from the folded and thrust-faulted Cretaceous

sedimentary rocks of the Chihuahua Trough. The topographic low at 2:00 (approximately 5 mi (8 km) to the west) is Quitman Gap. Along Quitman Gap, steeply dipping formations of Cretaceous age are exposed, many of which manifest evidence of thrust faulting and low-grade contact metamorphism where Cretaceous formations are in contact with intrusive rocks of the Northern Quitman Mountains.

The northwest-oriented Red Light Basin extends for approximately 35 mi (56 km) from its northernmost extent between the Northern Quitman Mountains and Bluff Mesa to the Rio Grande. The basin is drained by an intermittent trunk stream (Red Light draw), which discharges at the Rio Grande. The surface elevation at the uppermost reaches of the basin is approximately 4,500 ft (1370 m), and the elevation at the river is about 3,200 ft (975 m). The Red Light Basin is one of several Tertiary bolsons that were breached by the ancestral Rio Grande. The others were the Hueco, Green River, Presidio, and Redford bolsons. The incision of the bolsons by the river led to the formation of tributary streams that carried massive volumes of sediment to the Rio Grande and then southeastward along the path of the channel.

Continue 7.3 mi 11.7 km) on FM 1111.

110.5 mi (177.8 km)

On the left are the steeply dipping Finlay and Cox formations (Cretaceous) of Devil Ridge (Figure 1.24). Love Hogback (Figure 1.25) forms the southernmost part of the Devil Ridge thrust at the north end of the Eagle Mountains. In the distance, the Eagle Mountains are at 10:00.

The central area of the Eagle Mountains formed from rhyolite and trachyte flows and a syenite plug that intruded the thick sequence of folded and thrust-faulted Cretaceous rocks as well as the younger rhyolites and trachytes (Underwood, 1963; Albritton and Smith, 1965; Figure 1.26).

Continue 6.8 mi (10.9 km) south.

Mileage 117.3

Stop 1.5 - Geological setting of Red Light Basin

Stop here for discussions of the geology of the Red Light Basin and of igneous rocks that make up the core of the Eagle Mountains (Figure 1.27). Remove Geologic Map of Eagle Mountains and Vicinity (Underwood, 1963) from envelop.

The Chihuahua Trough was the major "negative" structural element (basin) in western Trans-Pecos Texas and adjacent areas of northeastern Mexico during the Middle to Late Mesozoic Era. The Diablo Platform, a Late Paleozoic feature, was the major "positive" structural element (Reaser and Underwood, 1980).

More than 19,700 ft (6,000 m) of sediment accumulated in the trough. The sediments were deformed during the Laramide orogeny to produce the folded and faulted mountains of the Chihuahua Tectonic Belt. The Southern Quitman Mountains, the Indio Mountains, the Eagle

Mountains, and Devil Ridge form major components of folded and faulted rocks of the Chihuahua Trough (Reaser and Underwood, 1980).

The Diablo Platform was the central positive feature of the Trans-Pecos region during the Paleozoic and Mesozoic eras. The Diablo Platform and the Coahuila Platform to the south acted as buttresses during the Laramide orogeny, as formations were thrust northeastward. The northeastern edge of thrusting is bounded by the southwestern margin of the Diablo Platform. The intensity of folding increases toward the west and southwest from the plateau margin. The prism of Mesozoic sediments decreases in thickness from 19,700 ft (6,000 m) in the trough to less than 2,000 ft (600 m) toward the north and eastward on the platform. The change in thickness of the sediments influenced the character of deformation (Reaser and Underwood, 1980).

Indio Mountains, Eagle Mountains and Devil Ridge

Although part of the same mountain range, the Eagle Mountains, Indio Mountains and Devil Ridge manifest markedly different structural styles.

In the Indio Mountains, several folded thrust blocks (primarily Yucca, Bluff, and Cox formations) are exposed east of the Indio Fault (normal fault). West of that fault, an imbricate thrust sheet (primarily Yucca Formation) is preserved on the downthrown block (see Cross Section F-F′, Quadrangle Map No. 26; Underwood, 1963).

Overall, the Indio Mountains are characterized by complex thrust faults and mostly open, symmetrical folds that are offset by normal faults and thrust faults (see Cross Section F-F′ from Underwood, 1963).

Mesozoic rocks of the Eagle Mountains are largely covered by thick sequences of volcanic rocks that obscure many details of Laramide folds and thrust faults. The Devil Ridge thrust fault, for example, cannot be traced with certainty through the mountains, although a few thrust faults have been mapped in places. The main part of the mountains appears to occupy the trough of a syncline which might have formed as a result of subsidence following extrusion of a large mass of magma (Gillerman, 1953).

Two east-northeast striking faults (Rhyolite Fault and Wind Canyon Fault) are significant structural features of the Eagle Mountains (see map of Geology of Eagle Mountains, Underwood, 1963). Underwood (1963) surmised that both faults might have developed during Laramide compression as a set of conjugate shear fractures, with dominant strike-slip movement. Reorientation of the stress field during Basin-and-Range faulting produced vertical movement along each fault (Underwood, 1963).

The principal direction of deformation at Devil Ridge was northeastward, along two imbricate thrust blocks: the Red Hills and Devil Ridge thrust blocks (see Cross Section A-A'; Underwood, 1962). At Love Hogback, the southeasternmost extent of Devil Ridge, the Yucca Formation, the oldest Cretaceous formation in the region, rests unconformably on the Chispa Summit Formation,

the youngest Cretaceous formation. Underwood (1963) estimated stratigraphic separation of about 7,900 ft (2,400 m) between the Yucca and the Chispa Summit, with horizontal movement of 19,000 ft (5,800 m) along the Red Hills and Devil Ridge thrust blocks.

Reaser and Underwood (1980) summarize differences between the structural characteristics of the Eagle Mountains, Indio Mountains, and Devil Ridge as follows:

1. Eagle Mountains: major east- to east-northeast-trending faults; open folds broken by younger faults.

2. Indio Mountains: complex system of thrust faults and open folds.

3. Devil Ridge: less complex thrust faults with minor folds.

Southern Quitman Mountains

The following blocks of text are abstracted from Albritton and Smith (1965), Jones and Reaser (1970), and Reaser and Underwood (1980).

The Southern Quitman Mountains are part of a northwest-trending, nearly recumbent anticline (Jones and Reaser, 1970). In the Southern Quitman range, thrusting, overturning, and asymmetry of folds are oriented eastward or northward toward the Diablo Platform (Jones and Reaser, 1970). The west limb of the anticline has been eroded and faulted, and a large part of the inverted eastern limb along the Rio Grande has been reduced by erosion to a series of narrow, resistant limestone ridges separated by narrow strike valleys formed from less resistant beds of limestone, sandstone, and shale (Jones and Reaser, 1970; Reaser and Underwood, 1980).

Cross Sections A-A′ - E-E′ (Jones and Reaser, 1970) reveal that overturning of beds increases from north to south along the mountain range. In the southernmost areas of the range near the Rio Grande, many beds are overturned 45° to 60° northeastward (see Cross Sections B-B′ - D-D′ from Reaser and Underwood, 1980); and locally some beds are rotated nearly 180° (see Cross Section E-E from Jones and Reaser, 1970).

Rocks in the northern part of the Southern Quitman Mountains are broken by the Quitman thrust fault (Figures 1.28-1.31; and Jones and Reaser, 1970). Jones and Reaser (1970) estimated movement along the fault to be about 4,900 ft (1,500 m) east-northeastward. Along with the Red Hills and Devil Ridge thrust faults toward the east, the Quitman thrust fault forms the third thrust block south of Sierra Blanca. Along the trace of the fault, overturned beds of the Quitman, Cox, Finlay, and Benevides formations (all Cretaceous) are thrust over a normal sequence of the Cox Formation.

The Quitman thrust fault can be traced southeastward about 8 mi (12.9 km) to the vicinity of Smuggler's Gap (see accompanying geological map by Jones and Reaser, 1970). Albritton and Smith (1965, p. 105) surmise that the fault extends northward beneath surficial deposits another 5.0 mi (8.1 km).

Igneous rocks of the Eagle Mountains

Gillerman (1953) mapped the igneous rocks of the Eagle Mountains. He differentiated three extrusive volcanic units and referred to them as (1) lower rhyolite, (2) trachyte porphyry and (3) upper rhyolite. He also described three distinct intrusive rock groups: (1) Eagle Peak syenite, (2) rhyolite dikes and sills, and (3) diabase dikes. Underwood's geological map of the Eagle Mountains (Underwood, 1963) incorporates the lithological designations found in Gillerman (1953). Those designations are also used in this guidebook. Cross sections C-C′ and D-D′ (refer to the geological map by Underwood (1963)) illustrate the stratigraphic association between the three extrusive units and the Eagle Peak syenite.

Gillerman's descriptions of the **extrusive units** are as follows (Gillerman, 1953):

The **lower rhyolite** consists of 500 to 1,000 ft of rhyolite flows, flow breccia, tuffaceous sediments, volcanic breccia, and welded tuffs. They were laid down upon an uneven erosion surface of moderate relief and are in unconformable contact with rocks of Late Cretaceous to Early Cretaceous age (see Cross Sections C-C′ and D-D′; Underwood, 1963).

On the west and southwest side of the mountains, tuffaceous sediments and volcanic breccia predominate. The tuffaceous sediments are buff-colored, thin-bedded, well-stratified and dip about 30° northeast. The volcanic breccia is thick-bedded, light gray or buff, and also dips about 30° northeast. The breccia contains many volcanic bombs as much as 6 in. (15.2 cm) in diameter and fragments of rhyolite, quartzite, and limestone. Quartz and feldspar crystals are present in the tuffaceous sediments and the volcanic breccia.

The **trachyte porphyry** occupies much of the area of the northwestern Eagle Mountains, where it is as much as 600 ft (183 m) thick. It is not present on the southwestern side of the mountains. The trachyte porphyry is a dark red to reddish-purple rock with large orthoclase phenocrysts in a fine-grained groundmass of orthoclase and a little quartz. Magnetite and hematite are abundant. Albitized plagioclase feldspars are present locally, and graphic intergrowths of albite and quartz are common. The rock weathers to grayish pink.

The **upper rhyolite** consists of as much as 1,500 ft (460 m) of rhyolite and flow breccias, with a few interbedded volcanic breccias, tuffaceous sediments, and spherulitic rhyolitic flows. Two major types of rhyolite are present. A light-gray flow breccia contains many fragments of earlier solidified parts of the same lava, as well as fragments of other rock types picked up by the flowing mass. Phenocrysts of quartz and sericitized feldspar are present. Flow-banding is generally prominently developed, with the extraneous material strung out as elongated and flattened fragments; vesicles are prominent. The flow breccia breaks with a rough fracture; it weathers to rounded hills and in some places stands as towering spires and cliffs with rounded contours.

The second type is a dense hard flinty rhyolite porphyry, gray to green or buff, with conspicuous, though small, phenocrysts of quartz and some feldspar. The rock breaks with a conchoidal fracture. Jointing is conspicuous and well developed, and results in angular blocky outcrops and many large and small steep cliffs and narrow canyons. Adjacent to the syenite plug, the rock is more calcic in composition, trending toward andesite, and has been recrystallized into a dark-gray, slightly coarser-grained rock. Quartz and large oligoclase phenocrysts, some albitized, are set in a groundmass of quartz and oligoclase.

Gillerman's descriptions of the **intrusive rocks** are as follows (Gillerman, 1953):

Many sills and irregularly shaped masses of rhyolite intrude the sedimentary rocks in the regions adjacent to the contact of the sedimentary rocks and the lower rhyolitic series. These intrusives are allied to the flows of the lower rhyolitic series. They are part of the same parent magma, being merely offshoots that penetrated the sedimentary rocks adjacent to the vents during the volcanic activity. The rhyolite is buff-colored, fine-grained, and contains quartz and sericitized feldspar phenocrysts. Limonite specks are common. The rhyolite is weathered and soft, except where silicified along fault and fracture planes.

The **Eagle Peak syenite** is a brownish-gray medium-grained rock with large phenocrysts of feldspar, chiefly orthoclase, which occurs in the central and highest part of the mountains and is exposed on Eagle Peak. The syenite crops out as a roughly elliptical-shaped body with, in the main, almost vertical contacts with the rhyolite. The rock is composed chiefly of orthoclase and oligoclase, with small amounts of quartz. Altered biotite is abundant; a few grains of zircon and some secondary carbonate minerals are also present.

The syenite appears to have intruded the upper rhyolitic series as a small stock. Two small, isolated areas are present east of the main body and represent offshoots of the main mass. To the south, the contacts with the rhyolite are not vertical, as on the other sides of the stock, but are concordant with the flows. The syenite apparently split some of the flows apart at this locality and invaded them as a sill-like protrusion from the main stock.

Diabase dikes are present on the north, northeast, and southwest sides of the mountains. The diabase is dark blue-gray, dense, medium-grained, and even-textured. Thin section studies show this rock to be composed chiefly of long thin laths of plagioclase feldspar. The mafic minerals have been completely altered, and grains of calcite and specks of magnetite and limonite are abundant. A prominent dike is found south-southwest of Eagle Peak, near the mouth of Snowline Canyon (refer to Underwood (1963)). The dike at this place is as much 50 ft (15 m) wide. Quartz is present, and the rock may be called a quartz diabase. Plagioclase feldspar, chlorite, and calcite are the most conspicuous minerals in the dike at this locality.

The lower rhyolites and trachytes predominate in the northern and northwestern areas of the mountains. The contact between the lower rhyolites and the overlying trachytes is seen as a sharp color contrast between the lighter colored rhyolites and the darker trachytes. Upper rhyolites

predominate in the central and southwestern areas of the mountains. Syenite forms the highest peaks. All of the above formations are examined in greater detail along the paved road to Eagle Peak (Day 2 road log).

In the late 1970s, graduate students from The University of Texas at El Paso (Legett (1979 and Verrillo (1979)) conducted more detailed mapping of the extrusive volcanic flows of the western Eagle Mountains. They renamed Gillerman's extrusive units and divided each into members, based on variations in composition and areal distribution.

The table below lists the lithological designations described by Gillerman (1953) in the left column and those proposed by Legett (1979) and Verrillo (1979) in the right column:

GILLERMAN (1953)	**LEGETT (1979) AND VERRILLO (1979)**
Upper Rhyolite	**High Mill Tuff** – 250 to 600 m
	Eagle Bluff Member – 0 to 200 m, lithic welded tuff
	Cottonwood Canyon Member
	Cottonwood Canyon Tuff – 265 to 400 m, densely welded tuff
	Silver Eagle Tuff – 10 to 15 m, moderately welded tuff
	Epiclastic Unit – 0 to 13 m, crystal tuff
Trachyte Porphyry	**Frenchman Canyon Trachyte** – 0 to 500 m, welded tuffs and lava flows divided into:
	Upper unit – 130 to 400 m, devitrified trachyte, and
	Lower unit – 0 to 130 m, densely welded tuff
Lower Rhyolite	**Carpenter Canyon Tuff** – 25 to 330 m
	Panther Peak member – 10 to 330 m, welded tuff
	Indian Springs member – 25 to 135 m, poorly welded ash flow and air fall tuffs

A geologic map of the western Eagle Mountains (Figure 1.32 from Hoffer and others, 1980) replaces the designations of Gillerman (1953) with the above formations and members proposed by Leggett (1979) and Verrillo (1979). The distribution of extrusive rocks is shown to be more varied with respect to composition than represented by Gillerman (1953) and Underwood (1963). The map adds more lithological detail so that the rhyolites and trachytes are shown as a more complex assemblage of extrusive rocks than might be inferred from the more general

representations of Gillerman (1953) and Underwood (1963). Figure 1.32 is included to illustrate the detail and complexity added by Legett (1979) and Verrillo (1979). To simplify descriptions of igneous rocks of the Eagle Mountains, this guidebook defaults to the lithologic descriptions of Gillerman (1953) and Underwood (1963).

Return to Sierra Blanca from this point (19 mi; 48.3 km).

136.30 mi (219 km)

Turn right (east) on to I-10 access road and merge with highway.

142.3 mi (229 km)

The ranch house south of the highway was the field headquarters for field operations during the low-level radioactive waste site investigation conducted by the UT-BEG (1991 – 1994). The house and 10,000 acres surrounding the house were the Fasken Ranch, which had been acquired by the State of Texas before Eagle Flat was nominated as a possible location for a processing and disposal facility. Although the investigation focused on the suitability of the ranch for processing and disposal, researchers with BEG covered more than 1,200 square-mi (3,110 km^2) to evaluate a wide range of matters (structural geology, seismicity, geomorphology and surface stability, surface water hydrology, hydrogeology and geochemistry, etc.) that had to be addressed before the Texas Natural Resources Conservation Commission (now Texas Commission on Environmental Quality [TCEQ]) could issue a license to the Texas Low-Level Radioactive Waste Disposal Authority (TLLRWDA) to develop and operate the site.

The matter of designating Eagle Flat as a site for the disposal of low-level radioactive waste was a highly controversial political matter (https://libcom.org/article/1996-8-sierra-blanca-community-opposes-nuclear-waste-site), and TCEQ responded by refusing to grant a license to TLLRWDA, based on nonspecific concerns about seismicity.

145.1 mi (233.7 km)

The prominent topographic low approximately 2 mi (3.2 km) south of the highway is Grayton Lake, a desert playa and the endpoint of all surface drainage in Northwest Eagle Flat. Yucca Mesa, Devil Ridge, and Love Hogback are in the distance.

149.1 mi (240 km)

Streeruwitz Hill is north of I-10. The hill is composed of rocks of the Allamoore and Hazel (Precambrian) formations and is capped by Hueco (Permian) limestone. For the next 12 miles (19 km), I-10 follows the southern edge of a pediment formed principally by the Allamoore and Hazel formations. The hills east of the Streeruwitz prominence and north of the highway are formed where Allamoore is overlain by Hazel. The light (grayish) scars in the distance are old open-pit talc mines and current talc mining operations of Natural Minerals, a subsidiary of Daltile.

The Allamoore pediment ends not far south of the highway, where a normal fault (down-to-the-south) forms the northern boundary of the Eagle Flat basin along the stretch of I-10 between Streeruwitz Hill and the Carrizo Mountains. Darling and others (1994) and Darling (1997) identified the pediment as a primary recharge area for much of Southeast Eagle Flat, on the basis of radiocarbon and tritium data that yield modern (post-bomb) signatures.

Water wells on the Allamoore Pediment are typically 200 ft (60 m) or less in depth and all produce water from thin and unconsolidated Quaternary alluvium and/or from Precambrian rocks on which the alluvium was deposited (Darling and others, 1994; Darling, 1997).

150.3 mi (242 km)

Straight ahead are the Carrizo Mountains. The highway traverses the northernmost extension of the Carrizo Mountains for the next 8.5 mi (13.7 km). There are many roadcut exposures of metaigneous and metasedimentary rocks of the Carrizo Mountains group along the road to Van Horn, but there are no safe places from which to examine rocks along the eastbound lanes of the highway. The best places from which to see these rocks and to discuss the Streeruwitz Fault are along the westbound lanes. This is on the agenda for Day 2 of the field trip.

158.8 mi (256 km)

The city of Van Horn lies straight ahead. Just north of the highway is Three-Mile Mountain, composed of Van Horn Sandstone (Precambrian), and overlain by Hueco limestone (Permian). The highway descends into a broad valley (Wild Horse Flat) that lies at the southern end of the north-northwest oriented Salt Flat Basin. Take Van Horn exit and continue 2.4 mi (3.9 km) to Hotel El Capitan.

161.4 mi (260 km)

Arrive at Hotel El Capitan.

REFERENCES - DAY ONE ROAD LOG

Albritton, C.C. Jr., and Smith, J.F. Jr., 1965, Geology of the Sierra Blanca area: U.S. Geol. Survey Professional Paper 479, 131 p.

Barker, D.S., 1977, Northern Trans-Pecos magmatic province: introduction and comparison with the Kenya rift: Geol. Society of America Bull, v. 80, p. 2075-2080.

Barker, D.S., 1987, Tertiary alkaline magmatism in Trans-Pecos Texas. Geol. Society Spec. Pub. 30, 415-431.

Collins, E.W., and Raney, J.A., 1993, Late Cenozoic faults of the region surrounding the Eagle Flat study area, northwestern Trans-Pecos Texas: Univ. of Texas at Austin, Bureau of Economic Geology final contract report prepared for Texas Low-Level Radioactive Waste Disposal Authority, 74 p.

Darling, B.K., Hibbs, B.J., and Dutton, A.R., 1994, Ground-water hydrology and hydrochemistry of Eagle Flat and surrounding area: Univ. of Texas at Austin, Bureau of Economic Geology contract report prepared for Texas Low-Level Radioactive Waste Disposal Authority, 137 p.

Darling, B.K., 1997, Delineation of the Ground-water flow systems of the Eagle Flat and Red Light basisn of Trans-Pecos Texas: Univ. of Texas at Austin Ph.D. dissertation, 179 p.

Darling, B.K., and Hibbs, B.J., 2001, The aquifers of Red Light Draw, Green River Valley, and Eagle Flat: Texas Water Development Board Report 356, Chapter 16, p. 226-240.

Darling, B.K., Hibbs, B.J., and Sharp, J.M, Jr., 2017, Integration of Pleistocene groundwater ages along flow paths in two West Texas Bolson aquifers: Presentation at GSA Annual Meeting in Seattle, Oct. 2017.

Dietrich, J. W., Owen, D. E., Shelby, C. A., and Barnes, V. E., 1983, Geologic Atlas of Texas, Van Horn-El Paso Sheet: The University of Texas at Austin, Bureau of Economic Geology, Geologic Atlas of Texas, map scale 1:250,000.

Elliott, B.A., 2018, Petrogenesis of heavy rare earth element enriched rhyolite: source and magmatic evolution of the Round Top laccolith, Trans-Pecos Texas: Minerals 2018, 8, 423; doi: 10.3390/min8100423.

Fisher, R.S. and Fisher, W.F. III, 1990, Integration of ground-water and vadose-zone geochemistry to investigate hydrochemical evolution: a case study in arid lands of the northern Chihuahuan Desert, Trans-Pecos Texas: The University of Texas at Austin Bureau of Economic Geology Geological Circular 90-5, 36 p.

Gates, J.S., and White, E.E., 1976, Test drilling for ground water in Hudspeth, Culberson, and Presidio counties in westernmost Texas: U.S. Geol. Survey open-file report 76-338, 76 p.

Gates, J.S., White, D.E., Stanley, W.D., and Ackermann, H.D., 1980, Availability of fresh and slightly saline ground water in the basin of westernmost Texas: Texas Department of Water Resources Report 256, 108 p.

Gillerman, E., 1953, Fluorspar deposits of the Eagle Mountains, Trans-Pecos Texas: U.S. Geol. Survey Bull. 987, 98 p.

Goodell, P., Ayala, S., Karplus, M., Velasco, A; and Mahar, A.I., 2023, Critical minerals in West Texas: Univ, of Texas at El Paso unpublished paper prepared for AIPG-Texas 2023 field trip guidebook, 6 p.

Gustavson and Associates, 2014, Amended NI 43-101, Preliminary economic assessment, Round Top Project, Sierra Blanca, Texas, prepared for Texas Rare Earth Resources, 159 p.

Harbour, R.L., 1972, Geology of the northern Franklin Mountains, Trans-Pecos Texas: U.S. Geol. Survey Bulletin 1298, 129 p.

Henry, C.D., and McDowell, F.W., 1986, Geochronology of magmatism in the Tertiary volcanic field, Trans-Pecos Texas. In Bureau of Economic Geology Guidebook; University of Texas at Austin, v. 23, p 99-122.

Henry, C.D., and Price, J.G., 1984, Variations in caldera development in the Tertiary volcanic field of Trans-Pecos Texas. J Geophys Res, 89, 8765-8786.

Henry, C.D., Price, J.G., Miser, D.E., 1989, Geology and Tertiary igneous activity of the Hen Egg Mountain and Christmas Mountains quadrangles, Bid Bend region, Trans-Pecos Texas. In Report of Investigations, Univ. of Texas at Austin Bureau of Econ. Geol., Austin, TX, USA.

Henry, C.D., Price, J.G., and James, E.W., 1991, Mid-Cenozoic stress evolution in the southern Cordillera, Texas and Mexico: transition from continental arc to intra-plate extension. Jour. Geophys. Res., 96.

Hoffer, J.M., ,1970, Petrology and mineralogy of the Campus Andesite pluton, El Paso, Texas: Univ. of Texas at Austin Bureau of Economic Geology Miscellaneous Map 36, 1:500,000, 8 p.   ,

Hoffer, J.M., Legett, B.D., and Verrillo, D.E., 1980, Tertiary volcanics of the western Eagle Mountains, Hudspeth County, Texas: New Mexico Geological Society Guidebook 31st Field Conference, Trans-Pecos Texas, p. 237-240.

Jones, B.R., and Reaser, D.F., 1970, Geology of Southern Quitman Mountains, Hudspeth County, Texas: Univ. of Texas at Austin, Bureau of Economic Geology, Geologic Quadrangle Map No. 39.

Kyger, N., 2013, Geology and geochemistry of the Sierra Blanca rare earth complex, Sierra Blanca, Texas: Univ. of Texas at El Paso M.S. thesis, 355 p.

Langford, R. P., 1993, Landscape Evolution of Eagle Flat and Red Light Basins, Chihuahuan Desert, South-Central Trans-Pecos Texas: Univ. of Texas at Austin Bureau of Economic Geology contract report prepared for Texas Low-Level Radioactive Waste Disposal Authority.

Leggett, B.D., 1979, Tertiary volcanics of the northwest Eagle Mountains, Hudspeth County, Texas: Univ. of Texas at El Paso M.S. thesis.

Mahar, M.A., and Goodell, P.C., 2023, Timing and origin of alkaline magmatism at the shoulder of the southern RGR, Sierra Blanca: Univ. of Texas at El Paso unpublished research paper prepared for AIPG-Texas 2023 field trip guidebook, 7 p.

Matthews, W.K., III and Adams, J.A.S., 1986, Geochemistry, age, and structure of the Sierra Blanca and Finlay Mountain intrusions, Hudspeth County, Texas: Univ. of Texas at Austin Bureau of Economic Geology Guidebook 23 p. 207-224.

McAnulty, W.N. Sr., 1974, Fluorspar in Texas: Univ. of Texas at Austin, Bureau of Economic Geology Handbook 3, 31 p.

McDowell, F.W., 1979, Potassium-argon dating in the Trans-Pecos volcanic field, *in* Walton A.W. and Henry, C.D. editors, Cenozoic geology of the Trans-Pecos volcanic field of Texas, University of Texas at Austin – Bureau of Economic Geology Guidebook No, 19, p. 10 – 18.

Muehlberger, W.R., Belcher, R.C., and Goetz, L.K., 1978, Quaternary faulting in Trans-Pecos Texas: Geology, v. 6, p. 337-340.

Murry, D.H., 1980, Mineralization in the northern Quitman Mountains, Hudspeth County, Texas, *in* Dickerson, P.W. *et al.*, eds., New Mexico Geological Society 31st Field Conference Guidebook, p. 267-270.

Price, J.G., Henry, C.D, and Standen A.R., 1983, Annotated Bibliography of Mineral Deposits in Trans-Pecos Texas: Univ. of Texas at Austin, Bureau of Economic Geology, Texas Mining and Mineral Resources Research Institute Mineral Resources Circular No. 73, 108 p..

Price, J.G., and Henry, C.D., 1986, Field trip road log: Day 0 – El Paso to Van Horn, *in* Price, J.G., Henry, C.D., Parker, D.F., and Barker, D.S., eds, Igneous geology of Trans-Pecos Texas, field trip guide and research articles: Univ. of Texas at Austin Bureau of Economic Geology, Texas Mining and Minerals Resources Research Institute Guidebook 23, p. 9 -12.

Price, J.G., Rubin J.N., Henry, C.D., Pinkston, T.L., Tweedy, S.W., Koppenaal, D.W., 1990, Rare-metal enriched peraluminous rhyolites in a continental arc, Sierra Blanca area, Trans-Pecos Texas; Chemical modification by vapor-phase crystallization, *in* Stein, H.J., and Hannah, J.L., eds., Ore-bearing granite systems; Petrogenesis and mineralizing processes: Geological Society of America Special Paper 246, p. 103-120.

Raney, J.A., 1991, Review of the geology and hydrology of the Eagle Flat area, Hudspeth County, Texas: Univ. of Texas at Austin, Bureau of Economic Geology final contract report prepared for Texas Low-Level Radioactive Waste Disposal Authority, 20 p.

Raney, J. A., Kreitler, C. W., Darling, B., Wermund, E. G., Blount, J., Hill, R., 1991, Preliminary Evaluation of the Eagle Flat Region Hudspeth County, Texas: Univ. of Texas at Austin, Bureau of Economic Geology contract report prepared for Texas Low-Level Radioactive Waste Disposal Authority, 30 p.

Raney, J. A., Collins, E. W., Darling, B., 1992, Eagle Flat Project, Hudspeth County, Texas: Univ. of Texas at Austin Bureau of Economic Geology contract report prepared for Texas Low-Level Radioactive Waste Disposal Authority, 83 p.

Raney, J.A., and Collins, E., 1993, Regional geologic setting of the Eagle Flat study area, Hudspeth County, Texas: Univ. of Texas at Austin, Bureau of Economic Geology contract report prepared for Texas Low-Level Radioactive Waste Disposal Authority, 53 p.

Reaser, D.F., and Underwood, J.R., Jr., 1980, Tectonic style and deformational environment in the Eagle-Southern Quitman Mountains, western Trans-Pecos Texas, *in* Dickerson, P.W., and Hoffer, J.M., eds., New Mexico Geological Socoety Thirty-First Field Conference and Guidebook, p. 123 – 130.

Rubin J.N., Price, J.G., Henry, C.D., Koppenaal, D.W., 1987a, Cryolite-bearing and rare metal enriched rhyolite, Sierra Blanca Peaks, Hudspeth County, Texas. American Mineralogist, v. 72, p. 1122-1130.

Rubin, J. N., Price, JG., Henry, C.D., Pinkston, T.L., Tweedy, S.W., Koppenaal, D.W., Peterson, S.B., Harlan, H.M., Miller, W.T., Thompson, R.J., Grabowski, R.B., Laybourn, D.P., Schrock, G.E., Johnson, A., Staes, D.G., Gaines, R.V., Miller, F.H., 1987b, Mineralogy of Beryllium Deposits Near Sierra Blanca, Texas: Bureau of Mines / Minerals yearbook area reports: domestic 1987, Volume 2, p. 601-614.

Rubin, J.N., Price, J.G., Henry, C.D., Kyle, J.R., 1990, Geology of the Beryllium-Rare Earth Element Deposits at Sierra Blanca, West Texas, in Kyle, J.J., Thompson, T.B., eds, Industrial Mineral Resources of the Delaware Basin, Texas and New Mexico: Guidebook Prepared for Society of Economic Geologists Field Conference – 24 -27 October 1990, p. 191-203.

Rubin, J.N., Henry, C.D., Pinkston, T.L., Tweedy, S.W., Koppenaal, D.W., 1993, The mobility of zirconium and other "immobile" elements during hydrothermal alteration. Chem. Geol. 110, 29-47.

Scanlon, B. R., Goldsmith, R. S., Gustavson, T. C, 1994, Evaluation of Unsaturated Flow in Fissured Sediments in the Chihuahuan Desert, Texas: Univ. of Texas at Austin Bureau of Economic Geology contract report prepared for Texas Low-Level Radioactive Waste Disposal Authority, 78 p.

Seager, W.R., 1980, Quaternary fault system in the Tularosa and Hueco Basins, southern New Mexico and West Texas, in Dickerson, P.W., and Hoffer, J.M., eds., Trans-Pecos region, southeastern New Mexico and West Texas: New Mexico Geol. Society 31sr Field Conference Guidebook, p. 131-135.

Seni, S. J., Raney, J. A., 1992, Characterization of Mineral and Geothermal Resources in the Eagle Flat Region, West Texas: Univ. of Texas at Austin Bureau of Economic Geology contract report prepared for Texas Low-Level Radioactive Waste Disposal Authority, 33 p.

Shannon, W.M., 1986, Lithogeochemical Characterization of Intrusive Rocks Comprising the Quitman-Sierra Blanca Igneous Complex, Hudspeth County, Texas. M. S. Thesis, University of Texas at El Paso.

Shannon, W.M., and Goodell, P.C., 1986, Lithogeochemistry of Intrusive Rocks of the Quitman-Sierra Blanca Igneous Complex, Hudspeth County, Texas: In Jonathan, J.G., Price, G., Henry, C.D., Parker, D.F., Barker, D.S., Eds., Igneous Geology of Trans-Pecos Texas: Bureau of Economic Geology Guidebook 23, University of Texas at Austin, p. 225-226.

Sharp, J.M. Jr., 2001, Regional groundwater flow systems in Trans-Pecos Texas: Texas Water Development Board Report 356, Chapter 4, p. 41-55.

Shelley, D., 1992, *Igneous and Metamorphic Rocks under Microscope: Classification, Textures, Microstructures and Mineral Preferred-Orientations*. Chapman and Hall, UK, London.

Twiss, P.C., 1979, Geologic Atlas of Texas, Marfa Sheet: The University of Texas at Austin, Bureau of Economic Geologic, Geologic Atlas of Texas, map scale 1:250,000.

Uliana, M., 2000, Delineation of Regional Groundwater Flow Paths and Their Relation to Structural Features in the Salt and Toyah Basin, Trans-Pecos Texas: Univ. of Texas at Austin Ph.D. dissertation, 215 p.

Uliana, M. and Sharp, J.M. Jr., 2001, Tracing regional flow paths to major springs in Trans-Pecos Texas using geochemical data and geochemical models: Chemical Geology, p. 53-72.

Uliana, M., Banner, J.L., and Sharp, J.M. Jr., 2007, Regional groundwater flow paths in Trans-Pecos Texas inferred from oxygen, hydrogen, and strontium isotopes: Journal of Hydrology, p. 334-346.

Underwood, J.R. Jr., 1962, Geology of the Eagle Mountains and Vicinity, Trans-Pecos Texas: Univ. of Texas at Austin Ph.D. dissertation, 560 p.

Underwood, J.R. Jr. ,1963, Geologic Map of the Eagle Mountains and Vicinity, Hudspeth County, Texas: Univ. of Texas at Austin, Bureau of Economic Geology, Quadrangle Map No. 26.

Verrillo, D.E., 1979, Geology and petrography of the Tertiary volcanic rocks in the southwest Eagle Mountains, Hudspeth County, Texas: Univ. of Texas at El Paso M.S. thesis.

Wermund, E. G., Raney, J. A., 1992, Analysis of Lineations in the Eagle Flat Study Area, Hudspeth County, Texas: Univ. of Texas at Austin Bureau of Economic Geology contract report prepared for Texas Low-Level Radioactive Waste Disposal Authority.

White, D.E., Gates, J.S., Smith, T.J., and Fry, B.J., 1980, Ground-water data for the Salt Basin, Eagle Flat, Red Light Draw, Green River Valley, and Presidio Bolson in westernmost Texas: Texas Department of Water Resources Report 259, 97 p.

Winograd, I.A., 1962, Interbasin movement of ground water at the Nevada Test Site: U.S. Geol. Survey Professional Paper 450-C, p. C108-C111.

Winograd, I.A., and Thodarson, W., 1975, Hydrogeological and hydrogeochemical framework, south central Great Basin, with special reference to the Nevada Test Site: U.S. Geol. Professional Paper 712-C.

GEOLOGY OF HUDSPETH COUNTY, TEXAS

**GUIDEBOOK OF AIPG-TEXAS
SPRING FIELD TRIP
APRIL 21 – 23, 2023**

FIGURES – DAY ONE
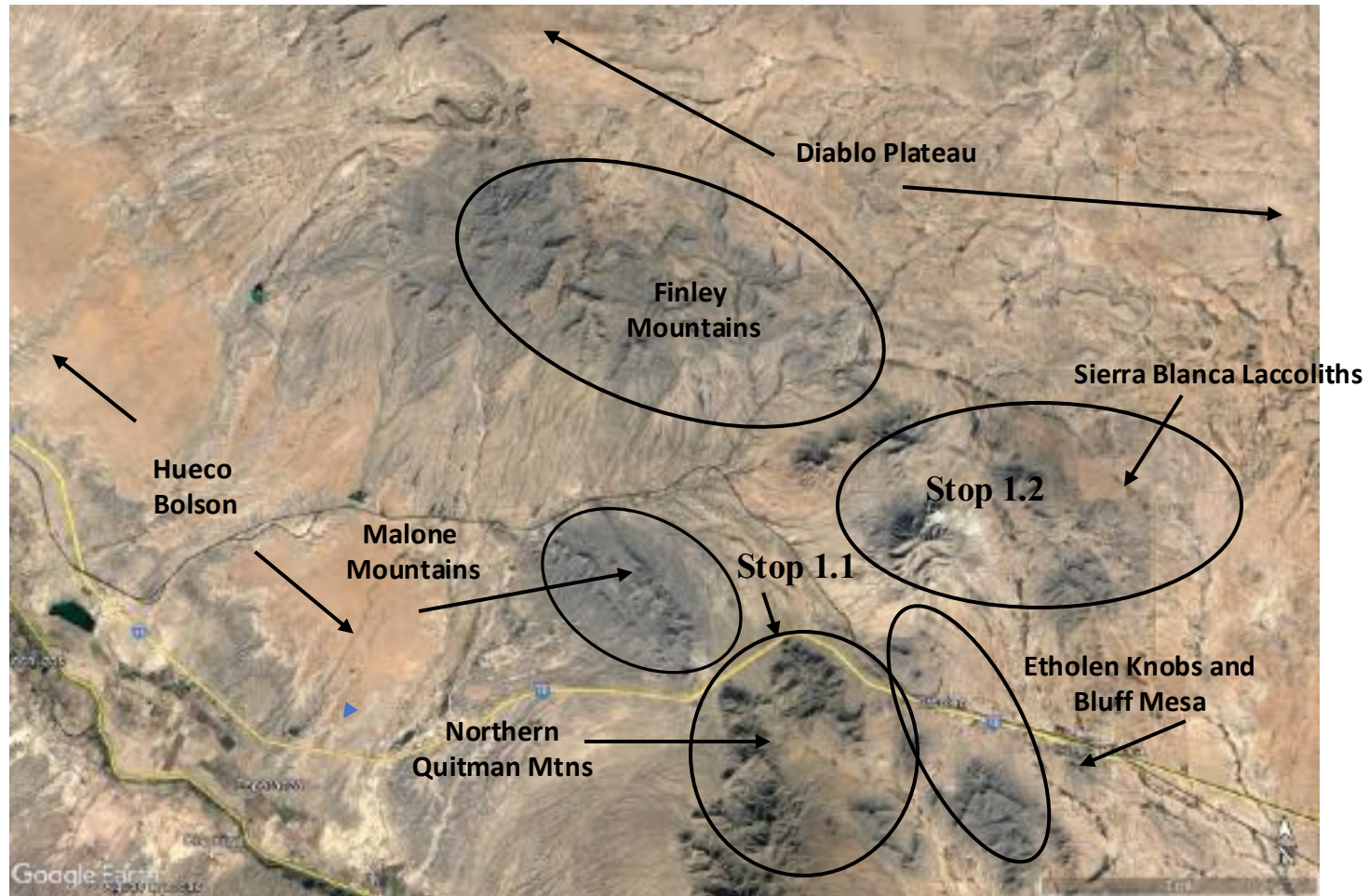
Figure 1.01 – Geological structures discussed at Stops 1.1 and 1.2.

Figure 1.02a   **Figure 1.02b**

Figure 1.02a - Field trip participants gather at rest station for overview of geological structures delineated in Figure 16. Sierra Blanca Mountain and Round Top laccolith are in background. **Figure 1.02b** - Professor Philip C Goodell (UTEP) leads discussion of geology of Chihuahua Trough, Northern Quitman Mountains, Sierra Blanca laccoliths and REE enrichment. Photos by Diane Darling

Figure 1.03a

Figure 1.03b

Figure 1.03a - Old checkpoint at entrance to abandoned Mile High desert resort. **Figure 1.03b** - Main office of abandoned Mile High desert resort. The checkpoint and main office are not in use. Photos by BK Darling

Figure 1.04a   Photo by BK Darling

Figure 1.04a - Google Earth image showing Sierra Blanca laccoliths and Etholen Knobs. **Figure 1.04b** – Etholen Knobs, as seen from I-10 access road..

Figure 1.05a

Photo by Paul Warren

Figure 1.05b

{Photo by BK Darling

Figure 1.05a – Sample of quartz rhyolite porphyry from main quarry.. **Figure 1.05b** - View of debris at base of quarry wall. Note benches cut above
quarry wall.

Figure 1.06a

Figure 1.06b

Figure 1.6a - Quarry owner/operator Dennis Walker (white hard hat) explains operations at Sierra Blanca Quarry. **Figure 1.6b** - Field trip participants examine specimens of rock for uranium mineralization. Uranium mineralization is a common at all of the laccoliths. Although rare earth elements occur the laccoliths, the greatest degree of enrichment is at Round Top, noted especially for the abundance of heavy rare earth elements (HREE). Photos by Diane Darling

Figure 1.07 - Wide-angle view of rock crusher and main quarry. Benches cut to stabilize slope and to allow for further development of the quarry are seen above quarry wall in background. Photo by Paul Warren

Figure 1.08a

Figure 1.08b

Figure 1.08a - Rock crusher at main quarry. **Figure 1.08b** - Closeup view of rock crusher. Rock is run first through a jaw crusher and then through a cone crusher to reduce fragments to specified size range. Fragments that are larger than specified by Union Pacific are returned to the quarry by a conveyor system that empties the fragments into the jaw crusher for further processing. Photos by BK Darling.

Figure 1.09a

Figure 1.09b

Figure 1.09a - Conveyor system returning over-sized fragments to crusher. **Figure 1.09b** - Crushed rock that meets ballast size specification are transported by a second conveyor and then deposited in pile at end of conveyor system. Photos by BK Darling.

Figure 1.10a

Figure 1.10b

Figure 1.10a - Crushed rock is deposited at washer. **Figure 1.10b** - Washed rock is transported by conveyor to end of conveyor   line where it is deposited in piles and allowed to dry.   Photos by BK Darling.

Figure 1.11a

Figure 1.11b

Figure 1.11a Washed rock on conveyor. **Figure 1.11b** - Washed rock deposited at end of conveyor system.   Photos by BK Darling.

Figure 1.12a

Figure 1.12b

Figure 1.12a - Piles of crushed rock at rail loading site.   **Figure 1.12b** - Rail loading point for crushed rock. Photos by BK Darling.

Figure 1.13a

Figure 1.13b

Figure 1.13a – Sierra Blanca Mountain as seen from I-10, near Stop 1.1. **Figure 113b** – Round Top Mountain as seen from I-10 near Stop 1.1. Photos by BK Darling

Figure 1.14a

Figure 1.14b

Figure 1.14a - Taking a break for lunch at Delfina's.   **Figure 1.14b** - Waiting for staff to take lunch orders. Photos by Mike Jacobs.
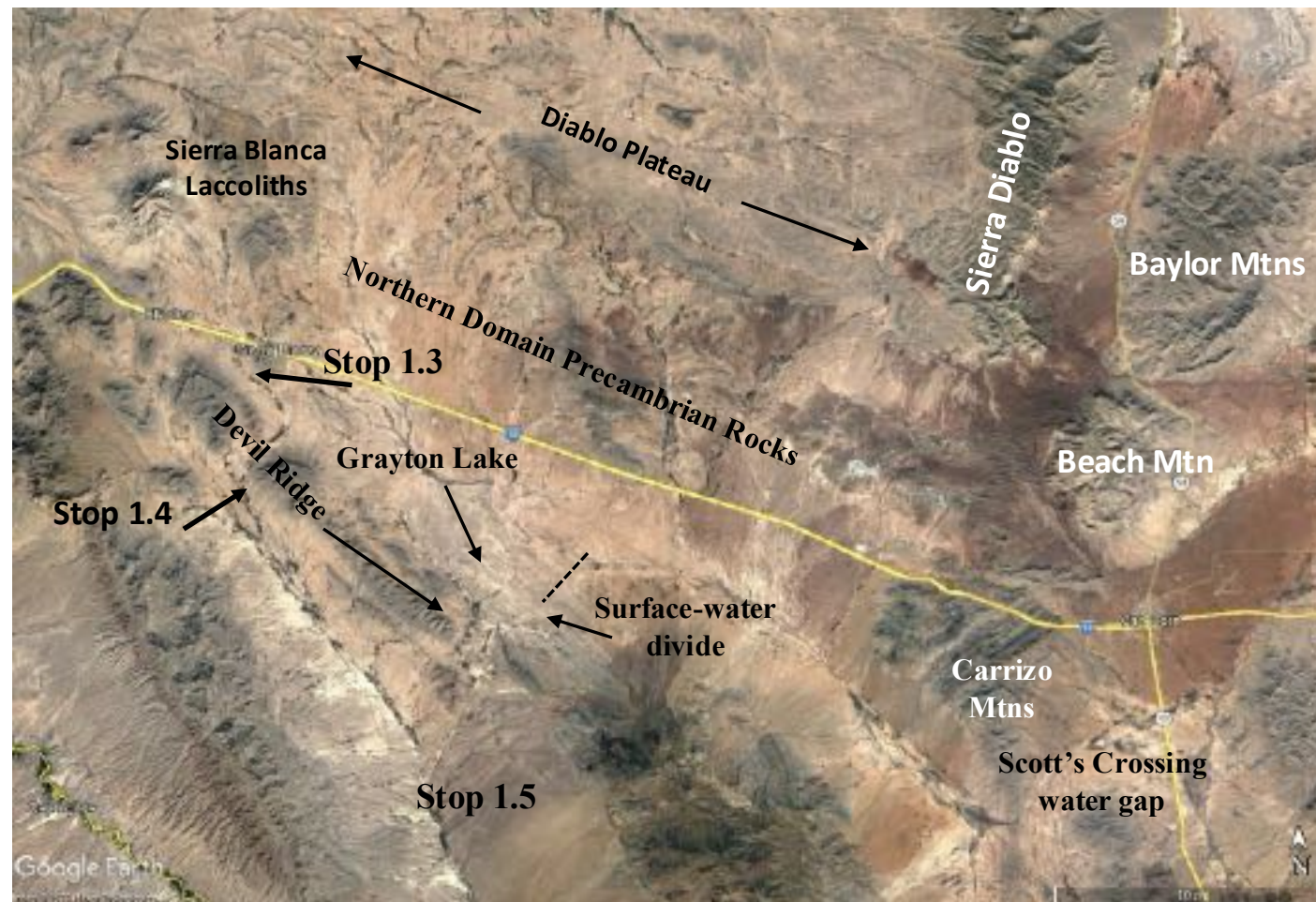
Figure 1.15 – Google Earth image of Eagle Flat Basin and surrounding highlands

Figure 1.16 – Contour map of depth to groundwater (feet below surface). Source: Darling and others (1994 and Darling (1997)
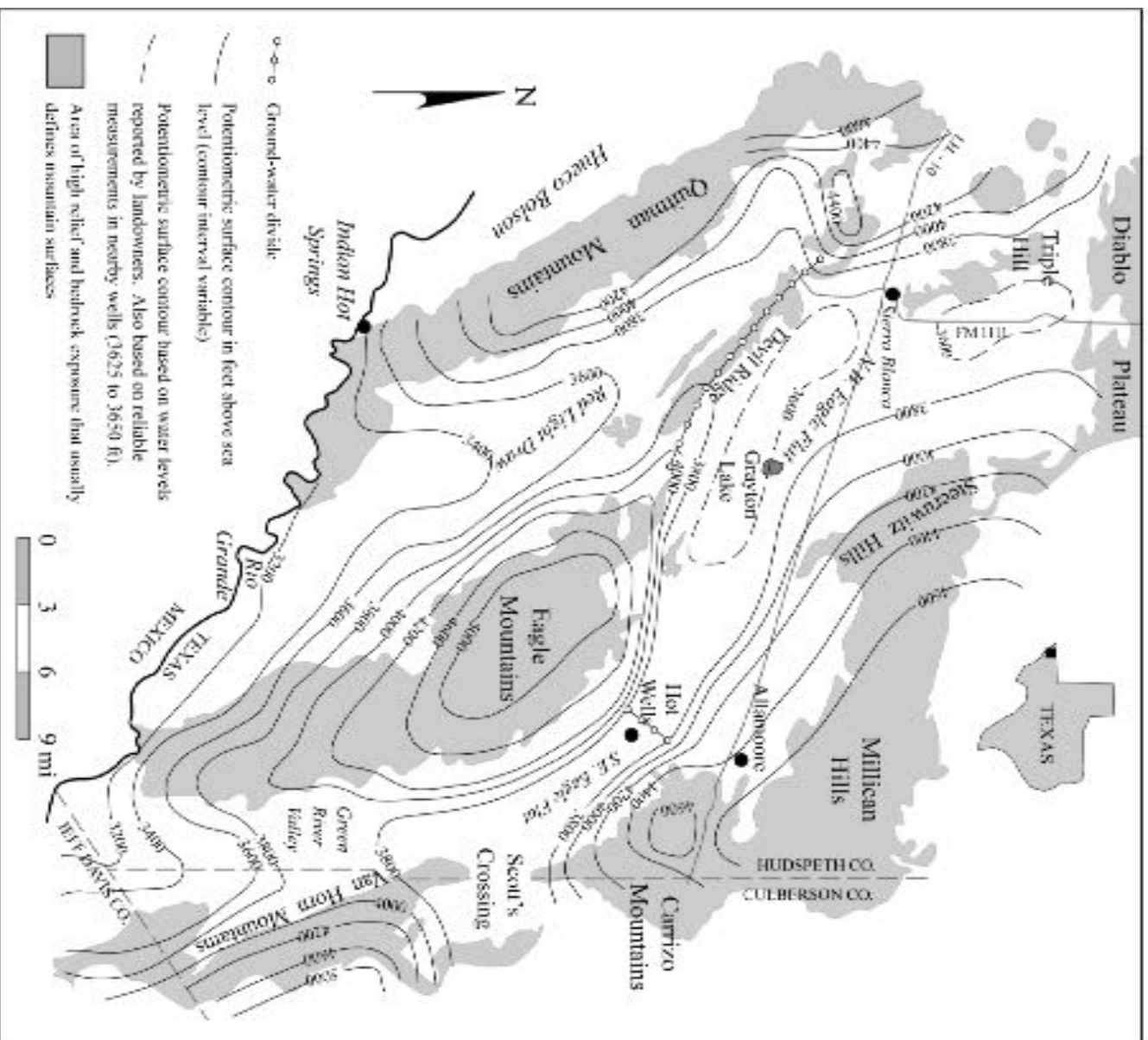
Figure 1.17 - Potentiometric surface water table contours – Eagle Flat, Red Light Draw, Green River Valley and bounding Mountains. Source: Darling, 1997, modified from Darling and others (1994).
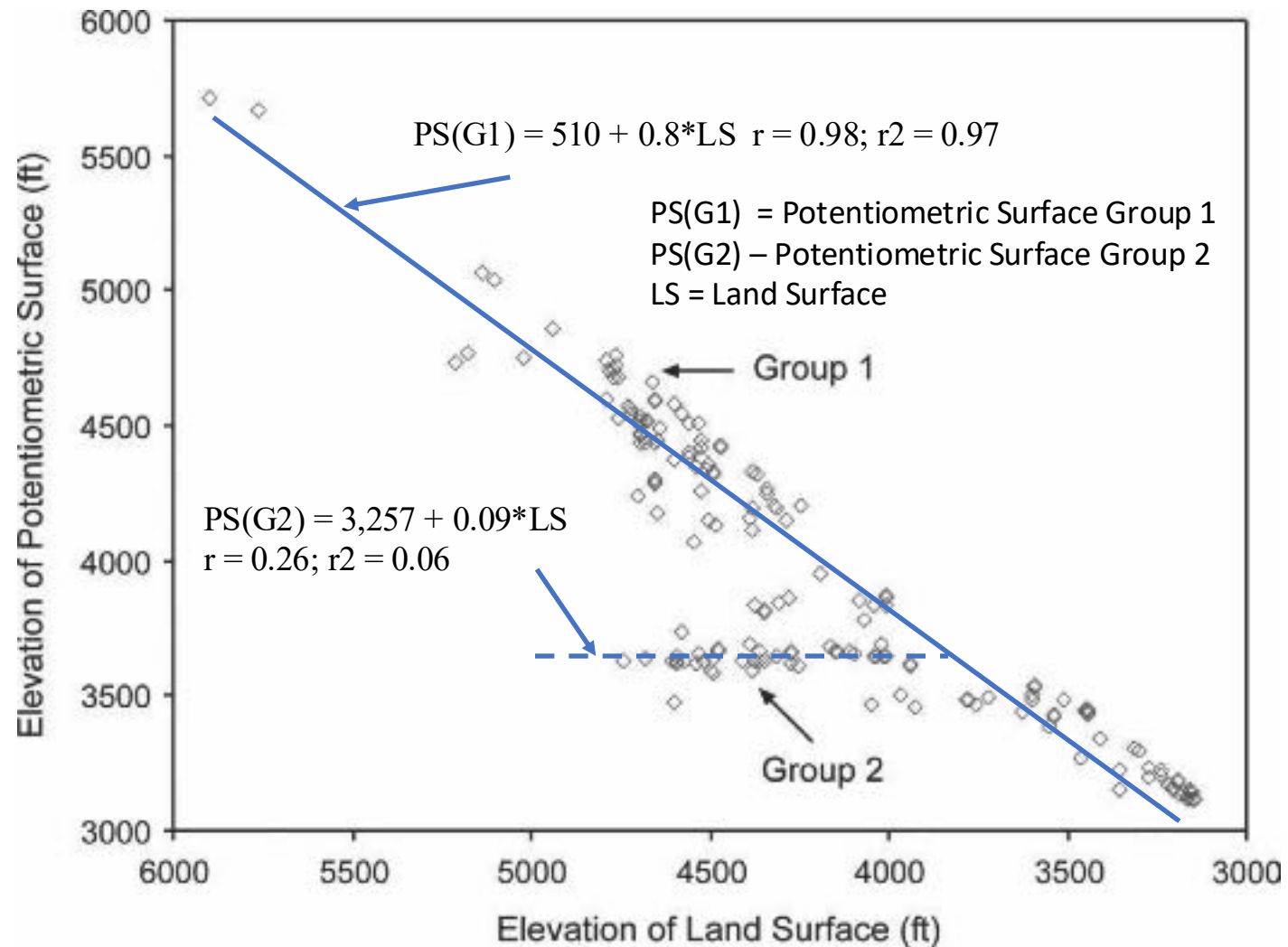
Figure 1.18 – Elevations of potentiometric surface and land. The least=squares regression lines and correlation coefficients are interpreted to indicate two groundwater systems: 1) Group 1, gravity-driven and local in scale and 2) Group 2, regional and trans-basin boundary. After Darling (1997).
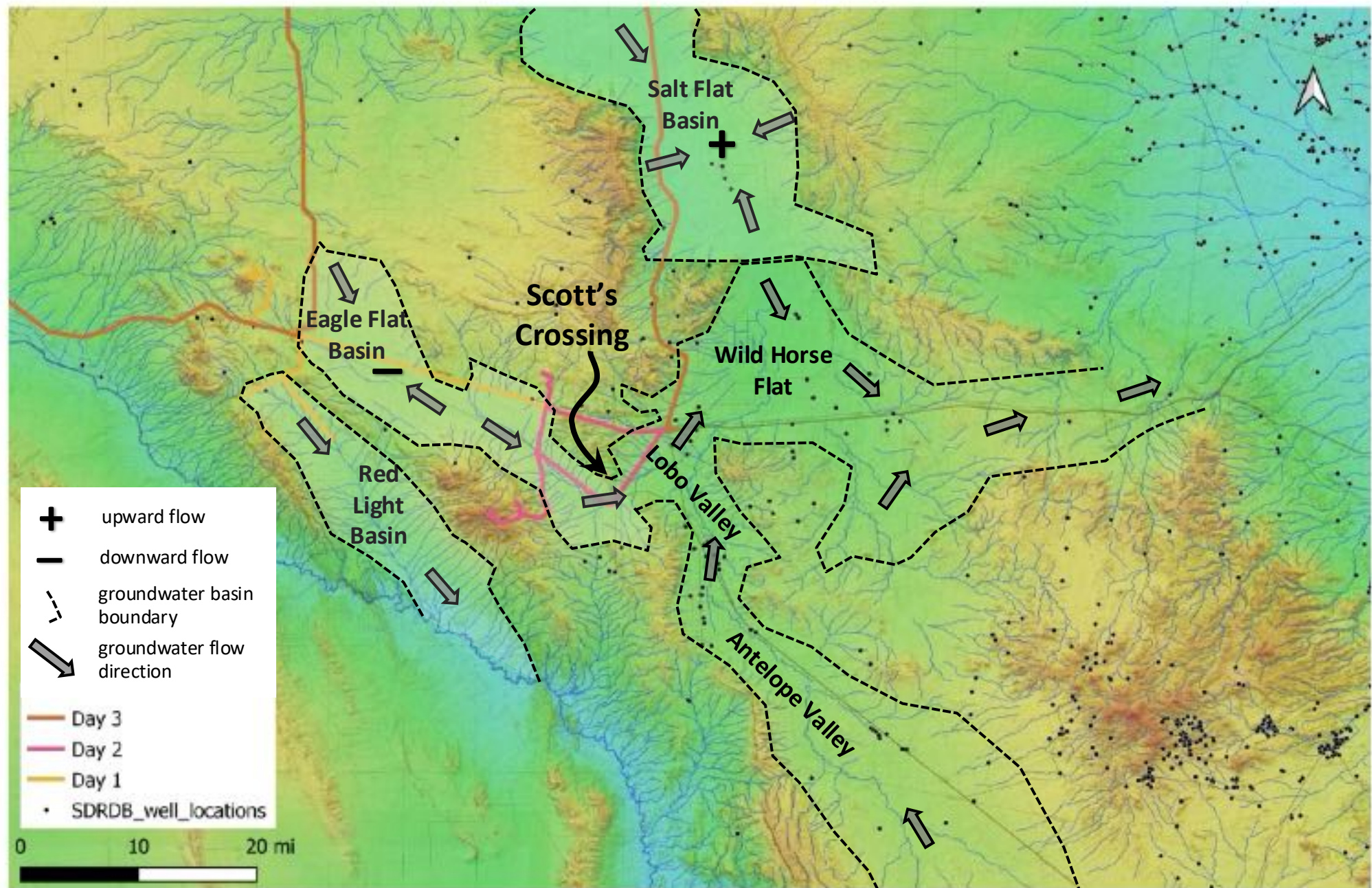
Figure 1.19 – Representation of regional groundwater flow in Cenozoic basins of Trans-Pecos Texas. Figure by Paul Warren and BK Darling.

83
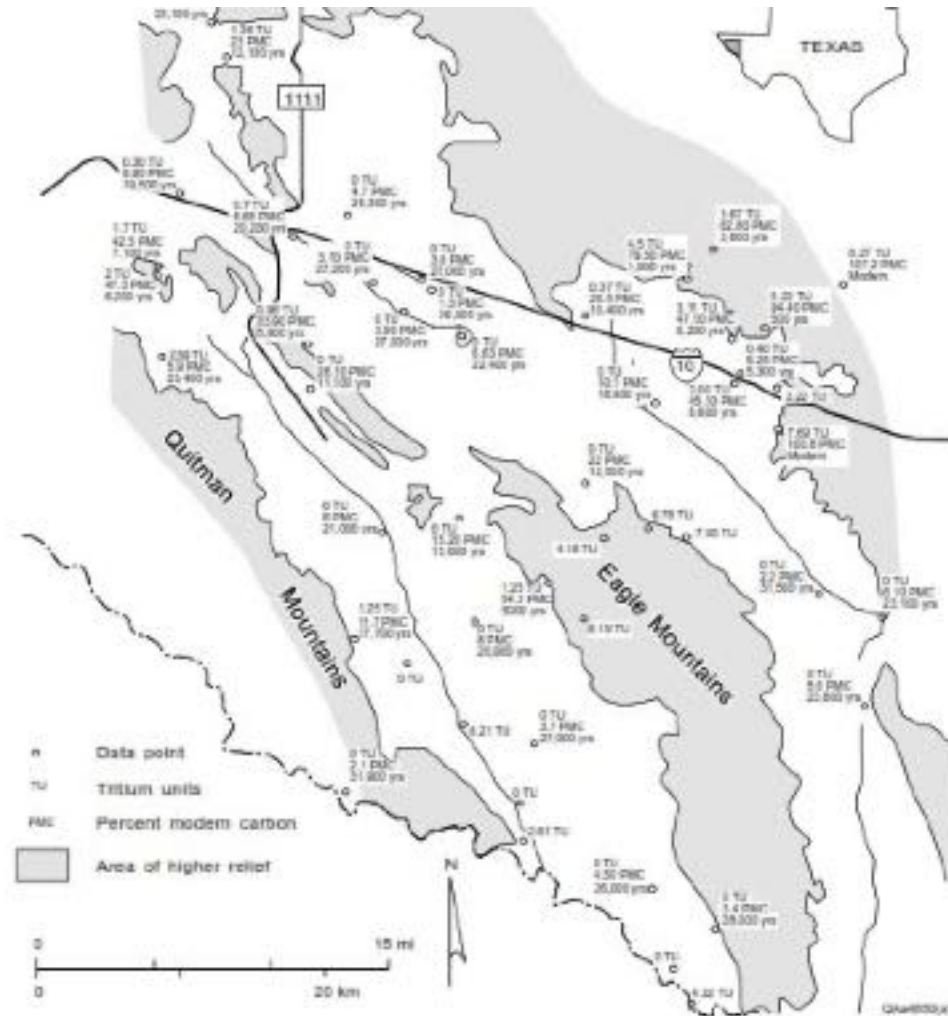
Figure 1.20 – ^3H (TU) and ^{14}C (PMC) in samples of groundwater from Eagle Flat and surrounding area. Isotope data from Darling and others (1994).

84
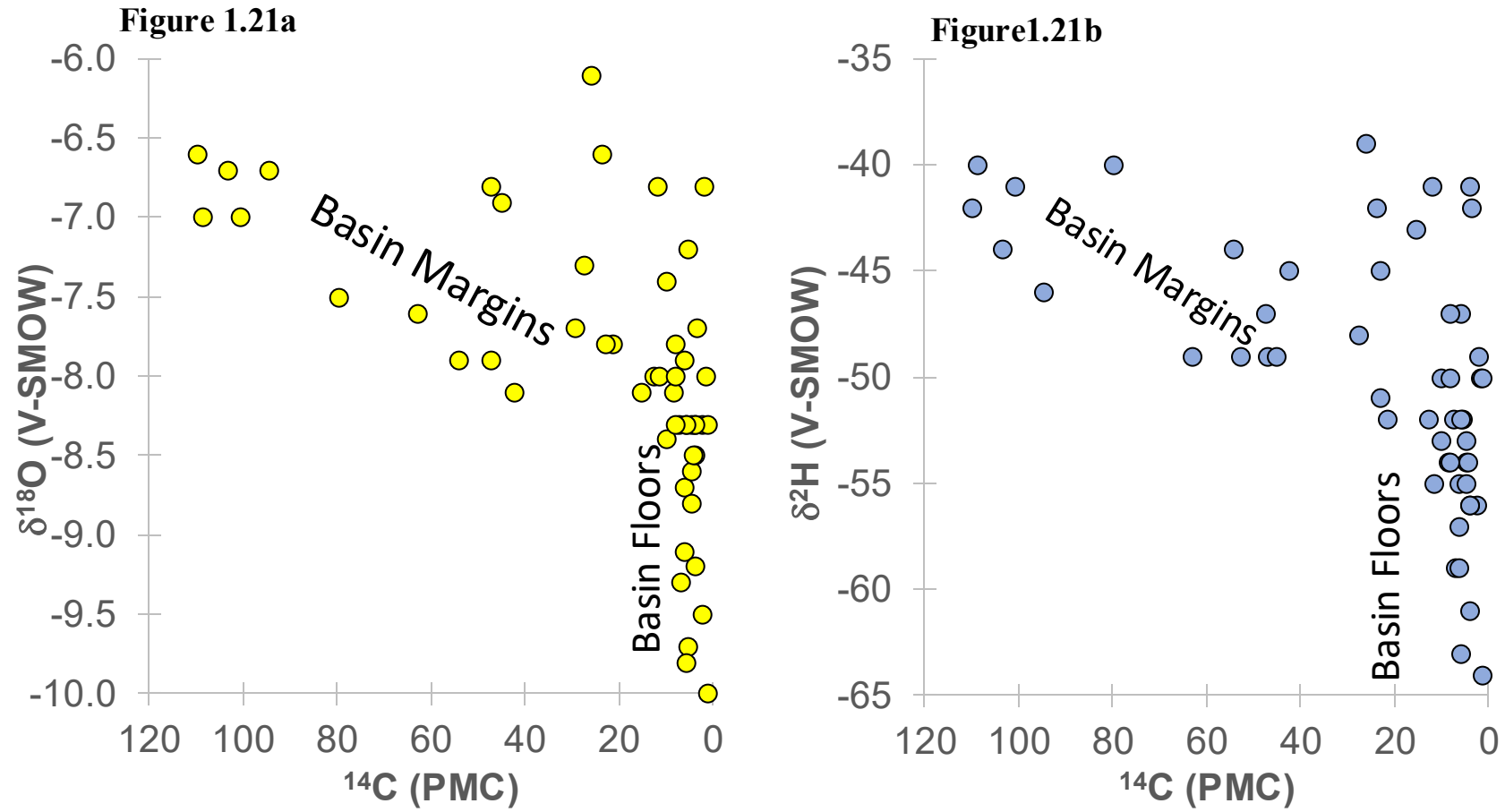
Figure 1.21a – $\delta^{18}O$ and ^{14}C in groundwater samples from Eagle Flat and surrounding area. **Figure 1.21b** – δ^2H and ^{14}C in groundwater samples from Eagle Flat and Surrounding area. Source: Darling and others (1994).

Figure 1.22a

Figure 1.22b

Figure 1.22a– Left: Yucca Mesa, looking south on FM 1111; Right: Yucca Mesa, looking east from FM 1111. Yucca Mesa is part of the Devil Ridge thrust. **Figure 1.22b** - Post-thrusting normal faults offset beds of the Bluff Mesa, Finlay, and Cox formations. Photos by BK Darling.

Figure 1.23 – Google Earth image showing Red Light Basin, surrounding highlands and Rio Grande

Figure 1.24 – Cox Sandstone and Finlay Formation dipping toward the southwest along Devil Ridge. Photo by BK Darling.
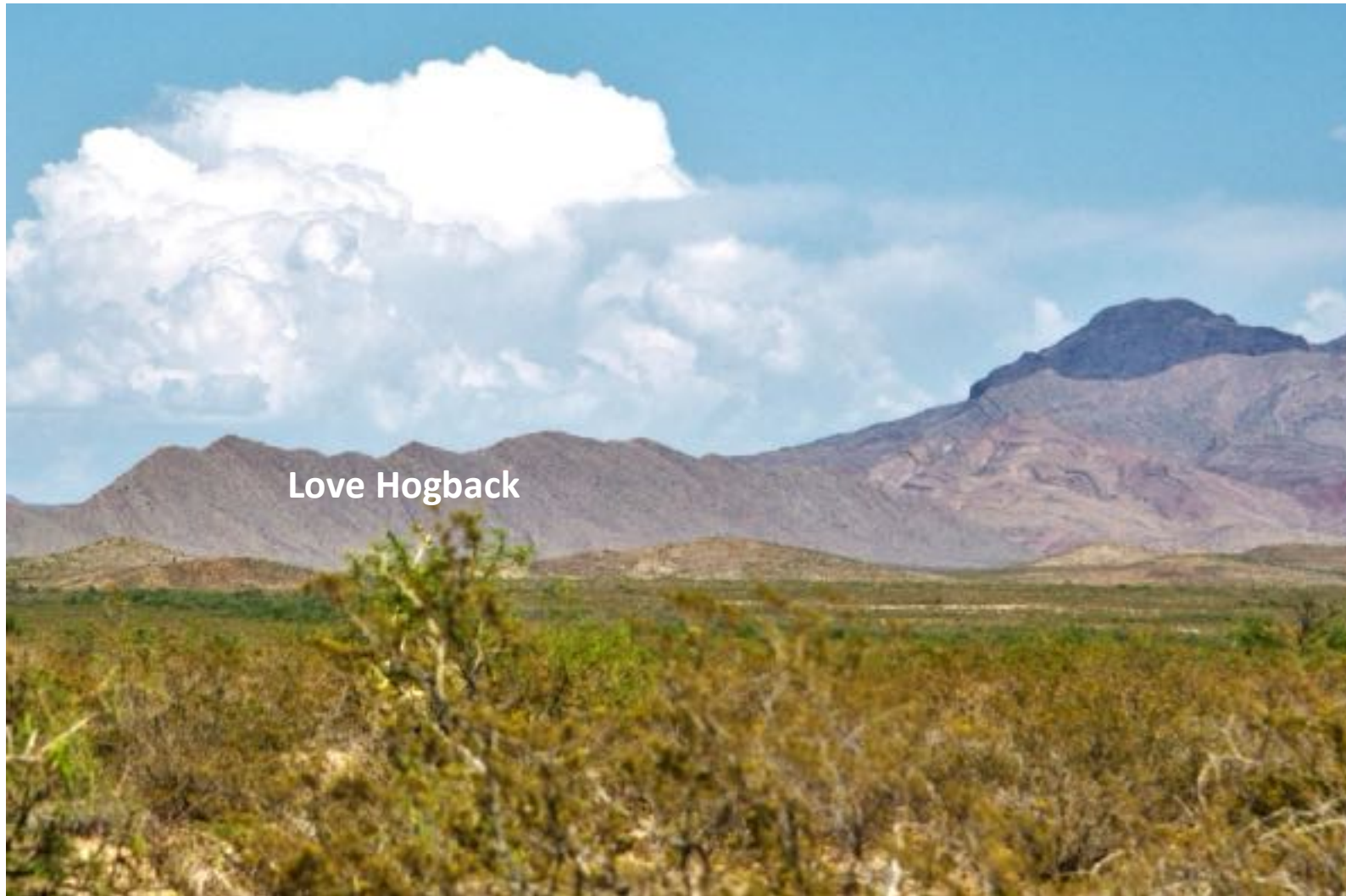
Figure 1.25 – Love Hogback, southernmost extent of Devil Ridge Thrust. Photo by BK Darling.

Figure 1.26 – Western Eagle Mountains. The white object near the highest elevation (to the right of Frenchman's Canyon) is the FAA radar station at Eagle Peak. The lower rhyolites, trachytes, upper rhyolites and the syenite are identified on the figure. Photo by BK Darling.

Figure 1.27 - Bruce Darling (center) leads discussion of stratigraphy and structural geology of Red Light Basin. Devil Ridge is in background. Photo by Diane Darling.

Figure 1.28a

Figure 1.28b

Figure 1.28a– Quitman thrust fault as seen from Quitman Gap Road.   Footwall beds are Cox sandstone, and thrust are hanging wall beds are overturned Bluff Mesa limestone. **Figure 1.28b** – Quitman thrust fault. Note upturning of Cox sandstone beds along footwall of thrust. Photos by BK Darling.
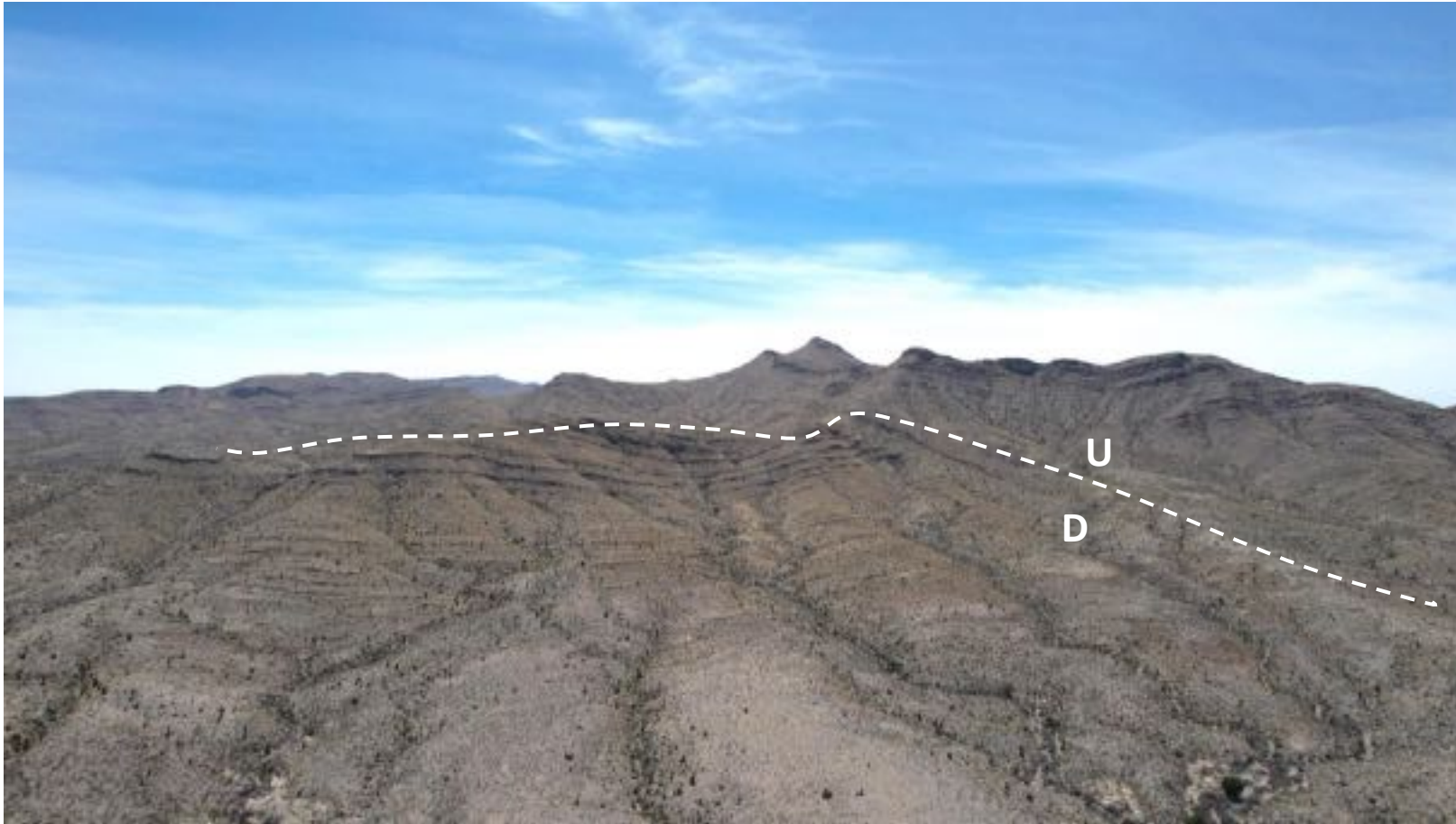
Figure 1.29 – Aerial oblique view of Quitman thrust fault as viewed from Quitman Gap road. Photo by Michael Jacobs.

Figure 1.30 - Wide-angle view of Quitman Thrust as seen from Quitman Gap Road. Photo by Paul Warren.

Figure 1.31 - Quick side trip on Quitman Gap Road to see Quitman Thrust Fault. Photo by Paul Warren.
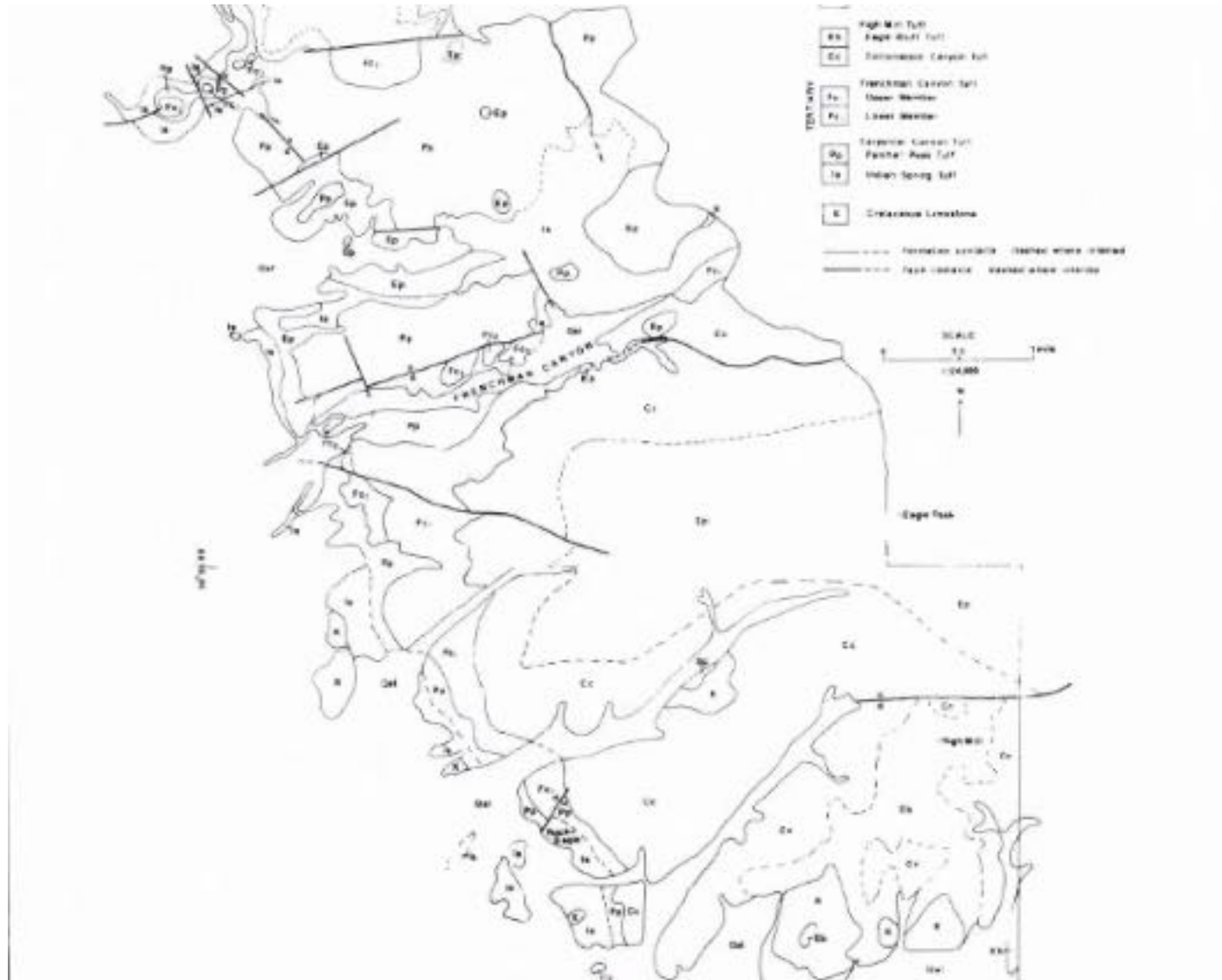
Figure 1.32 – Igneous formations of western Eagle Mountains, according to Hoffer and others (1980).,

GEOLOGY OF HUDSPETH COUNTY, TEXAS

**GUIDEBOOK OF AIPG-TEXAS
SPRING FIELD TRIP
APRIL 21 – 23, 2023**

**Day One
Supplemental Material**

Goodell, P., Ayala, S., Karplus, M., Velasco, A; and Mahar, A.I., 2023, Critical minerals in West Texas

Mahar, M.A., and Goodell, P.C., 2023, Timing and origin of alkaline magmatism at the shoulder of the southern RGR, Sierra Blanca

SUPPLEMENT 1

Goodell, P., Ayala, S., Karplus, M., Velasco, A; and Mahar, A.I., 2023, Critical minerals in West Texas

Critical Minerals in West Texas

Philip C. Goodell, Solymar Ayala, Marianne Karplus, Aaron Velasco, Mohammad Ali Mahar

Department of Earth and Environmental Sciences

University of Texas at El Paso

The importance of Critical Minerals (CM) has finally come to the forefront of national awareness, these being the natural materials essential to a highly technological societies that are imported from other countries. Most of the CM are actually chemicals, not minerals, and their specifics vary with country and over time, but there are approximately 50 of them, depending on how you count them.

The geology of Trans-Pecos Texas is characterized as a rift shoulder with part of the Delaware Basin on the east. The shoulder consists of uplifted portions of the North American craton terminating westward at the actual rift boundary faults, at the western boundary of the Diablo Platform and the Texas Linament. Extensional magmatism is thought to have initiated with the ignimbrite flareup, starting approximately 40 ma., with the eventual formation of 8 calderas in West Texas and many laccoliths. Some laccolith groups in semicircles suggest they may be precursors to calderas. Detailed structural response of the rift appears to have followed magmatism by maybe up to tens of millions of years. The Salt Graben north of Van Horn is a branch of the Rio Grande Rift.

To the east of Trans Pecos is the rest of the Delaware Basin, then the Central Basin Platform and the Midland Basin, together comprising the world class Permian Basin. To the west of the Trans Pecos is the Chihuahua Trough in northern Chihuahua, preceded by the Pedregosa and ProtoPedregosa Basins.

Rift Shoulder Mineralization Model

Mineralization at convergent plate margins has long been modeled by porphyry copper deposits at depth and a rich variety of epithermal deposits towards and at the surface. A vast amount of literature has been directed to this topic. A model for divergent plate margins has been lacking, but a sketch is provided here, following presentations given in Howari et al. 2022, and under continued development. Rift shoulders contain and are the source of many CM.

Figure 1 shows the development of bimodal magmatism at a generic rift shoulder, principally the development of multiple large felsic magma chambers. Rising closer to the surface these magmas result in families of laccoliths, or with continued development, in calderas and voluminous ash-flow tuffs, as shown in Figure 2. Known sites of CM deposits are inserted into Figure 2. Both laccoliths and calderas are not shown on the same diagram; calderas are shown because they are more complex.

Deep in these felsic systems may form the standard porphyry Mo deposits, and there may be LCT (lithium, cesium, tantalum) or NYF (niobium, yttrium, fluorine) pegmatites. Mineralization in extensional regimes is dominated by fluorine transport in contrast to chlorine transport in compressional regimes. Up the magmatic systems may be igneous breccia pipes, laccoliths, or caldera systems. Some porphyry Mo systems top out as topaz rhyolites.

CM within the rift shoulder systems are several. Re is enriched and recovered in Mo porphyries, and Ta is known to be present. Be, Li, and Cs pegmatites are widespread with some giant deposits (Tanko, Manitoba for Cs,).

With respect to the Rio Grande Rift, Figure 3, the following deposits or potential targets are identified, with the latter ones in West Texas.   In central Colorado the Climax Mo deposit sits just east of the Mosquito fault, the eastern boundary of the RG Rift, and is part of a cluster of Mo intrusives. In northern New Mexico the Questa Mo deposit and a lesser occurrence are located on the rift shoulder just east of the eastern boundary fault. In southern New Mexico the Wind Mountain laccolith on the Diablo Plateau is enriched in Zr, and other laccoliths are under study. At the eastern margin of the Diablo Plateau is the Cave Peak Mo breccia pipe, which has been extensively drilled and is known to contain Nb. Immediately east

of the central Diablo Plateau in the Salt Graben is a deposit of Li enriched clays (and brines) apparently leached from the laccoliths. At the southern end of the Diablo Plateau are the Sierra Blanca, Texas group of laccoliths including now famous Round Top, and adjacent Little Round Top and Little Blanca, all mineralized with heavy rare earths (HREEs). A significant Be deposit is present in adjacent carbonate rocks. Deep drilling encountered massive quartz which was never penetrated. On the western side of the Davis Mountains is a large zone of alteration known as White-Medley where Be anomalies occur. In the Southern Quitman mountains up Davis Arroyo a swarm of anomalous quartz veins exist. Drilling at 800 feet encountered massive quartz which was never penetrated. Uranium deposits and occurrences are widespread in West Texas, the U having been leached from the volcanic glass.

The rift shoulder model of Critical Minerals in caldera environments is presented and West Texas examples are noted.   These are not the only CM in West Texas.

Howari,F., Salman,A., Goodell,P., 2022, Uranium Geology of the Middle East and North Africa: Elsevier, 273 p.

West, M., Ni, J., Baldridge,S., Wilson,D., Aster,R., Gao,S.,Grand,S., 2004, Crust and upper mantle shear wave structure of the southwest United States: Journal of Geophysical Research v 109, #82, https://doi.org/10.1029/2003jB002575.

Figure 1. Regional Vertical cross section of rift (left) and crust (rigth) super impose over La Ristra velocity model Modified from Howari et al., 2022 and West et al., 2004.

Volcanic basement and intrusive host

A Magma chamber.
B Down-dropped central caldera block.
C Inter-caldera volcanic facies.
D Pre-caldera andesite volcanic pile.
E Outflow facies of ash-flow tuff 1.
F Outflow facies of ash-flow tuff 2.
G Volcaniclastic of AFT 1.
H Volcaniclastic of AFT 2.
I Lacustrine Facies of AFT 1.
J Lacustrine Facies of AFT 2.
K Critical Mineral Disseminated Granite.
L Mafic Intrusion.

1. Pegmatite, famous sites including southern Calif. New England, Brazil, Pakistan, Afganistan, Russia Ta CalTan central Africa, Tanco Manitoba i-Cs.
2. U and Re recovery successful in porphyry Mo deposits, other trace elements present.
3. Magmatic hydrothermal veins, often in ring dike intrusives, magmatic hydro thermal veins, often in ring dikes or radial dikes: caldera boundary breccias (7) (Moonlight mine, McDermit caldera, NE Nevada), Cave Peak, W Tx.
4. Rhyolite flow dome, rhyolite flow domes : may be resurgent, veins and dis seminations Pinto Canyon, Tx. (U+): (Ag Bolivia)
5. Pyroclastic flows and floor breccias.
6. Mafic component of bimodal magmatism, sometimes as mafic flow and flow breccias (ferrobasalts on the caldera floor) deposit in vesicles in Mc Dermit caldera, NE Nev.
7. Intracaldera fill, ash, volcaniclastic and lake sediment, landslide facies: preresurgence .
8. Magmatic resurgence, included with rhyolite domes in 4.
9. Post resurgence intracaldera fill, ash, volcaniclastic, and lake sediment, land slide facies, may or may not be present, may or may not be distinguishable from 7, 8 .
10. Intracaldera other outside the caldera, out flow facies included with 11, 12 and 13.

11. Step faults and other structural zones in outflow welded tuffs, Nopal 1, Margaritas, Pena Blanca, Chih. Mc Mammoth mine, W Tx,
12. Altered vitrophyre at base of welded tuff, Nopal 1.
13. Lapilli tuff, lithophasae, stratigraphic control.
14. Unwelded basal carbonate-lithic rich AFT, permeable and reactive, at SporMt. Utah, the world's largest Be deposit.
15. Conglomerate, arkose, and sandstone in channels cut into volcanic basement and at times containing organic material. Talahasse Creek, Colorado; Sonora, Calif., Egypt.
16. G and H, volcaniclastic facies.
17. Mary Jane Aiken MS study area ranch, Brewster Co. Tx.
18. Playa or calcrete facies, Australia, SW US.
19. Brines within 17 and 18.

Figure 2. Magmas, Caldera Volcanism, Volcaniclastics, and Basement geologic units (alphabetical) and potential mineral deposits (numerical).

Figure 3. Rio Grande rift shoulder and Critical Mineral Deposits.
Serveral are known porphyry Mo deposits.

SUPPLEMENT 2

Mahar, M.A., and Goodell, P.C., 2023, Timing and origin of alkaline magmatism at the shoulder of the southern RGR, Sierra Blanca

Timing and origin of alkaline magmatism within and at the shoulder of the southern Rio Grande Rift Sierra Blanca, Texas

Munazzam Ali Mahar and Philip C Goodell

Department of Earth, Environmental, and Resource Sciences
University of Texas at El Paso

ABSTRACT

Zircon U–Pb ages and Hf-O isotopic composition provided the important constraints for the timing and origin of caldera-related alkaline magmatism at the western and eastern part of the southern RGR (RGR) and alkali rhyolite emplaced within the rift shoulder. Quitman Mountain in Texas and Sierra Candelaria in northern Chihuahua marks the eastern and western margin of RGR, while Triple Hills is one of the five shallowly emplaced rhyolitic laccolith within the adjacent eastern cratonic shoulder of the RGR. Our new zircon U-Pb geochronological data assigned a weighted mean age of 35.2 ± 0.59 and 29 ± 0.5 Ma to the monazite and syenite exposed in the eastern and western margin of RGR, respectively. The Sierra Candeleria syenite yielded dominant nonradiogenic initial hafnium isotope composition with εHf (t) ranging from -5.1 to + 0.4, this is comparable to the 35 Ma monzonite exposed in the Quitman Caldera at the eastern margin of the RGR. The Quitman monzonite inheritance free zircons yielded typical mantle-like oxygen isotope composition with mean $\delta^{18}O = 5.7$ ‰. The U–Pb ages, absence of inheritance, mildly negative Hf isotope composition and mantle–like oxygen isotope composition suggest that the differentiated alkaline magma is primarily derived from the partial melting of enriched subcontinental lithospheric mantle. However, it is likely that the required heat is provided by the decompressing asthenospheric melt associated wi th the incipient rifting sometime before 35 Ma in the eastern and around 30 Ma in the western part of the rift. The Triple Hills rhyolitic laccolith located at the shoulder of the rift is dated at 37 ± 0.6 Ma. Triple Hills showed significant zircon inheritance of 1153-1062 Ma. Based on ~1.1 Ga zircon inheritances coupled with non-radiogenic Hf isotopic composition (ε Hf (t) = 0 to -10), we suggest involvement of older Red Bluff-type granitic basement in the generation of felsic magmas beneath the shoulder of the rift. The acquisition of new isotopic data is currently underway through the examination of core samples from Round Top drill holes, as well as surface samples taken from Little Blanca and Little Round Top laccoliths. These new da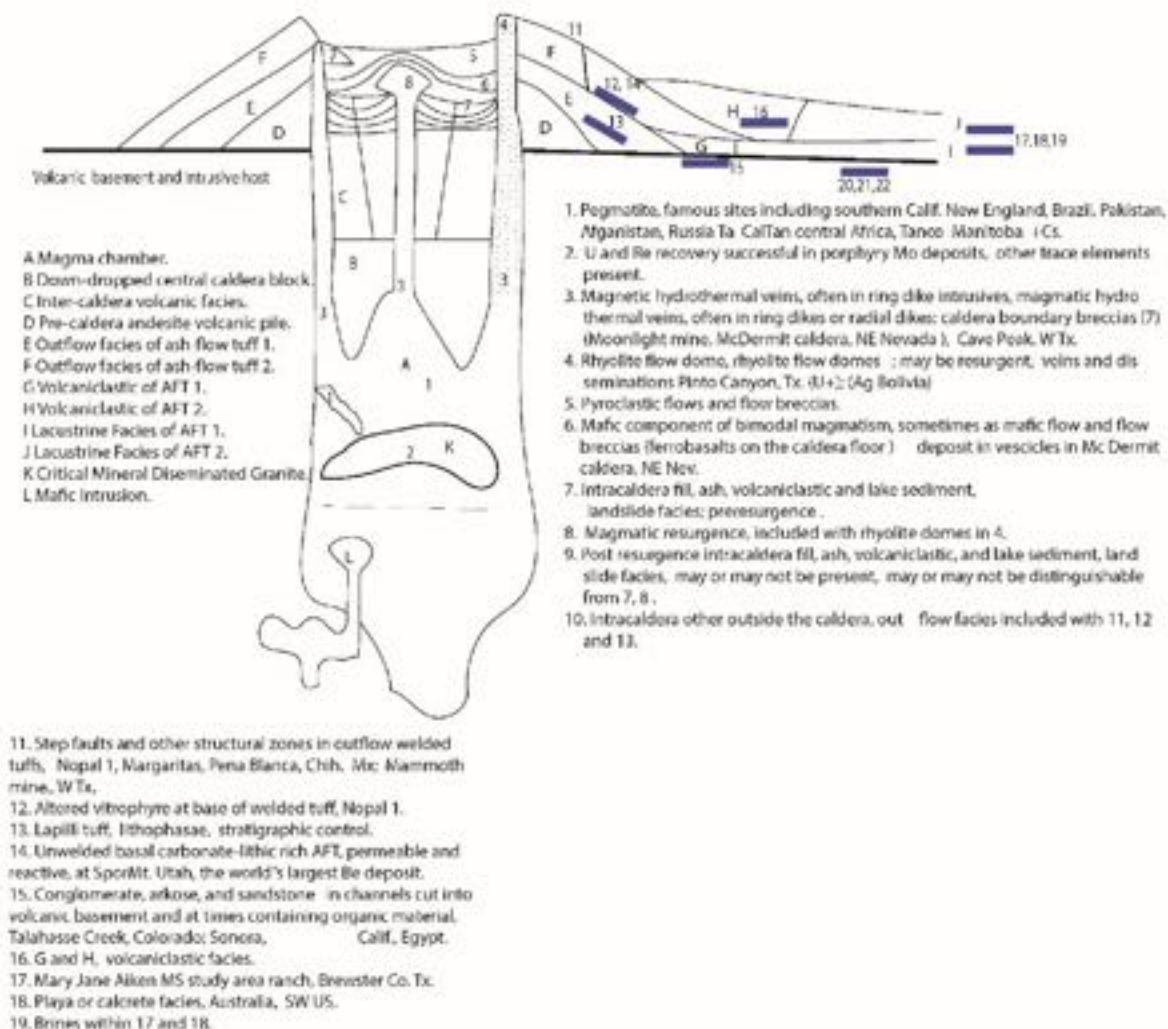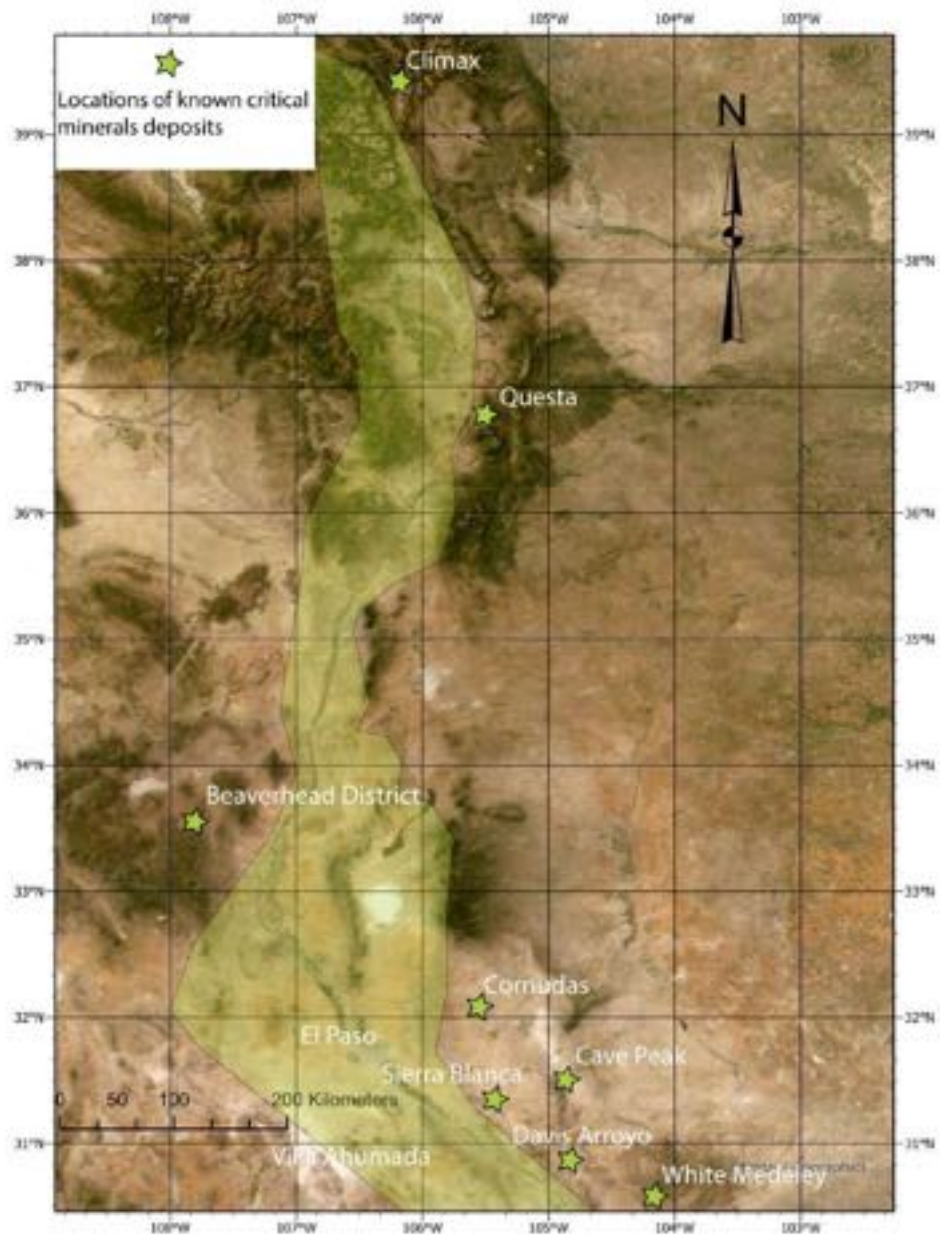ta will not only provide a comprehensive understanding about the genesis of the Y + HREEs deposit hosted by the Round Top Mountains but also promises to render deeper insights into the generation of REE-enriched felsic magmas at the shoulder of rifts elsewhere in the world.

INTRODUCTION

In the present work, we provide U–Pb ages on zircons and zircon Hf-O isotope composition of quartz monzonite exposed in the Quitman Mountain, Sierra Blanca, Texas, syenite from Sierra Candelaria, Chihuahua emplaced in the eastern and western part of southern RGR, respectively. We also provide geochronological as well as Hf isotopic data from the Triple Hills rhyolite

emplaced within the eastern cratonic shoulder of RGR in Sierra Blanca Texas. (Fig. 1). The study showed implications for the thermomagmatic and tectonic evolution of the southern RGR.

GEOLOGICAL SETTING

Eastern and western margin of RGR

Quitman Caldera Complex, known as Quitman Mountains, is located on the eastern boundary of Rio Grande rift. Quitman Mts mark the western extremity of volcanic centers in west Texas (Fig. 1). Quitman Mts are composed of both extrusive and intrusive rocks with layered tuffs, rhyolite to trachytic units in the center while intrusive surrounds the volcanic rocks.
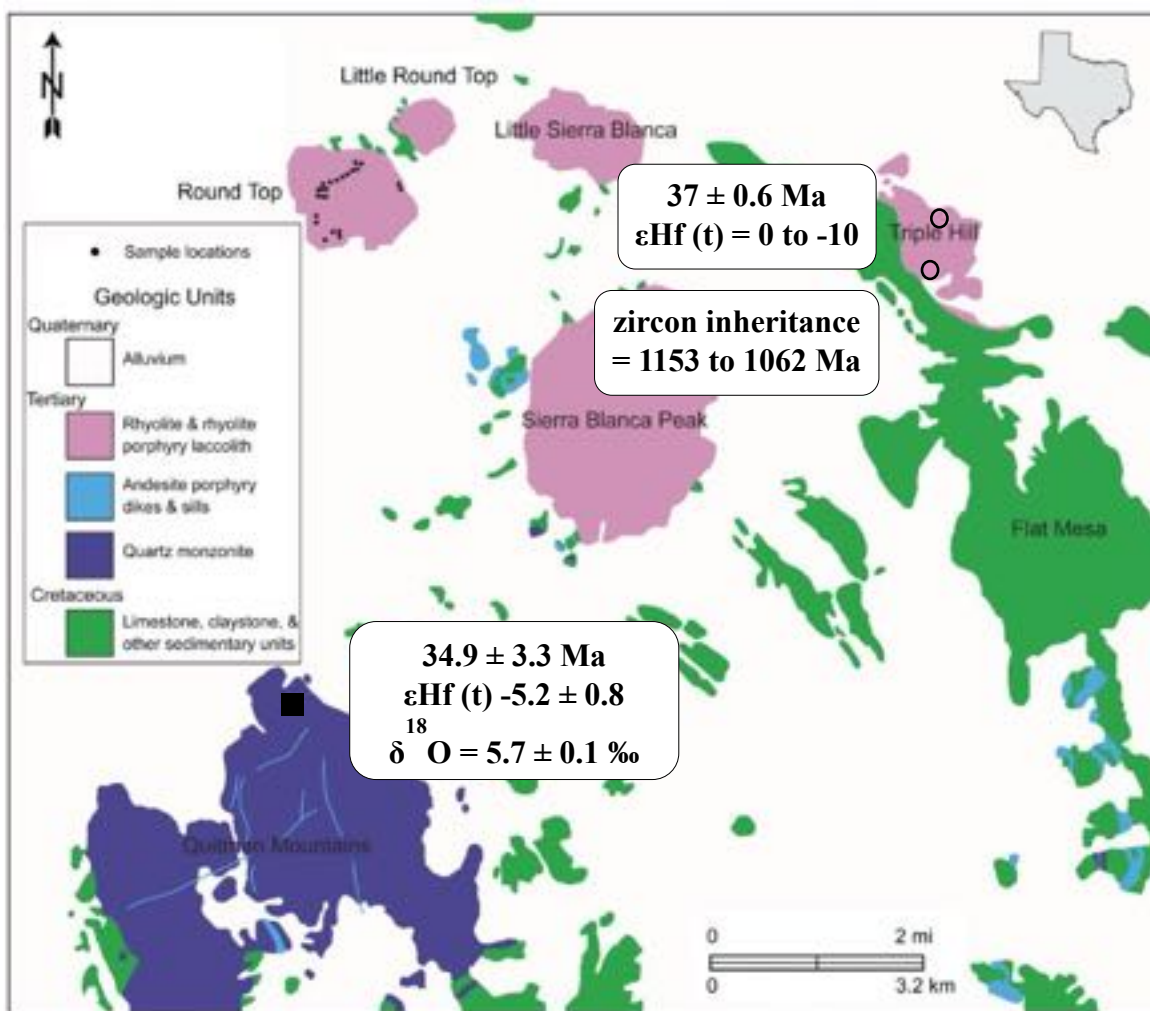
Figure 1. Geologic map of the Sierra Blanca Complex and surrounding rhyolite laccoliths (adopted from Dietrich et al., 1983). Sierra Candeleria (not shown) is located in the western part of the rift in Chihuahua.

Sierra Candelaria is at the southern end of a horst within the southward extended RGR and lies close to the western margin of the RGR in northern Chihuahua. Sierra Candelaria is texturally and compositionally comparable to the Quitman stock monzonite in the eastern part of the RGR as well as to the west Texas porphyry syenite laccoliths at the rift shoulder. Sierra

2

Candelaria syenite possibly represents the plutonic deeper part of a collapsed caldera similar to the Needle pluton syenites and other alkaline calderas in new Mexico and west Texas that intruded the Cretaceous sedimentary host rock and partly covered by the recent alluvium. No age data is available for the Sierra Candeleria syenite prior to this study.

Eastern Shoulder of RGR: Sierra Blanca rhyolite laccolith Complex

Sierra Blanca rhyolitic laccoliths are part of the Trans-Pecos Magmatic Province of Texas (Henry and McDowell 1986). The Sierra Blanca peaks are a series of five peraluminous rhyolite laccoliths in the Hudspeth County Sierra Blanca. (Fig. 1). Triple Hills is the western most laccolith and generally considered the oldest of the other four laccoliths. So far, the only age data are available for the Sierra Blanca laccolith which is dated at 36.2 ± 0.6 Ma (based on K/Ar in biotite; Henry and McDowell 1986). However, based on evolving geochemistry (i.e., enrichment of incompatible REE), Triple Hill is considered the most primitive and thus oldest of all the laccoliths followed by Sierra Blanca. The rest of the REE-enriched three laccoliths, Round Top, Little Sierra Blanca, and Little Round Top are speculated to be emplaced synchronously. (Shannon and Goodell 1986; Price et al. 1990). Recently, Piccione et al., 2019 based on U-Pb fluorite and nacrite dating of a vein within the Round Top proposed that the REE-enrichment occurred due to the fluid-induced mobility of REE at ca. 6.2 ± 0.4 Ma, about 30 million years after the emplacement of the laccoliths.

SAMPLE DESCRIPTION

One Sample ST was collected from the grey medium to coarse grained monzonite is exposed in the northern part of the Quitman Caldera. A total of four samples; SC1, SC6, SC8 and SC10 were collected from the course to medium-grained Sierra Candelaria syenite. Two samples TH3 and TH5 were collected from Triple Hills laccolith representing the felsic magmatic rocks emplaced within the cratonic shoulder of the rift. Figure 2 shows the BSE and CL images of the studied samples.

METHODS

The zircon U-Pb and Hf isotopic measurements were performed by multicollector (MC) LA-ICP-MS at the Arizona LaserChron Center, University of Arizona. Zircon oxygen isotope measurements were carried out using the Cameca IMS-1280 SIMS at the Wisconsin Secondary Ion Mass Spectrometer Laboratory (WiscSIMS) facility, University of Wisconsin.

PRELIMINARY RESULTS

Major and trace element geochemistry

We are currently writing the manuscript to be submitted soon, here, we briefly present some of the salient feature to better understand the timing and origin of southern RGR and its shoulder. Geochemically, the studied rocks are high-K and fall in the shoshonite field, the Sierra Candelaria samples are classified as syenite while Quitman Caldera sample falls at the boundary between syenite, monzonite and quartz monzonite. Alkaline rocks from both calderas show similar REE and trace element patterns on the primitive mantle normalized plots (Fig. 3). On the tectonic discrimination plots rocks fall in the within plate granite field. Geochemically, all the rhyolite laccoliths are high-K alkali-calcic to alkalic rhyolite and showed within-plate type granitic composition. Except Sierra Blanca and Triple Hills, other laccoliths, Round Top, Little Round Top and Little Blanca showed enriched HREE composition (Fig. 4). Triple Hills showed

enrichment in LREE. Similar Eu anomaly suggested fractionation crystallization process for the generation of RT, LRT, LB and SB.
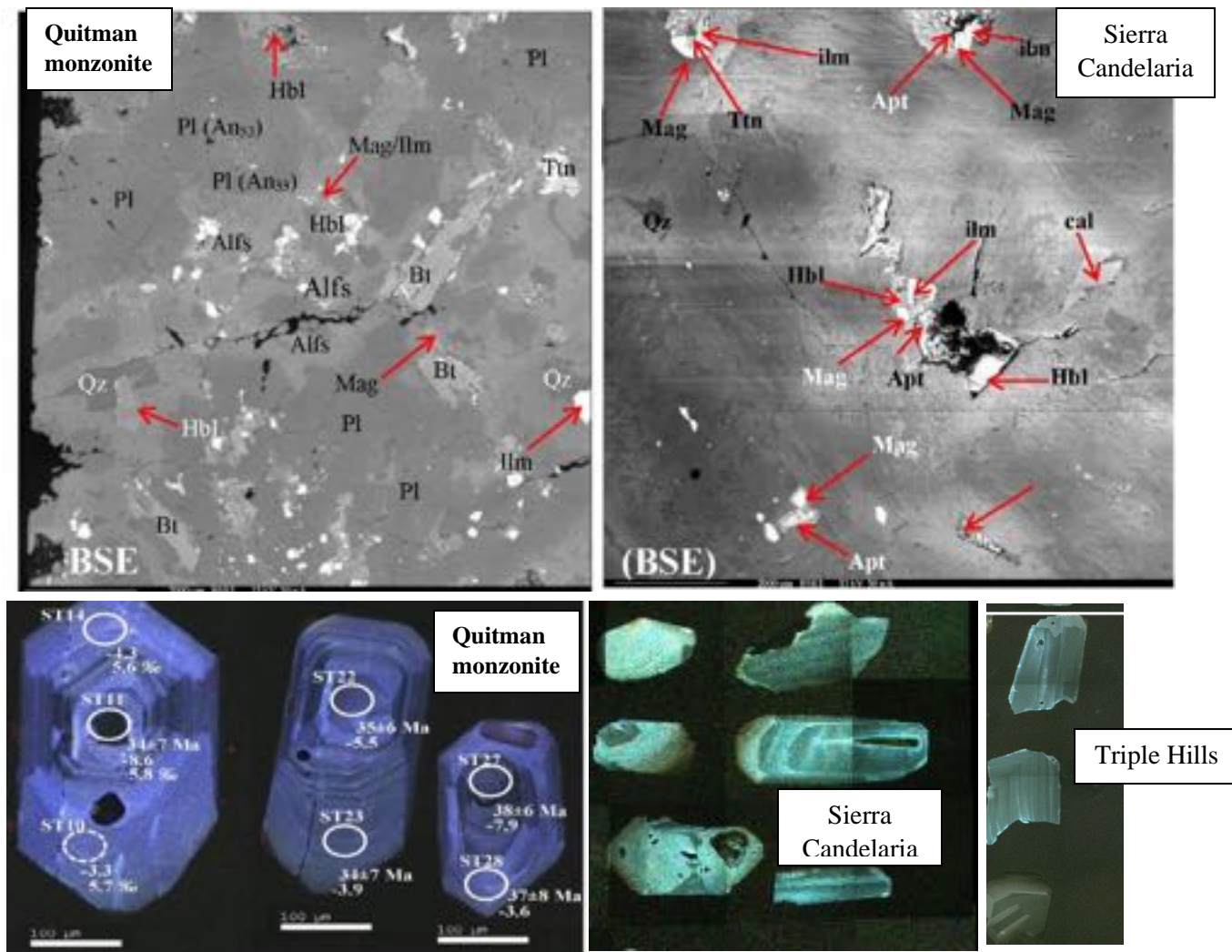
Figure 2. BSE images of Quitman and Sierra Candelaria samples with minerals labeled, CL images of some of the analyzed zircons are also shown.

Zircon U-Pb geochronology

The monzonite and syenite from Quitman Mountains and Sierra Candeleria yielded weighted mean age of 35.2 ± 0.59 and 29.3 ± 1.0 Ma (Fig. 1). Two samples from Triple Hills yielded a weighted mean age of 37 ± 0.6 Ma (Fig. 1).

Zircon Hf and oxygen isotopic composition

Quitman Mountains yielded nonradiogenic εHf (t) values ranging from -9.5 to +0.8 with a weighted mean of -5.08 ± 0.75. Samples from Sierra Candeleria yielded consistent less variable weighted mean Hf isotopic composition with εHf (t) varying from -2.5 to -3.9. Tertiary zircons from Triple Hills identical Hf isotopic composition to that of Quitman monzonite with ε Hf (t) varying from 0 to -10. For location see figure 1. Oxygen isotopic data was only acquired on zircons

4

extracted from Quitman monzonite. A total of 14 zircon spots from rim to core were analyzed on 10 zircon grains. The mean $\delta^{18}O$ is 5.7 ‰ (Fig. 1) ranging from 5.4 to 6.2 ‰ with a difference of only 0.8 ‰.
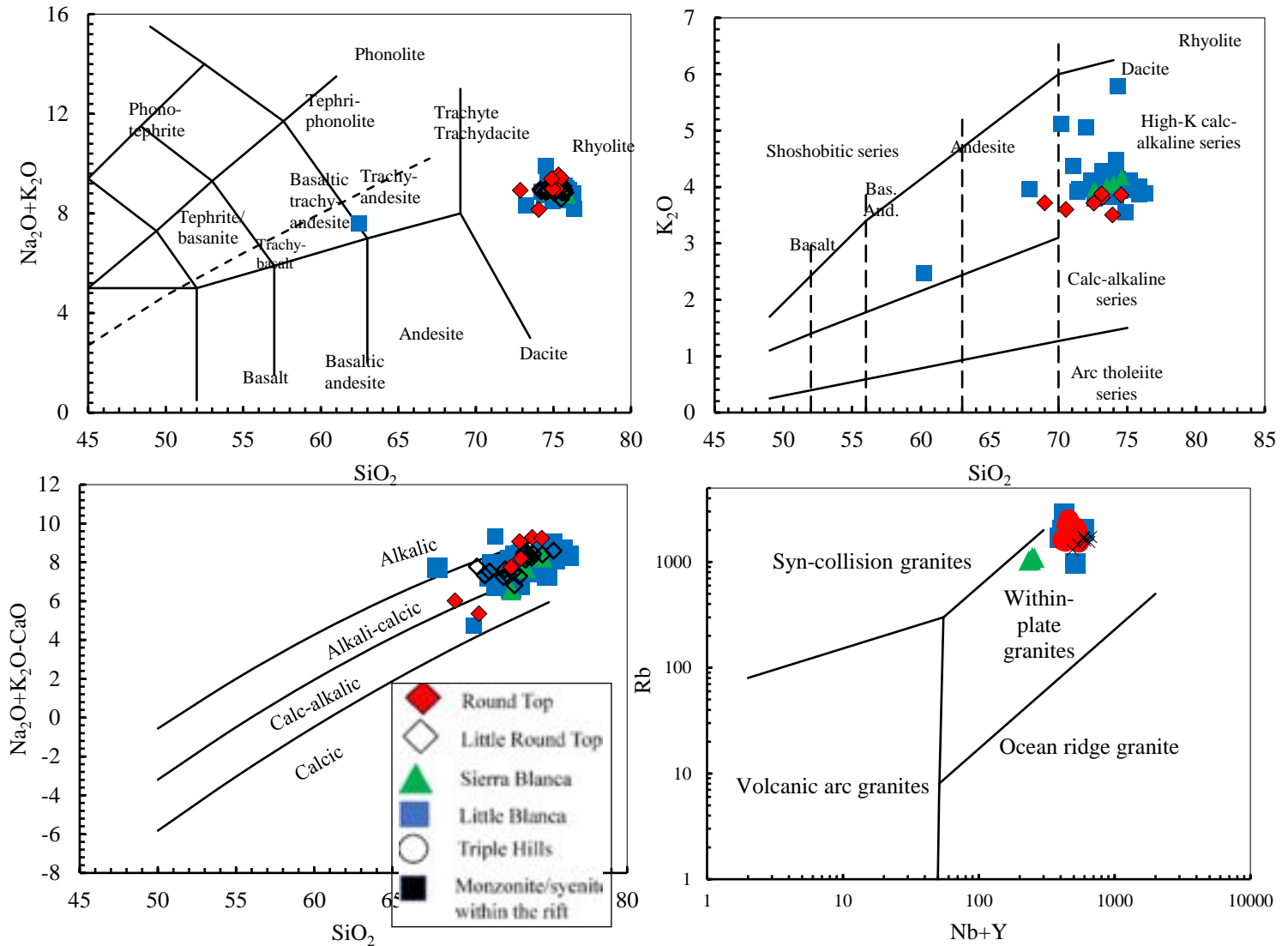
Figure 3. Geochemistry of studied samples.
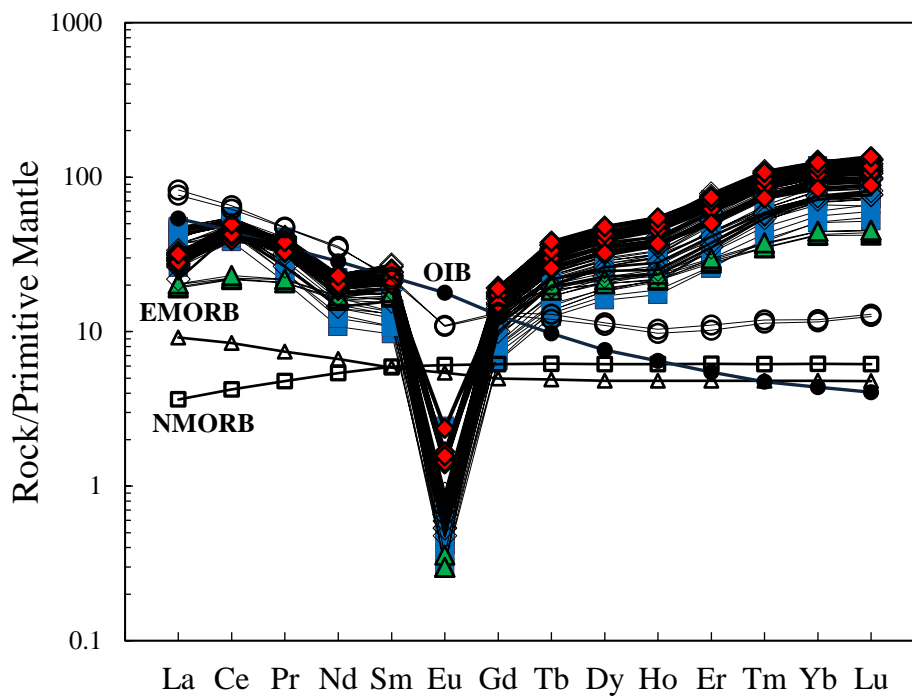
Figure 4. REE composition of studied samples.

PRELIMINARY CONCLUSIONS

- Based on the above Zircon U-Pb data, it is evident that the magmatism at the eastern margin of RGR is restricted to 35 Ma. While compositionally similar alkaline magmatism at the western margin of RGR started around 29 Ma. Triple Hills rhyolite emplaced within the eastern cratonic shoulder yielded an age of 37 Ma. Triple Hills rocks are the only samples yielded significant Red Bluff-type inherited zircons with dates ranging from 1153 to 1062 Ma.

- Hf isotopic composition of alkaline magmatic rocks within the rift as well as the rift shoulder yielded overlapping nonradiogenic Hf isotopic composition (negative ε Hf (t).

- Oxygen composition from Quitman monzonite yielded mantle-like oxygen isotopic composition of 5.7 ‰.

- The Hf-O isotopic data from alkaline rocks from the rift suggest that the source basaltic magma was generated by partial melting of enriched subcontinental lithospheric mantle. With little or no involvement of depleted [positive εHf (t)] asthenospheric mantle.

- Even though Triple Hills rhyolite yielded a similar Hf isotopic composition to that of alkaline rocks within the rift but have a significant Proterozoic zircon inheritance. These inherited zircons yielded identical εHf (t) values to the Proterozoic Red Bluff Granite Suite. These data from Triple Hills suggest involvement of Red Bluff-type granitic basement beneath rift shoulder.

WORK IN PROGRESS

Recently we received a grant to continue our work on Sierra Blanca laccolith. This work involves robust multi-mineral dating and Hf-O isotopic data of the laccoliths to fully understand the timing and origin of the Y +HREE deposit hosted by these rhyolites.

6

The following flow-chart explains the work plan for our ongoing research activities.

Type of samples

30 drill hole samples from two holes from Round Top deposit
30 surface samples from Little Round Top, and Little Blanca

Selected samples sent to Colorado School of Mines	→	Automated mineralogy, mapping of selected 1-inch round samples to locate target minerals like zircon, xenotime and fluorite.	→	**Timing of HREE mineralization** Mapped rock slabs sent to Stony Brook University for U-Pb dating and trace element composition.

Origin of magma sources Oxygen isotopic composition of identified zircons at UCLA	←	**Origin of magma sources** Hf isotopic measurements of zircons at the University of Arizona	←	**Timing of magma crystallization** U-Pb dating on zircon/ xenotime at the University of Arizona

LIST OF REFERENCES

Dietrich, J.W.; Owen, D.E.; Shelby, C.A.; Barnes, V.E., 1983. Geologic Atlas of Texas, map scale 1:250,000. In Geologic Atlas of Texas, Van Horn-El Paso Sheet; the University of Texas at Austin, Bureau of Economic Geology: Austin, TX, USA.

Henry, C D., and McDowell, F.W. (1986) Geochronology of magmatism in the Tertiary volcanic field, Trans-Pecos Texas. In J.G. Price et al, Eds., Igneous geology of Trans-Pecos Texas, p .99-122. Bureau of Economic Geology Guidebook 23, University of Texas at Austin.

Piccione, G., Rasbury, E.T., Elliott, B.A., Kyle, J.R., Jaret, S.J., Acerbo, A.S., Lanzirotti, A., Northrup, P., Wooton, K. and Parrish, R.R., 2019, Vein fluorite U-Pb dating demonstrates post–6.2 Ma rare-earth element mobilization associated with Rio Grande rifting: Geosphere 15, p. 1958-1972.

Shannon, W.M. and P.C. Goodell, 1986, Lithogeochemistry of intrusive rocks of the Quitman-Sierra Blanca igneous complex, Hudspeth County, Texas; in Igneous Geology of Trans-Pecos, Texas: Geol. Soc. Amer. Field Conf. Guidebook, p. 225-236.

GEOLOGY OF HUDSPETH COUNTY, TEXAS

GUIDEBOOK OF AIPG-TEXAS
SPRING FIELD TRIP
APRIL 21 – 23, 2023

ROAD LOG - DAY TWO

OVERVIEW OF ROAD LOG - DAY TWO

The Eagle Mountains are the focal point of Day Two. The road log begins with a stop along an access road to westbound I-10 for a discussion of the Precambrian rocks of the Carrizo Mountains, the Streeruwitz Thrust Fault, and the Texas Lineament. This is followed by a visit to the Natural Minerals talc mining operation at Allamoore, then a brief visit to an old railway stopping point where thermal groundwater was pumped from wells to replenish steam locomotives and to supply water to a hotel that offered hot baths sourced by the warm groundwater. From that point, the emphasis is on the structural geology and mineral deposits of the Eagle Mountains, the fluorspar deposits of Spar Valley, in particular. A paved road built and maintained by the Federal Aviation Administration is the path to Eagle Peak, the highest point of the Eagle Mountains and the highest paved road in Texas.

Road log by: Bruce K Darling and Michael Jacobs

Begin road log

0.0 mi (0.0 km)

Begin at intersection HW 54 and W. Broadway Street.

2.0 mi (3.2 km)

Merge with westbound I-10.

3.0 mi (4.8 km)

Three-Mile Mountain at 3:00. Permian Hueco Limestone on Precambrian Van Horn Sandstone.

3.98 mi (6.14 km)

Scenic overlook on right (Figure 2.01). Rocks are phyllitic slate of the Carrizo Mountains. The Van Horn Mountains are at 9:00 and the Carrizo Mountains are at 10:00. For the next 4.5 miles (7.3 km), the highway traverses exposures of Precambrian metaigneous and metasedimentary rocks of the Carrizo Mountains Group. The rocks exposed along this stretch of the highway are the northernmost extent of the southern domain of Precambrian formations in Culberson and Hudspeth counties and form the hanging wall of the Streeruwitz thrust fault.

4.82 mi (7.8 km)

Enter Hudspeth County and Mountain Time Zone.

6.9 mi (11.1 km)

Stop 2.1 - Road-cut exposures, rocks of Carrizo Mountains Group

Turn right on frontage road and stop at the first road cut.

The ridge at 3:00 is capped by Lower Cretaceous Cox Sandstone, faulted down against Precambrian. This is the Hillside Fault (Figure 2.01). The area is considered to be the type locality of the Texas lineament (Muehlberger, 1980).

Rocks of the Precambrian Carrizo Mountains Group are exposed in the road cut (Figures 2.02a,b – 2.30a,b). Carrizo Peak, on the south side of the highway, is a prominent feature of the northwestern part of the mountains and is underlain by Precambrian metarhyolite. Precambrian rocks in this area are bordered by scarps of Permian limestone on the south and north. The east and west sides of the mountains are flanked by unconsolidated basin fill sediments of Lobo Flat and Eagle Flat, respectively. The sequence of Precambrian rocks (Davidson, 1980) is estimated to be 19,000 ft (5,800 m).

Durfee (1982) described two domains in the Carrizo Mountains. Domain 1 in the central and eastern area is characterized by northwest-trending planar structures, in a regional ductile shear zone, that dip uniformly toward the southeast. Domain 2 encompasses the western and northwestern areas. This domain exhibits ductile and brittle tectonic fabrics. The two structural domains are separated by a complex listric normal fault zone. These data are interpreted in a tectonic model in which the Carrizo Mountains volcanic and sedimentary rocks were deposited in a subsiding basin and may have been buried to a depth of up to 9 miles (14.5 km) and subject to temperatures around 300°C (greenschist facies transition). The rocks were deformed as part of a regional ductile shear zone that resulted in mylonitic and schistose fabrics. Later brittle and ductile structures formed as domain 2 buckled and slid away from the main body of domain 1 along a series of listric normal faults.

Ewing (2016) describes rocks of the Carrizo Mountains Group as follows:

> Here, the present-day rock types are quartzite and metamorphosed arkose (feldspar-rich sandstone and conglomerate), schist (metamorphosed siltstone and shale), and marble, all interlayered with thick metamorphosed rhyolite flows and tuffs. The rhyolite yields ages from 1,382 to 1,377 Ma. The rocks are intruded by diabase sills dated at 1,286 Ma, granodiorite plutons, and some rhyolitic dikes, all of which predate metamorphism. The greater sedimentary content and the details of rock chemistry in the Carrizo Mountains

have led several geologists to propose an extensional setting, a rifting of the old continent to form a basin, possibly behind a volcanic arc.

Within 0.25 mile (0.4 km) north of Stop 2.1, rocks of the Carrizo Mountains Group are absent by erosion, and it is in the flats and low-lying hills here that Proterozoic formations that form the footwall of the Streeruwitz Thrust Fault (Allamoore, Tumbledown Mountain, and Hazel formations) are exposed. At several locations, rocks of the Carrizo Mountains Group overlie talc beds of the Allamoore Formation (Figure 2.04)

In this area, the Allamoore Formation (Ewing, 2016):

> … consists of about 1,000 ft (305 km) of carbonate rocks with rhyolite ash beds and some basalt. The base of this unit is a fault, so what originally lay beneath the Allamoore rocks is unknown. The carbonates include stromatolite fossils (hummocks formed by blue-green algae) and casts of salt crystals, which indicate shallow-water marine conditions with episodes of drying that allowed the salt to crystallize. A rhyolite ash bed near the top of the unit yields a U-Pb date of $1,256 \pm 5$ Ga. Above the Allamoore lies about 500 ft (152 m) of basaltic volcanic rocks and sandstone with volcanic material, plus a small amount of rhyolite. This is called the Tumbledown Formation, named after Tumbledown Mountain. Sandstone at the base of this unit contains rhyolite fragments interpreted to come from the Allamoore Formation, suggesting some erosion before Tumbledown deposition. A zircon-bearing rock near the top of the unit was dated at 1.43 ± 10 Ga. Chemically, these igneous rocks are similar to island arc basalts and also to basalts erupted within a tectonic plate.

After Stop 2.1, proceed west on access road and merge with I-10.

7.5 mi (12 km)

The Desert Rock quarry is at 2:00. Previously known as the Gifford-Hill rock crusher, the quarry began operation in 1925. Gifford-Hill produced crushed rock primarily as railroad ballast for about 60 years, with annual production of as much as 225,000 metric tons. In the last 20 years, crushed stone from the quarry has been produced primarily for decorative and landscaping purposes. The quarried rock is metarhyolite of the Carrizo Mountain Group (Figure 2.05).

The hills immediately northeast of the quarry and north of the railroad are made up of Lower Cretaceous conglomerates of the Campagrande and Cox formations (Figure 2.06). The rocks are on the downthrown side of the Hillside fault and are in contact with rocks of the Precambrian Carrizo Mountain Group.

7.6 mi (12.2 km)

Highway begins descent into Eagle Flat.

9.5 mi (15.3 km)

Take highway exit right and proceed 0.4 miles (0.65 km) to Hot Wells/Allamoore road.

9.9 mi (14.3 km)

The Natural Minerals talc plant (now closed) is north of the intersection of the Hot Wells/Allamoore road and the exit and entry lanes to I-10. Turn right on road to Allamoore. Follow lead vehicle 3.5 miles (5.6 km) on gravel road north to office of Natural Minerals. Follow lead vehicle 3.5 miles (5.6 km) on gravel road north to field office of Natural Minerals. The focus of Stop 2.2 (Figures 2.07a,b 0 2.09 a,b) will be on the occurrence and mining of talc from the Allamoore Formation.

13.5 mi (21.7 km)

Stop 2.2 - Natural Minerals talc mine

Price *et al.* (1983) observe that talc has been mined from numerous locations in the Allamoore Formation (Precambrian) since 1952. They note the following:

> Mining began on a small scale in 1952 and has expanded since then. From 1952 to 1982, annual production from the district has averaged 228,000 tons. Quartz and dolomite are the most common gangue minerals in the talc deposits. Much of the talc is calcined and sold to the ceramic industry as a synthetic diopside-like compound. Asbestiform amphiboles (richterite and actinolite), are found at a few localities. Locally abundant quartz-dolomite pseudomorphs after halite attest to the probable evaporitic environment of deposition of the magnesium-rich sedimentary rocks (possibly magnesite or dolomite) interbedded with cherts) that were metamorphosed to talc during late Precambrian time.

Price *et al.* (1983) cataloged 40 talc prospects and mines in the Allamoore area. In recent years, Natural Minerals (operating as a subsidiary of Daltile) acquired all of the mineral rights in the Allamoore area, with the objective of consolidating operations under the direction of a mining engineer, who has been charged with developing a development plan that does not rely on the inefficient and subeconomic high-grading approach used by many of the previous lease operators.

Kyle and Elliott (2021) note the following:

The commercial talc deposits occur within a narrow fold-and-thrust belt that represents the northernmost extent of a Grenville-age collisional belt (Grenville Front) that records a complex history of deformation and associated fluid flow (Davis, 2007; Davis and Mosher, 2015). The talc deposits generally occur in the immediate footwall of the Streeruwitz Thrust that displaced ~1.35-Ga metamorphic rocks over ~1.25-Ga foreland sedimentary and volcanic rocks. Talc formation was a product of the earliest deformation and alteration events that supplied silica to the Allamoore dolostones; development of talc-rich zones along structural conduits further influenced the nature of later deformation and fluid events. These processes record the collision of a north-verging continental mass with southern Laurentia that initially occurred ~1.15–1.12 Ga in the Llano region, with the collision continuing in western Texas until ~1.06–0.98 Ga (Davis and Mosher, 2015).

Daltile's mining engineer (Ben File) reports the following with regard to the Allamoore talc deposits:

1. The orebody dips approximately 70 degrees to the south.

2. Accounting for the steep dip, the average "true" thickness of the orebody is 400 ft.

3. Average annual production from the mine (American Mine) is 96,000 tons.

4. The company's processing plant at El Paso receives 84,000 tons per year. Plants at Muskogee, Oklahoma and Monterrey, Mexico receive 1,200 tons and 10,500 tons per year, respectively.

After visiting the talc mine, return 3.5 miles (5.6 km) south to I-10, then proceed another 4.3 miles (6.9 km) on Hot Wells road.

20.4 mi (32.8 km)

Stop 2.3 - Hot Wells

Stop at the railroad crossing, and pull over to left side of road (Figure 2.10). Hot Wells Road follows the approximate boundary between the western Carrizo Mountains and an eastern limit of Southeast Eagle Flat. The boundary between the uplift and the basin appears to be the West Van Horn Mountains Fault, a normal fault (down-to-the-west) that trends northward from the western margin of the Van Horn Mountains (Collins and Raney, 1993).

The location at the end of Hot Wells Road was a stopping point for steam locomotives that traveled the Texas & New Orleans rail line. According to the Texas State Historical Association, Hot Wells (https://www.tshaonline.org/handbook/entries/hot-wells-tx):

The town drew its name from wells that produced thermal water for the replenishment of locomotives and for a bath house at Hot Wells (Figure 2.11a,b). Records on file with the Texas Water Development Board (TWDB) show 1,000 ft (305 m) as the depth of each well, and a driller's log reports a mix of fine-grained to coarse-grained and very-coarse-grained deposits of basin fill.

Two wells were listed in TWDB's database, but obstructions in each well prevented the measurement of water levels (Darling and others, 1994). The temperature of a sample of groundwater collected from one of the wells in 1941 was 107°F (42°C). Darling and others (1994) uncovered an unlisted cased borehole between the two wells. A probe of the cased hole did not find an obstruction, and they reported depth to water of 620 ft (189 m) on 12/18/1992, a close match with depths reported by TWDB for other wells in that area of Southeast Eagle Flat.

Hot Wells is near the trace of the West Van Horn Mountains fault, as mapped by Collins and Raney (1993). It is the only area in which thermal water has been reported in Southeast Eagle Flat. Other occurrences of thermal groundwater in Eagle Flat are at Sierra Blanca, where a public water supply well drilled to 1,100 ft (335 m) in 1957 yielded water with a temperature of 100°F (38°C); and a water supply well at a prison approximately one mile south of Sierra Blanca which is reported to yield 100°F (38°C) groundwater.

The southwestern boundary of the trough between the Carrizo Mountains and the Eagle Mountains is formed by the East Eagle Mountains Fault (Collins and Raney, 1993); and it is in the trough underlying Southeast Eagle Flat where the thickest deposits of basin-fill are found in the Eagle Flat Basin.

The perspective from **Stop 2.3** offers a view of the northeast face of the Eagle Mountains. Prominent features from this point are the igneous core of the mountains, the Permian and Cretaceous sedimentary rocks that form a rim along the eastern front of the mountains, and the broad alluvial fan that reaches out into Southeast Eagle Flat as far as Eagle Flat Draw.

Remove **Geologic Map of Eagle Mountains** (Underwood, 1963) from envelop and refer to Figure 2.12. Locate "Hot Wells" and "Espy Ranch" between railroad Benchmarks 4,263 and 4,286 on map. The perspective from Hot Wells offers a clear view of important geological features along the northeast flank of the Eagle Mountains. The prominent ridge at 12:00 is known as "Espy Ridge". Exposed along the ridge are 1) metaquartzites, meta-arkoses, and amphibolites of Precambrian age, 2) Upper Permian Hueco Limestone, and 3) nine Cretaceous Period formations: Yucca Formation, Bluff Formation, Cox Sandstone, Finlay Limestone, Benevides Formation, Espy Limestone, Eagle Mountains Sandstone, Buda Limestone, and Chispa Summit Formation.

Espy Ridge is offset by three northwest-trending normal faults (Mine Fault, Spar Valley Fault, and Carpenter Fault), two prominent east-northeast-trending normal faults (Wind Canyon Fault and Rhyolite Fault), and many normal faults that break the Permian and Cretaceous formations into smaller blocks (Eagle Mountains Quad and Figure 2.12).

Just beyond the northwesternmost extent of Espy Ridge is a smaller but easily discernible mass of rocks of Permian age and Cretaceous age known as "Lone Hill". This area is broken into smaller blocks by two east-trending normal faults (Lone Hill Fault and Eagle Spring Fault). The northwest-trending Mine and Carpenter faults that cut through Espy Ridge appear to terminate at the Lone Hill Fault (Figure 2.12).

Return to vehicles, proceed across railroad tracks then through main gate to Cross L Ranch.

20.5 mi (33 km)

Follow paved road northwest. The road, known as Radar Road, continues for 13 miles (21 km), ending at the Federal Aviation Administration's radar station at Eagle Peak (Figure 2.12). For the next 6 miles (9.7 km), the road traverses the broad alluvial fan deposits spread toward the northeast from the Espy Ridge area. The fans extend as far to the northeast as Eagle Flat Draw. The Carrizo Mountains are north of the fans and the Van Horn Mountains are on the east.

26.4 mi (42.3 km)

The road turns toward the southwest, entering the easternmost extent of Wind Canyon. Rocks on either side of the road are dominantly Cox Sandstone (Cretaceous). From this point on, the road begins a steady ascent from the proximal area of the alluvial fan into the Eagle Mountains. The grade of the road is as much as 11 - 12 percent in the higher elevations of the mountains.

The house at 9:00 is a hunting lodge operated by the Cross L Ranch (Figure 2.12). Note the braided drainage pattern in the dry stream bed between Radar Road and the lodge. This drainage pattern is typical of streams that carry coarse sediment loads from steep terrains. The drainage pattern branches out into distributary channels where the stream discharges water and

sediment over the comparatively flatter surface of the alluvial fan that forms at the mouth of Wind Canyon (Figure 2.12).

27.4 mi (44 km)

The road begins to turn to the west-northwest as it enters the mouth of the narrow valley that follows the Spar Valley fault. Underwood's map of the Eagle Mountains (Underwood, 1963) shows the Spar Valley fault terminating at the Wind Canyon fault.

27.7 mi (44.6 km)

Turn right at unpaved road and follow lead vehicle 2 miles (3.2 km) to Spar Valley fluorspar mining site. Drive slowly. The road can be difficult to travel without four-wheel drive capability.

29.7 mi (47.8 km)

Stop 2.4 - Spar Valley mining site

Arrive at Spar Valley mining site.

The Espy Ridge – Lone Hill area of the Northeast Eagle Mountains is of special significance to the economic geology of the Eagle Mountains owing to the occurrence of fluorspar deposits. The Society of Economic Geologists' 1990 guidebook (Kyle, ed., 1990) includes the following with regard to fluorspar deposits of the Eagle Mountains:

> Fluorspar deposits are widespread in the Eagle Mountains. More than 30 occurrences are known in fissure veins along faults that cut a variety of igneous and sedimentary rocks and in disseminated bedding-replacement deposits in Cretaceous limestone. Fissure veins along major east-west normal faults appear to offer the greatest potential for commercial deposits; however, bedding-replacement deposits in limestone along bedding-plane faults have yielded most of the fluorspar produced in the district. Most of the 12,000 ± short tons of fluorspar shipped from deposits in the Eagle Mountains came from Spar Valley (Figure 2.13 of this guidebook). Spar Valley, a major drainage to the southeast in the east-central part of the Eagle Mountains, is developed along the northwest-trending Spar Valley fault.

A brief history of the discovery and mining of fluorspar from the Eagle Mountains is found in W.N. McAnulty (1974):

> Fluorspar was discovered in this district in 1919, but no ore was shipped until 1943. The U. S. Bureau of Mines conducted a program during 1943-45 designed to evaluate

the commercial potential of the district, which included geologic mapping, diamond drilling, trenching, and sampling.

Prospecting during 1942-48 resulted in discovery of fluorspar at several widely scattered places in the Eagle Mountains, especially in fissure veins in fault zones, northwest, southeast, south, and southwest of previously known deposits in Spar Valley. A 50-ton flotation plant was put in operation in Spar Valley in fall of 1945, and acid-grade concentrate was produced intermittently during 1945-46. Subsequently, the mill setup was changed to produce ceramic -grade concentrate.

From October 1945 to January 1949, a total of about 2,750 tons of acid- and ceramic-grade fluorspar concentrates was shipped. From November 1943 to October 1945, approximately 8,450 tons of metallurgical-grade fluorspar was shipped. Shipments from deposits in the Spar Valley area totaled about 11,400 tons. Fluorspar was discovered in the Eagle Springs area of the Eagle Mountains in the spring of 1943, and about 600 tons of metallurgical-grade fluorspar mined from deposits in that area was shipped in 1943. Fluorspar was discovered in the Rocky Ridge area in November 1943. Although an appreciable amount of exploratory excavating and sampling was done on Rocky Ridge deposits, little or no fluorspar was ever shipped. From1952 until 1970, the Eagle Mountains district received little attention.

A small amount of the fluorspar produced in Spar Valley was mined from veins and breccia zones along the Rhyolite fault where it crosses the upper end of Spar Valley. At places along the fault, brecciated zones up to 40 ft wide and 300 ft long are extensively fluoritized (McAnulty and Hoffer, 1980).

The only significant bedding-replacement deposits known in the Eagle Mountains are around the Northern and Southern Ore Body area in Spar Valley. They are confined to brecciated zones along bedding plane faults in the upper part of the (Cretaceous) Finlay Limestone.

Espy Ridge itself is offset by three northwest-trending normal faults (Mine Fault, Spar Valley Fault, and Carpenter Fault), two prominent east-northeast-trending normal faults (Wind Canyon Fault and Rhyolite Fault), and many normal faults that break the Permian and Cretaceous formation into smaller blocks (Figures 2.12 and 2.13). Just beyond the northwesternmost extent of Espy Ridge is a smaller but easily discernible mass of rocks of Permian age and Cretaceous age known as "Lone Hill". This area is broken into smaller blocks by two east-trending normal faults (Lone Hill Fault and Eagle Spring Fault). The northwest-trending Mine and Carpenter faults that cut through Espy Ridge appear to terminate at the Lone Hill Fault. Jacobs (1982) in his MS Thesis considers these areas to be along the northeast margins of the Eagle Mountains caldera and the many rhyolitic intrusions in this area to be emplaced as part of a ring-dike system.

Figure 2.14 is an oblique aerial photo taken from the Northern Ore Body at the head of Spar Valley looking to the southwest down the relatively broad Spar Valley. The valley follows the eastern margin of the Eagle Mountain caldera (Jacobs, 1982) and is occupied by two major faults, the Spar Valley fault and the Mine fault. Most of the productive mines are in this area, where the Mine Fault and Spar Valley faults intersect with the major east-west trending Rhyolite fault and other smaller east-west-trending faults.

The stop in Spar Valley is at the "Old Red Pit" locality (Figure 2.15), known as the Southern Ore Body. There were no underground diggings at this location and the ore is found as replacement deposits in the heavily altered limestones by silicification and fluoritization of the limestones. The ore here was at the surface and the mining was done in a series of trenches cut into the bedding. The ore lies along the Mine fault to the east with an associated rhyolite sill which underlies the Cox Sandstone, which can be seen on the east flank of the hill just south of the pit. The ore body horizon lies above reef beds in the lower part of the Finley Limestone. The ore occurs in a siliceous red limestone. It is in places vuggy and brecciated with many of the cavities filled with small fluorite crystals. Figures 2.16a and 2.16b show some examples of the ore found within the Old Red pit.

The most important and largest deposit of fluorite in the Spar Valley area is found at the Northern Ore Body (Figures 2.17 and 2.18). The deposit here is a bedding replacement body consisting of several beds of high-grade ore separated by beds of shale. The deposits are also associated with the reef beds within the lower Finley Limestone. The rhyolite present to the west of the shafts is an intrusive elongated plug based on field observations and interpretations of primary flow structures which are aligned along the direction of the hill This hill is mapped as part of the rhyolite ring dike system described by Jacobs (1982). Rhyolite is also present at the north end of the deposit, both in the underground and at the surface. The rhyolite adjacent to the shaft and faults and is highly silicified and brecciated. The fragments in this breccia are of both limestone and rhyolite. Veinlets and stringers of fluorite ore are present in the brecciated zone. The thickness of the replacement ore body beds varies with many being 5 to 10 feet (1.5 to 3 m) thick.

Figure 2.17, an aerial drone shot, shows a number of aligned shafts sunk down into the hill. The shafts in places go down 200 ft (61 m). This area is highly faulted and many of the ore zones are faulted off. At the time Gillerman (1953) and Underwood (1962, 1963) did their work in the Eagle Mountains, the geology and fluorspar in this area were not yet recognized as being a caldera feature. In the late 70s and early 80s, UTEP students interpreted the fluorspar deposits and associated faulting and igneous intrusions as 'features located within a down-dropped caldera block. Jacobs (1982) attributes much of the highly faulted and intruded rocks within the caldera as being due to the down=dropping of the caldera floor during the inception of the eruptions of massive volumes of volcanic rock. The massive volcanic rocks and syenites are also considered to be intra-caldera. Jacobs (1982) surmises that the floor collapsed with the caldera highly shattered and faulted. This formed multiple avenues for the movement of mineralizing

117

hydrothermal fluids. Most of the igneous intrusive dikes and sills in the Eagles are similar in geochemical character to the lower rhyolite; however there are some dikes and sills that are distinctively different. At this time, there is not a clear answer to the spatial relationship of these different intrusions to each other.

At the Northern Ore Body, the ore within the high-grade beds, averaging from 69-75% CaF_2, are coarsely crystalline, granular and vuggy in places. Many of the cavities are lined with large well-formed fluorite crystals and small clusters of crystals (Figures 2.16a,b). There are also many crosscutting veinlets and fissures of high-grade ore. The deposit has high-grade beds alternating with intervening lower-grade beds. In general, the lower-grade beds are shaly in nature and less permeable to the mineralizing fluids. Figure 2.18 is an aerial photo taken directly down one of the major shafts. It appears that some vertical fissures or mineralized beds can be seen on the walls of the shaft.

The mineralization and shafts here are closely associated with what Jacobs (1982) mapped as a fairly large rhyolite dike or stock-like intrusion and is part of what he interpreted to be the eastern segment of the ring-dike system of the Eagle Mountain caldera (Figure 2.19). It is one of the larger intrusive bodies delineated and segregated out of the 'Lower Rhyolite' sequence.

Figure 2.20 is a part of a topographic map of the northeast Eagle Mountains (Jacobs, 1982). The main focus of Jacobs' thesis (Jacobs, 1982) was to segregate out areas of intrusive igneous rocks from rocks previously mapped and lumped into the overall 'Lower Rhyolite' unit of Gillerman (1953) and Underwood (1962).

The location of the map is the Southern Ore Body which is in the saddle between the northern edge of the small hill south of where the 'well' is denoted on the map. The Northern Ore Body discussed above is approximately where the 'x' is beneath the TRD (Tertiary Rhyolite Dike) in the center of the map (Figure 2.20). The eastern fault on the map is the major Spar Valley Fault and the western fault on this map is the Mine Fault. Not shown on the map is the major east west Rhyolite Fault which cuts across the map just to the north of the TRD symbol. This fault supposedly cuts off most of the mineralization in the rocks of the Northern Ore Body (Gillerman, 1953).

Figures 2.19 and 2.20 show Jacobs' (Jacobs, 1982) interpretation of the location of the southern, eastern and northeastern Eagle Mountain Caldera boundaries based on the location and trend of the major faults and associated rhyolite and quartz latite intrusive bodies. This interpretation places the Spar Valley Mining district within the eastern boundary of the caldera. This location is just south of the northeast trending, elongated dike/plug (in red} shown to the right of the center of the map. Note that Figure 2.19 shows the Northern Ore Body and rhyolite intrusion cut off by the major east-west trending Rhyolite fault (Jacobs, 1982).

Smaller fluorspar mines can be seen from this location. Toward the northeast, a few diggings are apparent along the road that traverses along the flank of Espy Ridge near the head of Spar Valley. That is the Rhyolite Vein Mine and it lies along the east-west Rhyolite Fault (Figure 2.21). The mineralization appears to be in a fissure vein cutting through the wall rocks. A short adit, mentioned in Gillerman (1953) must now be collapsed as there is no evidence of the adit. As in the Northern Ore Body shaft directly across the Spar Valley drainage, near vertical fissures can be seen in the pit wall. Driving up the road to a saddle on Espy Ridge there is a minor rhyolite intrusive rock in the saddle. The saddle in Espy Ridge is formed and cut by the Rhyolite Fault.

From the Old Red Pit and looking south down Spar Valley, one can see diggings and a mine dump at about 2:00 on the upper part of a hill in the distance (Figure 2.22). This is the No. 4 Shaft Mine, located along a minor east-west fault. A couple of adits were driven into the hill to the southwest and to the north. There was some stoping along the southwest adit, and this appears to come to the surface at a trench to the southwest on the hillside in Figure 2.23. The mineralization and ore are found in fissure veins.

There are numerous other fluorspar deposits in the Eagle Mountains outside of Spar Valley, such as the Lucky Strike in the Eagle Spring mine areas. These mostly occur at the intersection of northwestward and east-west trending faults. These are numerous smaller isolated, highly silicified, replacement type deposits, most of which show the same northwestward orientation. The mineralization is similar to that found in the Southern Ore Body. Smaller vein and fissure deposits can also be found in the rhyolites.

Another place of interest that can be found in the northeast Eagle Mountains, in the Lone Hill area, is Eagle Spring, perhaps the most significant spring in Hudspeth County. From 1854 to 1882, the spring supplied water to stage traffic on the route the route between San Antonio and El Paso (Underwood, 1963). Stage traffic did not follow a more northern route through Eagle Flat because of the absence of springs and perennial streams. Figure 2.24 is a picture of the monument commemorating the Eagle Spring Stage Station.

The commemoration is as follows:

> EAGLE SPRING STAGE STAND - A station 1854-1882) for the stage coaches and wagon trains of the Overland-Chihuahua Trails, which linked the Pioneer West, brought heartening mail and passengers, and supplies, and quickened the life of this remote region, then far out on the lonely fringes of the frontier civilization".

Figure 2.25 is a drone aerial shot of the Eagle Spring stage stand.

After visit to Spar Valley, return 2 mi (3.2 km) to Radar Road.

31.7 mi (51 km)

Radar Road begins 0.70-mile (1.1 km) traverse of braided stream deposits at the mouth of Spar Valley. Lithologies encountered beyond this point of the drive to Eagle Peak are dominantly rhyolites, trachyte porphyries, and syenites. Follow road 1.1 miles (1.8 km) along Wind Canyon to Eagle Mountains Ranch House.

32.8 mi (52,8 km)

Arrive at Eagle Mountains Ranch. The ranch house is near the contact between trachyte porphyries and upper rhyolites of the Eagle Mountains igneous complex. Wait for gate to be unlocked and continue slowly along road. For the next half mile, rocks on either side of the road are upper rhyolites. At approximately 0.5 mile (0.8 km), the Eagle Peak syenite predominates on the road to the summit.

34.1 mi (54.9 km)

Radar Road makes a sharp turn into a north-northwest narrow canyon. Between the Eagle Mountains ranch house and this turn, the road has climbed approximately 700 ft (213 m) over a distance of 1.3 miles (2.1 km); that is, over a gradient of approximately 11 percent. From this point, Radar Road follows the narrow northwest-oriented canyon another 1.8 miles (2.9 km) to the FAA radar station. The elevation at the station is approximately 7,440 ft (2,270 m), and the steepness of the climb is 12.3 percent. Shift vehicles into low gear and do not exceed the posted speed limit.

35.9 mi (55 km)

Stop 2.5 - Eagle Peak

Pull into the parking area at the radar station. Eagle Peak is the prominent nob approximately 500 ft (152 m) northeast of the radar station (Figures 2.26a and 2.26b). The panoramic view from Eagle Peak is one of the most impressive in all of Texas (Figure 2.27 to 2.30). Much of the following text is taken from "The View from Eagle Peak: Physiographic and Geologic Setting of the Eagle Mountains Region" (Underwood, 1975). Figure 2.31 has been added to accompany the text. Features described by Underwood (1975) are identified on Figure 2.31 by bold letters.

> Eagle Mountains and vicinity … includes Devil Ridge (**A**), Eagle Mountains (**B**), and Indio Mountains (**C**). This superb geological laboratory includes: (1) well-exposed rocks ranging in age from Precambrian to Recent, including a small inlier of metamorphosed Precambrian sedimentary rocks, small inliers of lower Permian limestone, approximately 7,000 feet of marine Cretaceous rocks with varied composition and complex facies, an early Tertiary sequence of fine-grained flow and pyroclastic rocks , and intrusive rocks in the form of

dikes and sills and a small stock; (2) complicated structural relationships created by late Cretaceous to early Tertiary folding and thrust faulting and late Tertiary block faulting, and (3) a recently developed, through-flowing drainage system, the Rio Grande (**D**), that has created conspicuous alluvial fans and terraces. The Eagle Mountains (**B**), together with the Indio Mountains (**C**) and Devil Ridge (**A**), like other ranges in the region, form a horst that is flanked by grabens. The highlands and the partly filled intermontane basins constitute bolsons, e.g. Green River (**E**), Eagle Flat (**F**), and Red Light (**G**) bolsons.

The Eagle Mountains (**B**) are a topographically high mass of Tertiary volcanic and intrusive rock overlying marine limestone, shale, and quartz sandstone of Cretaceous age. In small areas on the north and northeast flanks, Permian limestone and Precambrian metasedimentary rocks are exposed.

Devil Ridge (**A**) is a northwesterly trending ridge that extends from the northwest flank of the Eagle Mountains (**B**) almost to Sierra Blanca, Texas. In Devil Ridge (**A**), Lower Cretaceous limestone, sandstone, and shale are thrust over Upper Cretaceous sandy limestone and shale. Small early Tertiary dikes and sills have penetrated the Cretaceous rocks.

The Indio Mountains (**C**), which extend southward from the Eagle Mountains (**B**) to the Rio Grande (**D**), are composed largely of marine strata of Cretaceous age. Tertiary volcanic rocks cover a large area in the southern part of the mountains; intrusive rocks are volumetrically minor and occur only in the northern Indios.

The map area is near the northwest end of the Laramide Chihuahua tectonic belt. The Eagle Mountains (**B**) are part of the eastern-most range of the belt, which begins more than 100 miles to the southeast near Ojinaga, Chihuahua and terminates at Sierra Blanca, Texas.

North to northwest-trending thrust faults are prominent in Devil Ridge (**A**) and in the Indio Mountains (**C**). The southwestward and westward movement of the overthrust block along some of the faults in the Indio Mountains (**C**) is opposite to the northeast movement of the overthrust blocks along the faults in the Devil Ridge (**A**) area. Late Tertiary normal faulting and subsequent erosion are responsible for the current topography.

The summit of Eagle Peak, 7,496 ft. (2,286 m) above sea level, the highest point in Hudspeth County and the eighth highest peak in Texas, affords an unexcelled view of the vast part of Trans-Pecos Texas and northern Chihuahua.

To the north, Guadalupe Peak (**H**), the highest point in Texas with an elevation above sea level of 8,752 ft (2,268 m), and El Capitan, only 500 feet (152 m) lower, are both remnants of the mighty Permian Capitan barrier reef that bordered the Delaware basin. These lofty

limestone masses separate the Hueco bolson (**I**) to the west from the Salt Basin (**J**) to the east. Sierra Diablo (**K**), a north-trending range along the eastern margin of the Diablo Plateau, overlooks the Salt Basin (**J**) to the east and contains the most nearly complete rock record of any physiographic feature in the region. In these mountains, rocks ranging in age from Precambrian through Cretaceous, excepting those of Cambrian, Triassic, and Jurassic age, are well exposed.

Salt Basin (**J**) is a remarkable smooth-floored depression more than 100 miles long, averaging 20 miles wide, into which water drains from all directions. This closed basin, the easternmost of those of the Basin-and-Range province, is a long, narrow north-trending half graben, bordered on the west by the Sierra Diablo (**K**) and on the east by the Delaware (**L**) and Apache (**M**) mountains.

The Delaware Mountains (**L**) are an elongate north-northwest trending fault block in which Permian sandstone and shale of the Delaware basin facies have been uplifted and exposed. In contrast, the Apache Mountains (**M**) are an aboveground northwest-trending part of the ancient Capitan Reef.

Much nearer and just north of Van Horn are the Beach (**N**) and Baylor (**O**) mountains, relatively small fault block composed) up the uneven skyline to the west and northwest.

The western boundary of the Red Light Basin is the Southern Quitman Mountains (**W**). The Southern Quitmans are folded and thrust-faulted Cretaceous rocks. Tertiary intrusive and flow rocks make up most of the Northern Quitman Mountains (**X**).

Just north of the Quitmans (**X**) and near the western margin of the Diablo Plateau (**Y**) is easily the more distinctive feature of this panorama. Sierra Blanca (**Z**), "White Mountain", a laccolith with convex slopes sweeping gracefully to a summit 6.700 feet above sea level.

The Malone (**A***) and Finley (**B***) mountains, low ranges farther west and northwest on the western margin of the Diablo Plateau (**Y**), contain gently folded rocks large of Permian and Cretaceous age. The Malone Mountains (**A***) contain the only outcrop in Texas of marine strata of Jurassic age.

The Hueco (**C***) and Cordnudas (**D***) mountains, some 50-60 miles (80 – 96 km) northwest and north-northwest, respectively are relatively low-lying masses that extend northward into New Mexico. The Hueco Mountains (**C***), lying along the northwest margin of the Diablo Plateau (**Y**) and the east margin of the Hueco Bolson (**I**), is a barren range composed primarily of sedimentary rocks of Paleozoic age. Along the southern margin of the mountains there are scattered small outcrops of red granite which have been identified as Precambrian in age; to the north near the state line there are Tertiary

The Cornudas Mountains (**D***), some 20 miles east of the Huecos (**C***) and also along the New Mexico border, are composed of Cretaceous sedimentary rocks intruded by Tertiary alkalic igneous rocks similar to those in the Hueco Mountains (**C***).

This geologically spectacular region thus exposes a rock record that spans more than a billion years of earth history and a rock record that varies from scattered exposure of the very old Texas craton to the alluvium that was deposited by most recent flood of the Rio Grande.

48.4 mi(78 km)

Stop at intersection of Radar Road and dirt road. Turn right at intersection and follow dirt road parallel to railroad tracks. This path back to Van Horn follows the railroad tracks through the Scott's Cross water gap, 8 miles (12.9 km) southeast of the intersection (Fig. 2.32). The southern Carrizo Mountains are north of the railroad tracks, and Eagle Flat Draw is south of the road. Toward the south are the broad fans built toward the northeast by streams draining the Eagle Mountains and Espy Ridge. Further toward the south is Green River Valley.

56.4 mi (90.8 km)

Follow dirt road across railroad tracks and proceed northeast 8.3 miles (13.4 km) to Van Horn. Immediately northeast of the tracks is an arroyo. This is the point at which Eagle Flat Draw discharges into Lobo Valley. Toward the south-southeast are the northernmost rocks of the Van Horn Mountains. These mountains owe their present form to late Tertiary block-faulting. Structurally, the Van Horns are a northward-trending horst flanked on the east and west by intermontane basins (Twiss, 1957). Precambrian metasedimentary rocks are exposed in the northernmost areas of the mountains.

The road swings toward the northeast and enters the Lobo Flat area east of the Carrizo and Van Horn Mountains and south of the city of Van Horn. The road northeast of Scott's Crossing proceeds for 8 miles (12.9 km) to Van Horn.

REFERENCES

Collins, E.W., and Raney, J.A., 1993, Late Cenozoic faults of the region surrounding the Eagle Flat study area, northwestern Trans-Pecos Texas: Univ. of Texas at Austin, Bureau of Economic Geology final contract report prepared for Texas Low-Level Radioactive Waste Disposal Authority, 74 p.

Darling, B.K., Hibbs, B.J., and Dutton, A.R., 1994, Ground-water hydrology and hydrochemistry of Eagle Flat and surrounding area: Univ. of Texas at Austin, Bureau of Economic Geology contract report prepared for Texas Low-Level Radioactive Waste Disposal Authority, 173 p.

Davis, B.R., 2007, Complex structural and fluid flow evolution along the Grenville Front, Trans-Pecos Texas: Univ. of Texas at Austin, M.S. thesis, 231 p.

Davis, B.R., and Mosher, S., 2015, Complex structural and fluid flow evolution along the Grenville Front, west Texas: Geosphere, v. 11, no. 3, p. 868-898.

Davidson, D.M. Jr., 1980, Precambrian geology of the Van Horn Area, Texas: New Mexico Geological Society 31st Field Conference Guidebook, p. 151-154.

Durfee, B.A., 1982, Geology and structure of the Carrizo Mountain metarhyolites, Culberson and Hudspeth counties, Texas: Univ. of Texas at El Paso Ph.D., dissertation, 120 p.

Ewing, T.E., Texas Through Time: Univ. of Texas at Austin, Bureau of Economic Geology, 431 p.

Gillerman, E., 1953, Fluorspar deposits of the Eagle Mountains, Trans-Pecos Texas: U.S. Geological Survey Bull. 987, 98 p.

Jacobs., M.A., 1982, Tertiary rhyolite intrusives of the northeastern Eagle Mountains, Hudspeth County, Texas: Univ. of Texas at El Paso M.S. thesis.

Kyle, J.R., 2011, Geology of Texas industrial minerals: Austin Geological Society Bull., V. 7, p. 29-43.

Kyle, J.R. and Elliott, B.A., 2021, Texas mineral resources within or affected by Proterozoic basement structures, *in* Callahan, O.A. and Eichhubl, P., eds., The geologic basement of Texas: a volume in honor of Peter Flawn: Univ. of Texas at Austin, Bureau of Economic Geology, Report of Investigations 286, ch. 4.

McAnulty, W.N., 1974, Fluorspar in Texas: Univ. of Texas at Austin, Bureau of Economic Geology Handbook 3, 31 p.

McAnulty, W.N. and Hoffer, J.M., 1980, Second day road log from Van Horn to Tumbldown Mountain, Hazel Mine, Southern Wylie Mountains and return to Van Horn: New Mexico Geological Society, 31st Field Conference Guidebook, p. 19-25.

Muehlberger, W.R., 1980, Texas Lineament revisited *in* Trans Pecos Region: New Mexico Geological Society Guidebook, 31st Field Conference, eds. Dickerson, P.W.; Hoffer, J.M; Callender, J.F.

New Mexico Geological Society, 1990, Industrial Mineral Resources of the Delaware Basin, Texas and New Mexico, ed. Kyle R.

Price, J.G., Henry, C.D., and Standen, A.R., 1983, Annotated Bibliography of Mineral Deposits in Trans-Pecos Texas: Univ. of Texas at Austin, Bureau of Economic Geology, Mining and Minerals Resources Research Institute Mineral Resources Circular No. 73, 108 p.

Underwood, J.R., 1962, Geology of the Eagle Mountains and Vicinity, Trans-Pecos Texas: Univ. of Texas at Austin Ph.D. dissertation, 560 p.

_____, 1963, Geologic Map of the Eagle Mountains and Vicinity, Hudspeth County, Texas: Univ. of Texas at Austin, Bureau of Economic Geology, Quadrangle Map No. 26.

_____, 1975, The view from Eagle Peal: physiographic and geologic setting of the Eagle Mountains region *in* Geology of the Eagle Mountains and Vicinity, Trans-Pecos Texas Texas. Society of Economic Paleontologists and Mineralogists, Permian Basin Section Guidebook Pub. 75-15, p. 59-61.

GEOLOGY OF HUDSPETH COUNTY, TEXAS

**GUIDEBOOK OF AIPG-TEXAS
SPRING FIELD TRIP
APRIL 21 – 23, 2023**

FIGURES 2.01 – 2.32

Figure 2.01 – Locations of Stops 2.1 – 2.3 of Day Two road log.

Figure 2.02a

Figure 2.02b

Photos by Paul Warren

Figure 2.02a – Metaigneous rocks at roadcut (Stop 2.1) **Figure 2.02b** – Field trip participants examine metaigneous rocks of Carrizo Mountain Group at Stop 2.1. Photos by Paul Warren.

Figure 2.03a

Figure 2.03b

Figure 2.03a – Phyllite exposed along roadcut at Stop 2.1. **Figure 2.03b** – Metarhyolite exposed along roadcut at Stop 2.1. Photos by BK Darling.

129
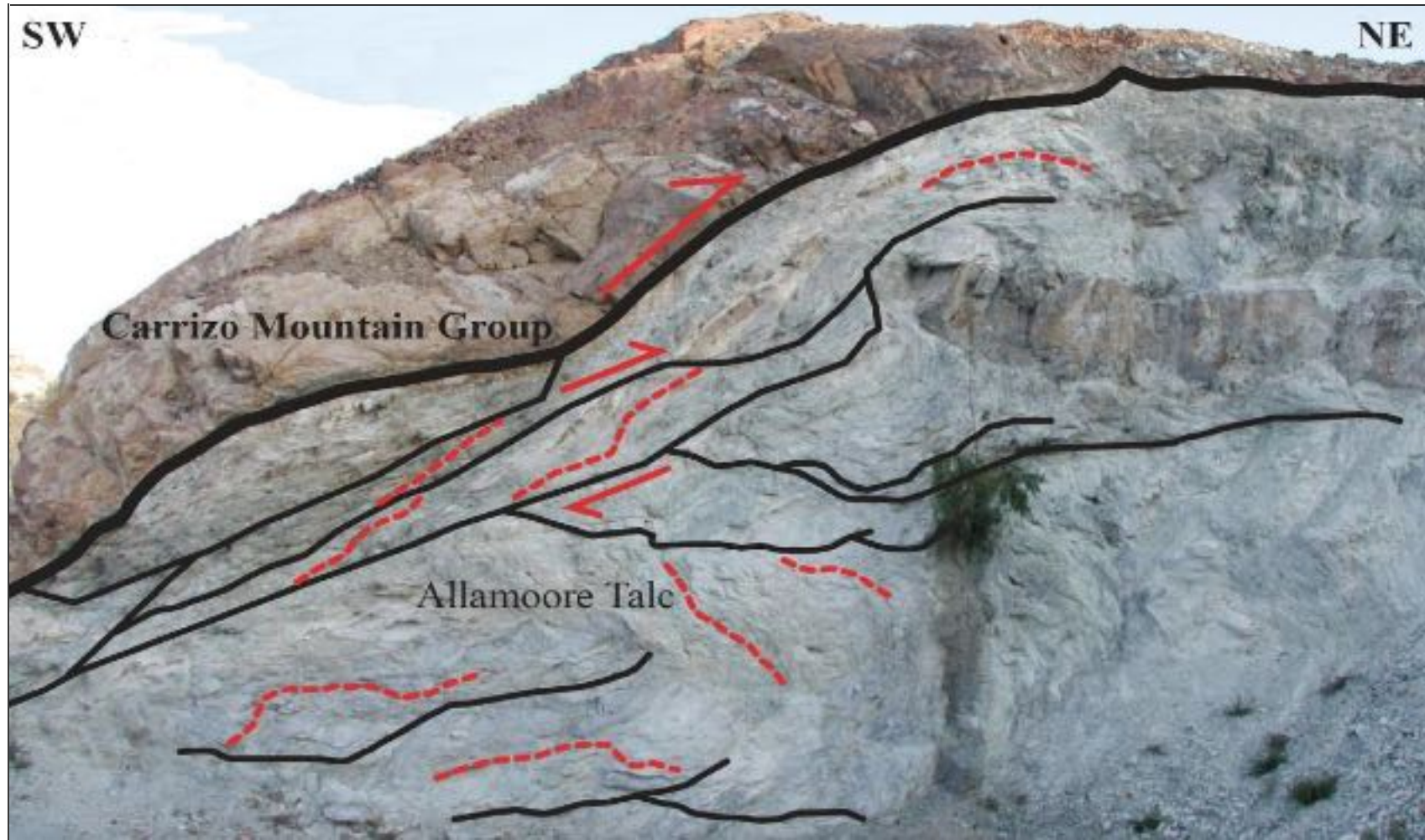
Figure 2.04 - Allamoore Formation talc and Carrizo Mountain Group along the Streeruwitz Thrust, Texola mine, Allamoore talc district, Hudspeth County, Texas. From Kyle (2011), after Davis (2007).

Figure 2.05 – Precambrian metarhyolite at Desert Rock quarry. Carrizo Mountains in background. Photo by BK Darling.

Figure 2.06 – Old area of main pit at Desert Rock quarry. The hill in background is composed of Campagrande and Cox formations (Cretaceous). The pit and the hill are separated by the Hillside fault (see **Figure 2.01**). Photo by BK Darling.

Figure 2.07a

Figure 2.07b

Figures 2.07a and 2.07b – Field trip participants gather in office of Natural Minerals to hear Ben File (mining engineer) explain occurrence and mining of talc and history of talc mining at Allamoore. Photos by Paul Warren.

Figures 2.08a and 2.08b – Examining exposures of talc and folds in talc at main quarry. Photos by BK Darling.

Figure 2.09a

Figure 2.09b

Figures 2.09a and 2.09b – Field trip participants examine folds in talc at main quarry. Photos by BK Darling.

Figure 2.10 – Stopping for lunch at Hot Wells and discussion of thermal groundwater and history of old Hot Wells hotel and thermal bath house. Eagle Mountains in background. Photo by Diane Darling.

Figure 2.11a

Figure 2.11b

Figures 2.11a and 2.11b – Concrete structures used to support pumps at old Hot Wells station, hotel, and bath house. Photos by BK Darling.

Figure 2.12 – Google Earth image of Eagle Mountains. Shown are the image is the path of Radar Road, Eagle Peak, other prominent geological features and major faults.

Figure 2.13 – Fluorspar mines of Spar Valley. From McAnulty (1974).

139

Figure 2.14 – Oblique aerial photograph looking southwest from the head of Spar Valley. Photo by Michael Jacobs.

Area of intense silicification and Fluoritization along mined trenches

Figure 2.15 – Overhead view of the Southern Ore Body – "Old Red Pit" area. Photo by Michael Jacobs.

Figure 2.16a

Figure 2.16b

Figures 2.16a and 2.16b – Silicified and brecciated rocks with quartz, calcite and fluorite crystal filled vugs and fractures Southern Ore Body, 'Old Red Pit'. Photos by Michael Jacobs.

Figure 2.17 – Oblique aerial view of the shafts in the Northern Ore Body.

Figure 2.18 – Overhead view of the main vertical shaft (200') in the Northern Ore Body.
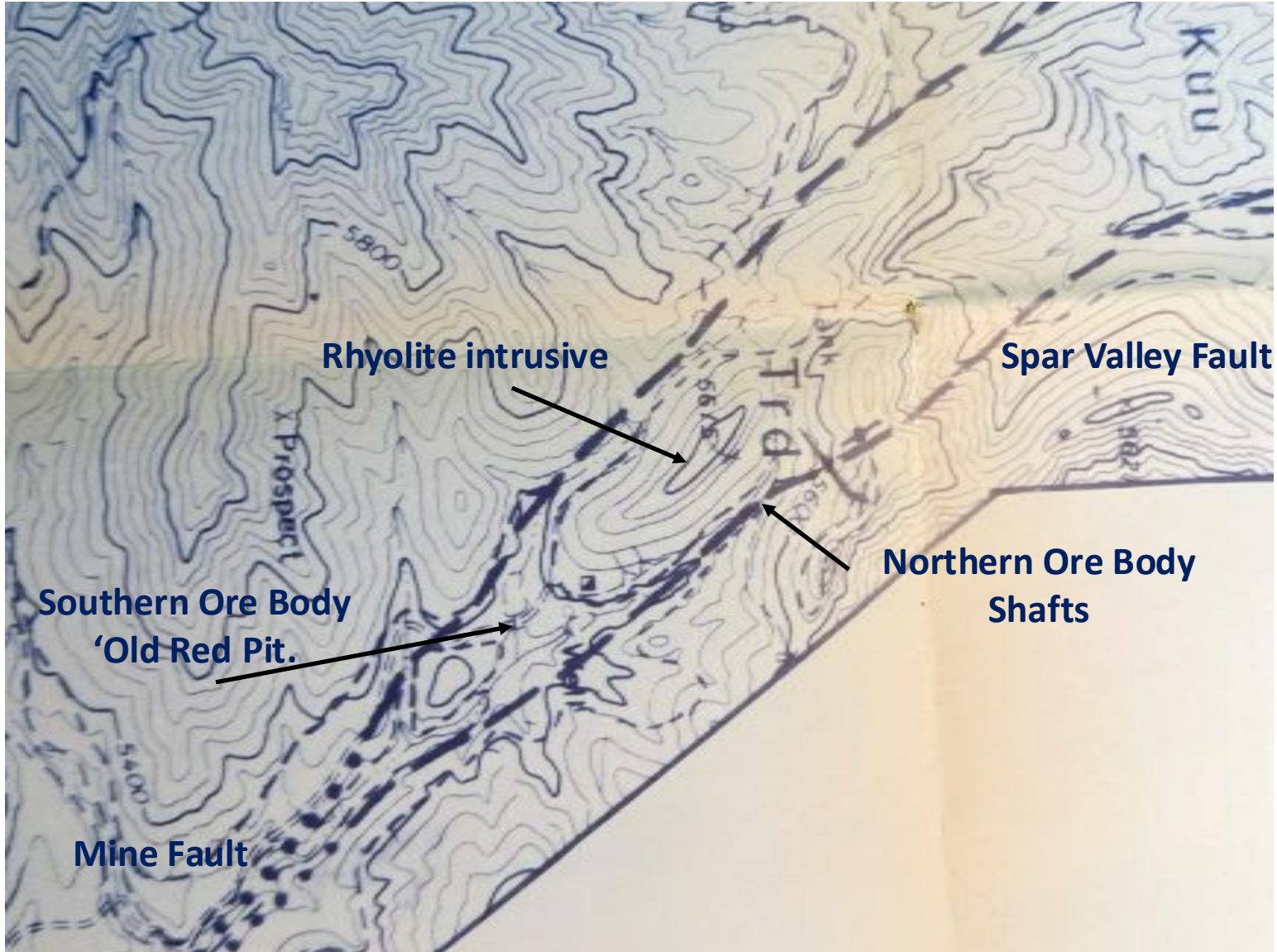
Figure 2.19 – Map showing the interpreted Eagle Mountain Caldera Boundary and major Intrusive rhyolitic ring dikes, sills and plugs (Jacobs, 1982).

Figure 2.21 – Aerial view of the Rhyolite Vein Mine located to the north on Espy Ridge.
Photo by Michael Jacobs.
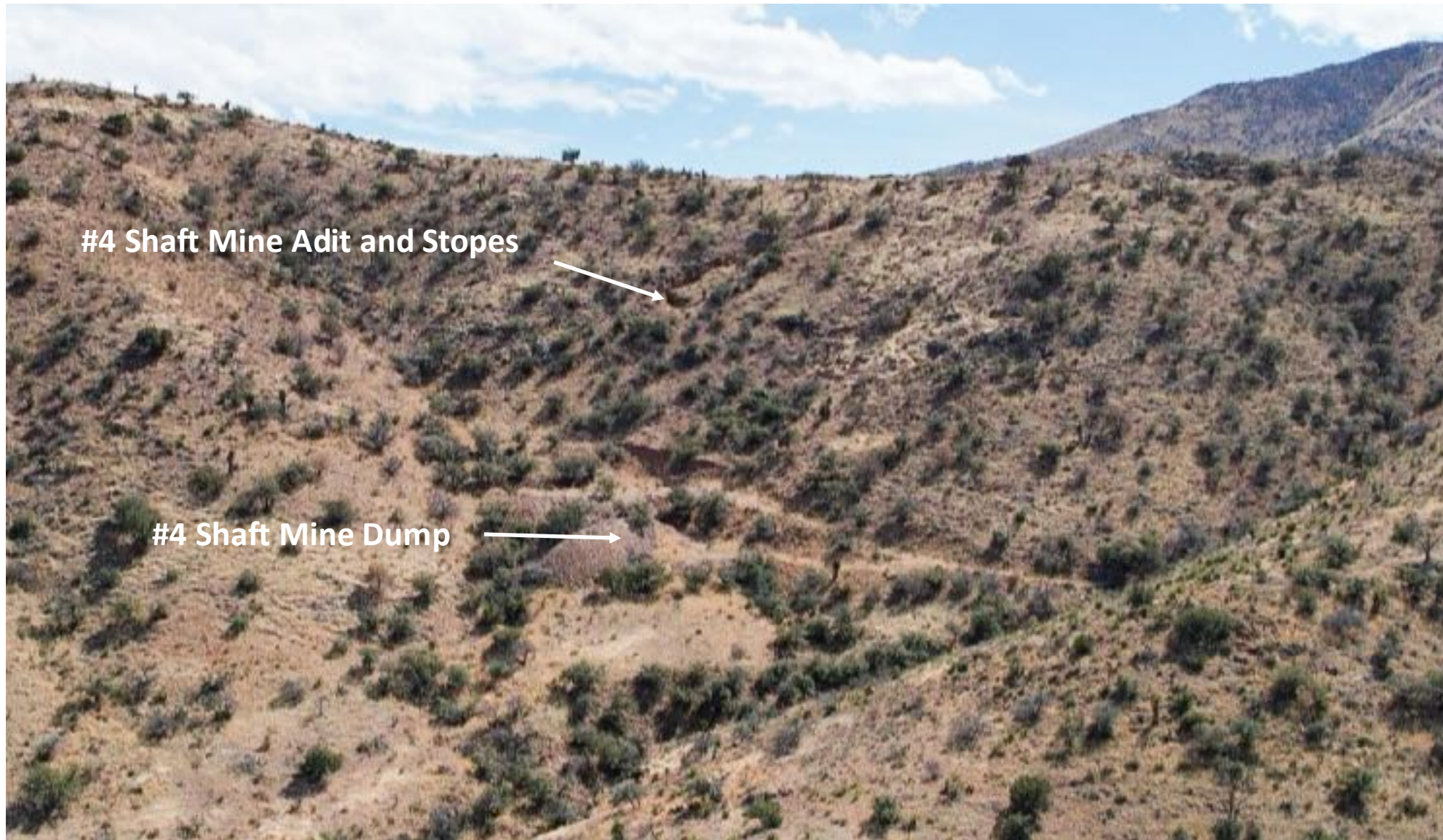
Figure 2.22 – Overhead view of the Southern Ore Body – "Old Red Pit" area – Spar Valley Stop. Photo by Michael Jacobs.

Figure 2.23 – Overhead view of the Southern Ore Body – "Old Red Pit" area – Spar Valley Stop. Photo by Michael Jacobs.

Figure 2.24 – Marker of the Butterfield Stage Station at Eagle Springs, northeast Eagle Mountains. Photo by Michael Jacobs.

Figure 2.25 – Oblique aerial photograph of the Eagle Spring Stagecoach Station. Photo by Michael Jacobs.

Figure 2.26a

Figure 2.26b

Figure 2.26a - Eagle Peak and FAA radar station as seen from paved road to the radar station. **Figure 2.26b -** Eagle Peak as seen from FAA radar station. Photos by BK Darling

Figure 2.27 – View toward the northwest across Red Light basin from FAA radar station. Quitman Mountains are in the background. Photo by BK Darling.

Figure 2.28 – View toward the southwest from road to FAA radar station. Diabase dike intrudes Eagle Peak syenite.. Southern Eagle Mountains and Indio Mountains are south of the diabase dike. Photo by Paul Warren.

Figure 2.29 – View toward the northeast from road to FAA radar station. Shown in the photo are Southeast Eagle Flat, Eagle Flat Draw, the Carrizo Mountains, Lobo Valley and Wild Horse Flat. The mountains in the upper right corer of the photo are the Wylie Mountains. Van Horn is in upper left quadrant of photo. Photo by Paul Warren.

Figure 2.30 – View toward the southwest across southern Red Light basin. Photo by BK Darling.

Figure 2.31 Geological features described by Underwood (1963)

Figure 2.32 – Return to Van Horn along road through Scott's Crossing

© Paul Q. Warren

GEOLOGY OF HUDSPETH COUNTY, TEXAS

GUIDEBOOK OF AIPG-TEXAS
SPRING FIELD TRIP
APRIL 21 – 23, 2023

ROAD LOG – DAY THREE

OVERVIEW OF ROAD LOG – DAY THREE

The Day 3 road log is a traverse around and over the Diablo Plateau. Beginning in Van Horn, the 150-mile (241 km) drive north along the Sierra Diablo escarpment to the Guadalupe Mountains, then west through the northernmost reaches of the Salt Basin graben, then south to Sierra Blanca lays out the complex geology of the plateau, emphasizing the key role that this structure played in the evolution of the basins and mountains south of the plateau.

Road log by: Bruce K Darling and Michael Jacobs

Begin road log

Begin at TX 54 and Broadway. Travel north on TX 54.

0.80 mi (1.3 km)

Bridge across arroyo. Beach Mountain is at 11:00, and the Baylor Mountains are straight ahead Figure 3.1). Wild Horse Flat is east of the highway.

Rocks that make up Beach Mountain range from Bliss Sandstone (Cambro-Ordovician) to El Paso Formation and Montoya Dolomite (Ordovician). Sections of the mountain are capped by Hueco Limestone (Permian Wolfcamp).

An eastward-dipping fault block, Beach Mountain is nearly circular in plan, with a diameter of approximately 5 mi (8 km). The mountain is bounded on the east by a fault which forms the southwestern boundary of the Salt Basin graben, and on the north by a northwest-trending fault that separates Beach Mountain from the Baylor Mountains to the northeast. Valleys cut in Precambrian rocks bound Beach Mountain on the northwest, west and south sides; and the mountain itself is cut by high-angle normal and minor thrust faults (McAnulty and Hoffer, 1980; Clark and Kyle, 1990)

The Baylor Mountains are a fault block that consists of El Paso Formation and Montoya Dolomite, capped by rocks of the Hueco Limestone and Bone Spring Formation (Permian - Leonardian).

The Delaware Mountains lie east of the Salt Basin. The mountains consist of fine-grained basinal clastic rocks equivalent to Capitan Limestone (Permian – Guadalupian) and older Permian shelf-edge carbonates (Clark and Kyle, 1990).

The Apache Mountains are south of the Delaware Mountains. The Apache Mountains are composed of members of the Capitan Limestone (Seven Rivers, Yates, and Tansill formations).

East of TX 54 lies the northernmost area of Wild Horse Flat, a southern extension of the Salt Basin. Wild Horse Flat is a major source of water to support irrigation in this area of Culberson County. In 1994, the City of El Paso purchased 20,000 acres north of Van Horn for $70/acre ($1.4 million), with the long-term objective of developing a well field to supply water for El Paso Water Utilities (Kreitler and Darling, 1997). The appraised dryland value of the property was estimated to be $60/acre, so El Paso paid $10 per acre for groundwater in storage. The average saturated thickness was estimated to be 425 ft (130 m). Assuming a conservative effective-porosity estimate of 15 percent and a recovery factor of 50 percent, the volume of recoverable water in storage would be 637,500 acre-ft. An acre-ft is equal to a volume of water 1 ft (0.3 m) deep over an area of 1 acre (approx. 326,000 gallons). El Paso has not attempted to develop the property.

9.8 mi (15.8 km)

Stop 3.1 - Beach Mountain, Baylor Mountains, southeastern Diablo Plateau and Hazel Mine

Pull over the right after crossing the bridge over Sulfur Creek. The highway follows the south Baylor Mountain fault at this point and then turns toward the north, along the west side of the Baylor Mountains (Figure 3.01). Along the northwest path of the road over Sulfur Creek, the prominent southeastern edge of the Diablo Plateau can be seen west of TX 54 (Figures 3.02a,b). The Hueco limestone lies on red shales and sandstones of the Hazel Formation (Proterozoic). At the point where the fault turns toward the north, the high escarpment that forms the Sierra Diablo can be seen at 11:00. In this area, the Van Horn Sandstone (Precambrian) is wedged between the Hueco and Hazel formations.

At the northward bend of TX 54, the road west of the highway leads to the Hazel Mine, approximately 2.4 mi (3.9 km) to the west (Figures 3.01 and 3.03). The Hazel mine (Price and others, 1983) was one of the oldest mines in Texas and the State's largest copper-producing property. The Hazel Mine was in operation from 1856 to 1947. From 1891 to 1947, the mine yielded 37 tons of ore containing 850,000 lbs of copper (1.1%), and 678,000 oz of silver (18 oz/ton). Between 1880 and 1886, an additional 80,000 tons of high-grade silver and copper ore were produced. The estimated total production from the Hazel Mine was 110,000 tons containing 1.5 million lbs of copper (0.7%) and 4 million oz of silver (36 oz/ton).

The mine works consisted of three main shafts, extensive underground drifts and stopes, and two open stopes. Deeper workings of the mine were flooded about 1900 (Flawn, 1952; McAnulty and Hoffer, 1980).

18.8 mi (30.3 km)

Stop 3.2 - Victorio and Babb flexures and left-lateral faults of Salt Basin

TX 54 crosses the North Baylor Mountain Fault (Figure 3.01). King (1965) and Goetz (1977) observed that the Victorio Flexure, a prominent northwest-trending monocline on the southern area of the Diablo Plateau, appears to project along a southeastern path across the Salt Basin, aligning with the North Baylor Mountain Fault, and continuing between the northern boundary of the Apache Mountains and the southernmost extent of the Delaware Mountains (Figures 3.04 – 3.05). Named for Victorio Peak, the flexure is exposed on the Sierra Diablo Escarpment (Figure 3.06).

Also shown on Figures 3.04 and 3.05 is the trace of the Babb Flexure, another northwest-trending monocline located about 12 mi (19 km) north of the Victorio Flexure. The Babb Flexure projects at the edge the Sierra Diablo escarpment where the prominent cliff makes a sharp turn toward the west-northwest (Figures 3.04 and 3.07).

The northwest trend of the escarpment along the Babb Flexure (Figure 3.04) continues for approximately 8.5 mi (13.7 km) before turning north-northwest. The flexure projects northwest across the northern Diablo Plateau as a down-to-north/northeast normal fault that runs just north of a Tertiary igneous intrusion (sill) known as Sierra Prieta. This linear trend can be projected further toward the northwest to align approximately with the Red Hills intrusion and smaller Tertiary intrusions exposed at Pump Station Hills (Figure 3.22). Mullican and Mace (2001) describe the Babb flexure as a west-northwest-trending monocline about 1 to 2 mi (1.6 to 3.2 km) wide with downward

displacement of strata on the north side of the flexure that may be traced about 40 mi (64 km) northwestward from the Salt Basin. King (1965) observes that the dip of Permian beds on both flexures ranges from 10° to 15° northward. Displacement along the flexures, based on differences in height of evenly bedded units at the upper and lower ends of the structures, is 1,700 ft (518 m) on the Victorio Flexure and 1,000 ft (305 m) on the Babb Flexure (King, 1965). The flexures may be the Permian or post-Permian expressions of a major pre-Permian strike-slip fault (King, 1965).

King (1965, p. 117) observes that the:

> Salt Basin is peculiarly segmented, apparently by west-northwestward-trending faults that extend short distances into the ranges which border it. Each segment is offset left laterally from the ones on either side, suggesting a possible strike-slip displacement along the west-northwestward-trending faults which bound them. Nevertheless, no such displacements can be observed where these faults enter the adjoining ranges. It seems more likely that the northward-trending structures, during their formation, reactivated an earlier west-northwestward-trending grain, and were modified by it.

The lateral offsets described by King (1965) are apparent in Figure 3.04. Continuing north from the North Baylor Mountain Fault, the Guadalupe Mountains are at 12:00. El Capitan, the prominent feature at the south end of the mountains, is made up of upper Permian reef carbonates that were built out over prograding basinal deposits exposed in the Delaware Mountains.

23.7 mi (38 km)

Stop 3.3 - Entrance to Blue Origin launch site

Entrance to Blue Origin Launch Site 1 (Figure 3.08). Take many photos here. Only Blue Origin employees are allowed in.

24.0 mi (42.2 km)

The highway curves to the northwest. The mouth of Victorio Canyon is at 9:00.

29.7 mi (47.8 km)

Stop 3.04 - Marble Canyon and Cave Peak

Figure 3.09 is a panoramic view of Marble Canyon and Cave Peak as seen from Stop 3.04. Cave Peak is a rhyolitic intrusion of Tertiary age. Extensive drilling in the intrusion revealed subcommercial stockwork molybdenum mineralization (Sharp, 1979). Neither Cave Peak nor Mable Canyon is available for inspection. All properties in this area, east and west of TX 54 are part of the Figure 2 Ranch, owned by Amazon founder, Jeff Bezos. (Rich Kyle led the discussion of Marble Canyon and Cave Peak systems (Figure 3.10)).

Urguhan and others (2023) describe the Marble Canyon Stock as an unmineralized, compositionally zoned alkalic pluton with a silica-undersaturated rim of monzodiorite, a transition phase of monzonite, and a silica-oversaturated core of quartz syenite, located approximately one mile southwest of Cave Peak (Figure 3.11). The silica content increases from an undersaturated periphery to the silica-over-saturated core, changing from 49 to 71% SiO_2 (Price et al., 1986). Nepheline-bearing dikes, quartz trachyte dikes, pegmatite, and aplite dikes are present throughout the stock (Price et al., 1986).

7

Metamorphism of Hueco Limestone and Bone Spring Limestone units developed a contact aureole of marble and hornfels around the stock (Bridge, 1986; Price and Henry, 1986). Calcite-brucite marble is mined around the Marble Canyon intrusion perimeter.

The Cave Peak intrusive system (Figures 3.11 and 3.12) consists of an outer rhyolite breccia with a hypabyssal rhyolitic core that has been overprinted by multiple magmatic and hydrothermal events. The breccia pipe has a diameter of approximately 2500-ft (762 m) at the surface. The complex appears to be hour-glass in shape, narrowing to ~800-ft (244 m) in diameter at approximately 1300-ft (396 m) depth before expanding (Sharp, 1979; Figure 3.12). The core consists of older quartz monzonite and quartz latite porphyries. The older phases have been cut by an alkali feldspar granite porphyry, biotite granite porphyry, aplite and late rhyolite dikes.

In a master's thesis on the Cave Peak molybdenum system, Ugurhan (2018) writes:

> The deposit belongs to the class of high-grade, rift-related, fluorine-rich Mo deposits commonly referred to as Climax-type porphyry Mo systems that are products of highly evolved rhyolite magmatism. The Cave Peak intrusive system consists of an outer rhyolite breccia mass with a complex intrusive core, overprinted by multiple hydrothermal events (refer to Figures 3.11 and 3.12 of this guidebook). Molybdenite is the primary Mo-bearing mineral and occurs as stockwork veinlets commonly with quartz, biotite and fluorite and as fine disseminations. At least three spatially and temporally different Mo zones were identified by exploration in the 1960s (Sharp, 1979). Elevated concentrations of F, Nb, Sn, and W are also present. The Marble Canyon Stock is an unmineralized, compositionally zoned, monzodiorite and monzonite to quartz syenite pluton located 1.5 km southwest of Cave Peak (refer to Figure 3.11 of this guidebook); previous studies have suggested a genetic link between the two plutons.
>
> The deposit shows a within-plate geochemical affinity, average (n=10) Nb, Rb, and Sr concentrations of 730, 690, and 61 ppm, respectively, and a highly differentiated magma series. Rare earth element (REE) concentrations are elevated, with average REE+Y concentrations of 758 ppm (n=10) and 437 ppm (n=9) for Cave Peak and Marble Canyon, respectively. Curvilinear trends are observed between Marble Canyon and Cave Peak rocks when major oxides plotted against silica on variation diagrams. Trace element plots of Rb, U, Th, and Mo also show these linear trends implying a link between Cave Peak and Marble Canyon. Quartz syenite and monzonite from the Marble Canyon Stock yielded zircon U-Pb ages of 36.2 ± 0.15 Ma and 36.1 ± 0.09 Ma, respectively. The youngest major intrusion at Cave Peak, an alkali feldspar granite porphyry, has a zircon U-Pb age of 34.8 ± 0.4 Ma, further suggesting these intrusions are related.

A summary paper prepared for this field guide (Kyle and Ugurhan, 2023) is included as a supplement attached to the Day Three road log.

32.1 mi (51.7 km)

West of HW 54 is the entrance to Figure 2 Ranch, Jeff Bezos' residence in West Texas (Figure 3.13).

34.5 ,mi (55.5 km)

Crossing southeast projection of Babb Flexure across the Salt Basin graben (Figures 3.4, 3.5 and 3.7).

50.0 mi (80.5 km)

Formations of Delaware Mountains Group

East of HW 54 are rocks of the Brushy Canyon, Cherry Canyon, and Bell Canyon formations (ascending order) of the Delaware Mountains Group. The above formations are composed of shelf sediments that prograded over a broad marine shelf into deep waters of the Delaware Basin during Middle Permian time (Figures 3.14 – 3.17). Overlying the Bell Canyon Formation is the Capitan Limestone (Permian - Guadalupian). The entire assemblage of rocks represents a shelf/shelf-margin/deep-basin sequence of northern Delaware Basin marine deposits.

 In a substantial summation of work on the Delaware Mountain Group, Nance (2006) writes:

The Delaware Basin during deposition of the Delaware Mountain Group was a deep- water basin bounded by carbonate-ramp (San Andres and Grayburg) and carbonate-rim (Goat Seep and Capitan) margins that developed on the western edge of the Central Basin Platform, the Northwest Shelf, and the Diablo Platform. The primary connection between the Delaware Basin intracratonic sea and the open ocean was through the Hovey Channel (see Figure 3.14 of this guidebook). Most deposition in the area during sea-level highstands was on the shelves and consisted of the mixed carbonate- siliciclastic San Andres Formation and Artesia Group (Grayburg, Queen, Seven Rivers, Yates, and Tansill Formations; Figure 3.15 of this guidebook). The Delaware Mountain Group shelf-derived siliciclastics and shelf- margin-derived detrital carbonates were deposited during intermittent sea-level lowstands. Basin subsidence outpaced sediment supply such that deep-water conditions were maintained until the close of the Guadalupian, after which Ochoan evaporites filled the basin and eventually blanketed the entire greater Permian Basin area. Onset of basin evaporite accumulation corresponded with demise of the Capitan Reef system and is hypothesized to mark closing of the Hovey Channel, which promoted progressive restriction of the basin from marine influx (King, 1948).

56.0 mi (90 km)

Turn left (west) on to HW 180.

65.0 mi (105 km)

Stop 3.05 - Gypsum playa of northern Salt Basin, and Guadalupe Mountains

Guadalupe Mountains as seen from the gypsum playa of the northernmost Salt Basin (Figure 3.18 and 3.19). The gypsum surface is formed from the evaporation of groundwater at the surface and in the uppermost part of the unsaturated zone. Boyd and Kreitler (1986) describe the northern Salt Basin as "a closed hydrologic system in which discharge of ground-water flow occurs in a series of playas, or salt flats."

> Ground water originating in peripheral consolidated rocks and alluvial fans flows toward the basin and discharges by evaporation from the salt flats. Progressive increases in salinity are characteristic of the water moving down gradient and are primarily attributed to evaporative concentration. Steady increases in sodium (Na^+) and chloride (Cl^-) and, to a lesser degree, magnesium (Mg^{+2}) and potassium (K^+) characterize increases in total dissolved solids (TDS). Intense evaporation above the water table in the salt flats concentrates the composition of brine to TDS values that range from 50,000 mg/L to greater than 300,000 mg/L. Precipitation of minerals from solution, primarily alkaline earth carbonates and gypsum, results in depletion of calcium (Ca^{2+}) and bicarbonate (HCO^{3-}) and relative enrichment of sulfate (SO_4^{2-})in the ground water. Inflowing ground water of a Ca-Mg-SO_4 composition undergoes evaporation and evolves to a final composition of Na-Mg-SO_4-Cl brine in the salt flats. Gypsum currently precipitates in the salt flats (see Figure 3.20 of this guidebook) at a depositional rate that ranges from 0.02 to 0.09 cm/yr. These deposits dso not likely represent relict lakebed sediments.

Continue 23 mi (37 km) west to FM 1111. Between the northern Salt Basin and FM 1111, HW 180 traverses relatively flat terrain of Permian carbonate rocks and undifferentiated rocks of Cretaceous age. Before leaving Salt Flat, observe hills formed by igneous rocks of the Sierra Tinaja Pinta, northwest of the Salt Flat and north of HW 180 (Figures 3.21 and 3.22).

Proceed 22.7 mi (36.5 km) west on HW 180 and turn right (south) at FM 1111.

87.7 mi (141 km)

Sierra Tinaja Pinta

Before turning south onto FM 1111, note prominent hills north of HW 180. The hills nearest HW 180 are igneous rocks of the Sierra Tinaja Pinta, mentioned above. Further to the north

are the volcanic rocks of the Cornudas Mountains (Figure 3.22). Gross (1965) describes the complex as follows:

> Igneous rocks in the Sierra Tinaja Pinta and Cornudas Station areas are part of a group of intrusions of Tertiary age that outline the northeastern margin of the Diablo Plateau; they are part of the larger alkalic petrographic province of Trans-Pecos Texas. Laccoliths, dikes, sills and a cone sheet were intruded into the Hueco and Victorio Peak Limestones of Permian age and into sandstone and limestone of Cretaceous age, which are paleontologically correlative with the Fredricksburg and Washita Groups of central Texas.
>
> The igneous rocks are of four types: (1) porphyritic analcime syenite and associated dike and contact rocks, (2) pyroxene trachyte, (3) porphyritic and analcime-nepheline syenite, and (4) olivine-analcime trachyte.

Turn left (south) at FM 1111.

91.7 mi (147.6 km)

Pump Station Hills

Pump Station Hills are located east and west of FM 1111 (Figure 3.22). Masson (1956) describes Pump Station Hills as:

> … a group of low, rounded knolls irregularly distributed on an elliptical area approximately 4 mi (6.5 km) long and 2.5 mi (4.0 km) wide in north-central Hudspeth County, Texas. The surrounding terrain is virtually featureless, and the hills themselves are topographically unimpressive. In most cases, exposed bedrock can be found only upon close inspection, and outcrops are restricted to the crests of hills. The locality derives its name from the natural-gas transmission pump station located near the center of the area at the intersection of Farm Road 1111 and the El Paso Natural Gas and Pasotex pipelines.
>
> Lithologically they resemble Precambrian granitic and rhyolitic rocks exposed elsewhere in Trans-Pecos Texas, but the hills are located within an alignment of shallow alkaline intrusive bodies which are believed to be Tertiary in age. Relations between the igneous rocks in question and the surrounding Paleozoic and Cretaceous sediments cannot be determined with certainty due to a lack of good exposures. Published opinion with regard to a Precambrian or Tertiary age for the Pump Station Hills has varied, but in recent papers it has been concluded that the rocks are Precambrian.

95.2 mi (153 km)

Red Hill intrusive (Tertiary) at 9:00, 4.3 mi (6.9 km) east of FM 1111.

99.3 mi (151 km)

Sierra Prieta intrusive (Tertiary) at 9:00 (Figure 3.22), 10 mi (16 km) east of FM 1111.

127.5 mi (205 km)

FM 1111 begins descent into Northwest Eagle Flat. The Diablo Plateau escarpment is not a sharp vertical break at this point, as it is in areas to the east and along the northward path of HW 54. Sierra Blanca Mountain and Triple Hill are at 2:00, 8 mi (12.9 km) to the southwest (Figure 3.23).

133.5 mi (215 km)

The Triple Hill laccolith is at 3:00, 2 mi (3.2 km) west of FM 1111.

Mileage 149.5

Intersection of FM 1111 and El Paso Street. Turn left and then pull into parking lot at convenience store and gas station one block to the east.

Sierra Blanca completes a traverse around and over the Diablo Plateau. On Days One and Two of the field trip, the plateau was seen only as a prominent escarpment from I-10 and the Eagle Mountains. Although portrayed as a major buttress against which compressive tectonic forces from the south were directed over tens of millions of years, the significance of this geological feature is not fully apparent until one sees the plateau from more than one side and from a broad surface that has not been subjected to deformation from the compressive and extensional forces that forged the mountains and basins to the south. It was the immovable object against which a great many forces were arrayed over millions of years of time.

Return to El Paso International Airport from here. Distance to airport is 83 mi (134 km). Total mileage on Day 3: 233 miles (375 km).

REFERENCES

Boyd, F.M., and Kreitler, C.W., 1986, Hydrogeology of a gypsum playa, northern Salt Basin, Texas: Univ. of Texas at Austin Bureau of Economic Geology Report of Inv. 159, 37 p.

Clark, K.F., and Kyle, J.R., 1990, Road log from Van Horn to Tumbledown Mountain talc deposit, Marble Canyon, Sierra Blanca, and El Paso *in* Kyle, J.R., ed., Industrial mineral resources of the Delaware Basin, Texas and New Mexico: Society of Economic Geologists Guidebook Series, V. 8, p. 53-83.

Flawn, P.T., 1952, The Hazel copper-silver mine, Culberson County, Texas: Univ. of Texas, Bureau of Economic Geology Report of Inv. No. 16, 22 p.

Gross, R.O., 1965, Geology of Sierra Tinaja Pinta and Cornudas Station areas, Hudspeth County, Texas: Univ. of Texas M.A. thesis, 119 p.

King, P.B., 1948, Geology of the southern Guadalupe Mountains, Texas: U.S. Geol. Survey Professional Paper 215, 179 p.

King, P.B.,1965, Geology of the Sierra Diablo Region: U.S. Geol. Survey Professional Paper 480, 185 p.

Kreitler, C.W., and Darling, B.K. 1997, Value of Ground Water: Unpublished paper presented at Seventh Annual Conference on Texas Water Law, November 1997, Austin, Texas, 15 p.

Kyle, J.R., and Ugurhan, M., 2023, Geology of the Cave Peak porphyry Mo deposit, Trans-Pecos Texas: Unpublished paper prepared for guidebook, 4 p.

Masson, P.H., 1956, Age of igneous rocks at Pump Station Hills, Hudspeth County, Texas: Amer. Association of Petroleum Geologists, V. 40, no. 3, p. 501-518.

McAnulty, W.N., and Hoffer, J.M., 1980, Second day road log from Van Horn to Tumbledown Mountain, Hazel Mine, Southern Wylie Mountains and return to Van Horn: New Mexico Geological Society, 31st Field Conf. Guidebook, p. 19-25.

Mullican, W.F., III, and Mace, R.E., 2001, *in* Mace, R.E., Mullican, W.F. III, and Angle, E.S., eds., Aquifers of West Texas: Texas Water Development Board Report 356, Chapter 18, p. 248-258.

Nance, H.S., 2006, Middle Permian basinal siliciclastic deposition in the Delaware Basin: the Delaware Mountain Group (Guadalupian): The University of Texas at Austin, Bureau of Economic Geology, Austin, TX, 80 p.

Price, J.G., Henry, C.D, and Standen A.R., 1983, Annotated Bibliography of Mineral Deposits in Trans-Pecos Texas: Univ. of Texas at Austin, Bureau of Economic Geology, Texas Mining and Mineral Resources Research Institute Mineral Resources Circular No. 73, 108 p.

Price, J.G., Henry, C.D., Dickerson, P.W. and Muehlberger, W.R., 1985, Summary of Tertiary stress orientations and tectonic history of Trans-Pecos Texas, *in* Structure and tectonics of Trans-Pecos Texas: West Texas Geological Society Field Conference, p. 149-151.

Price, J.G., and Henry, C.D., 1986, Field trip road log: Day 0 – El Paso to Van Horn, *in* Price, J.G., Henry, C.D., Parker, D.F., and Barker, D.S., eds, Igneous geology of Trans-Pecos Texas, field trip guide and research articles: Univ. of Texas at Austin Bureau of Economic Geology, Texas Mining and Minerals Resources Research Institute Guidebook 23, p. 9 -12.

Price, J.G., Henry, C.D., Barker, D.S. and Parker, D.F., 1987, Alkalic rocks of contrasting tectonic settings in Trans- Pecos Texas. Geological Society of America Special Paper, 215, p. 335-346.

Sharp, J.E.,1979, Cave Peak, a molybdenum-mineralized breccia pipe in Culberson County, Texas: Economic Geology, v. 74, p. 517-534.

Ugurhan, M., 2018, Characterization and timing of the Cave Peak porphyry molybdenum system, Culberson County, Texas: University of Texas at Austin M.S. thesis, 154 p.

Ugurhan, M. and Kyle J.R., 2023, Geology of the Cave Peak porphyry Mo deposit, TransPecos Texas: University of Texas at Austin – Bureau of Economic Geology paper included as supplement to this guidebook.

Ugurhan, M., Elliott, B.A., Kyle, J.R., Stockli, D.F., and Mathur, R., 2023, Geochemical evolution of the REE-enriched of the Cave Peak porphyry Mo-deposit, Trans-Pecos Texas, USA: Lithos (https://doi.org/10.1016/j.lithos.2023.107434)

Hazel Silver Mines, near Van Horn, Texas

GEOLOGY OF HUDSPETH COUNTY, TEXAS

GUIDEBOOK OF AIPG-TEXAS
SPRING FIELD TRIP

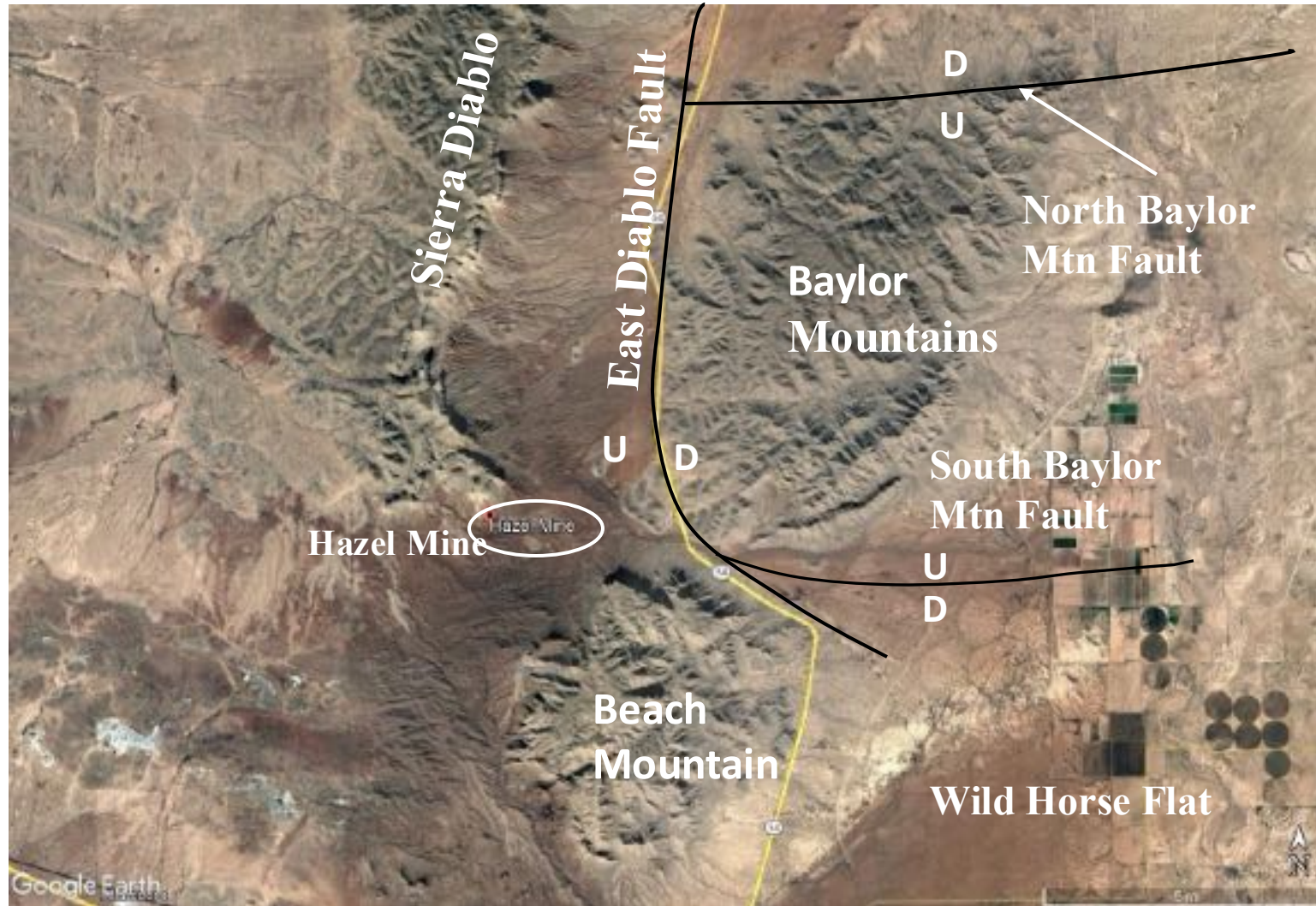## APRIL 21 – 23, 2023

DAY THREE – FIGURES 3.01 – 3.23

Figure 3.01 – Normal faults separating Baylor Mountains from Beach Mountain and Sierra Diablo. Also shown is location of Hazel Mine at southeastern tip of Diablo Plateau
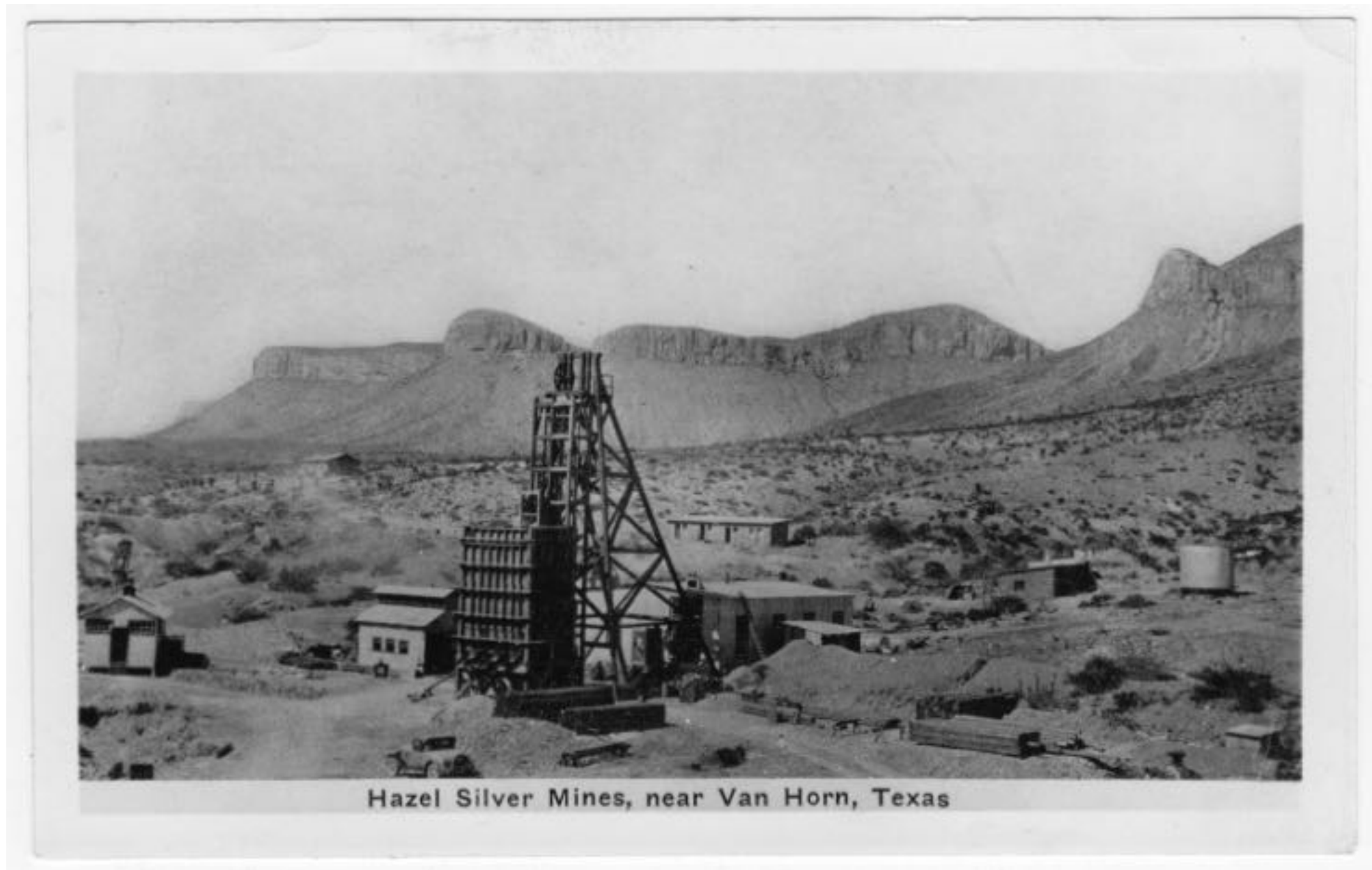
Figure 3.02a

Figure 3.02b

Figure 3.02a – Southern escarpment of Diablo Plateau. **Figure 3.02b** - Southeastern point of Diablo Plateau, as seen from HW 54.. Photos by BK Darling.

Hazel Silver Mines, near Van Horn, Texas

Figure 3.03 – Headframe erected at Hazel Silver Mine. Photo attributed to P.T. Flawn, approx. 1951.
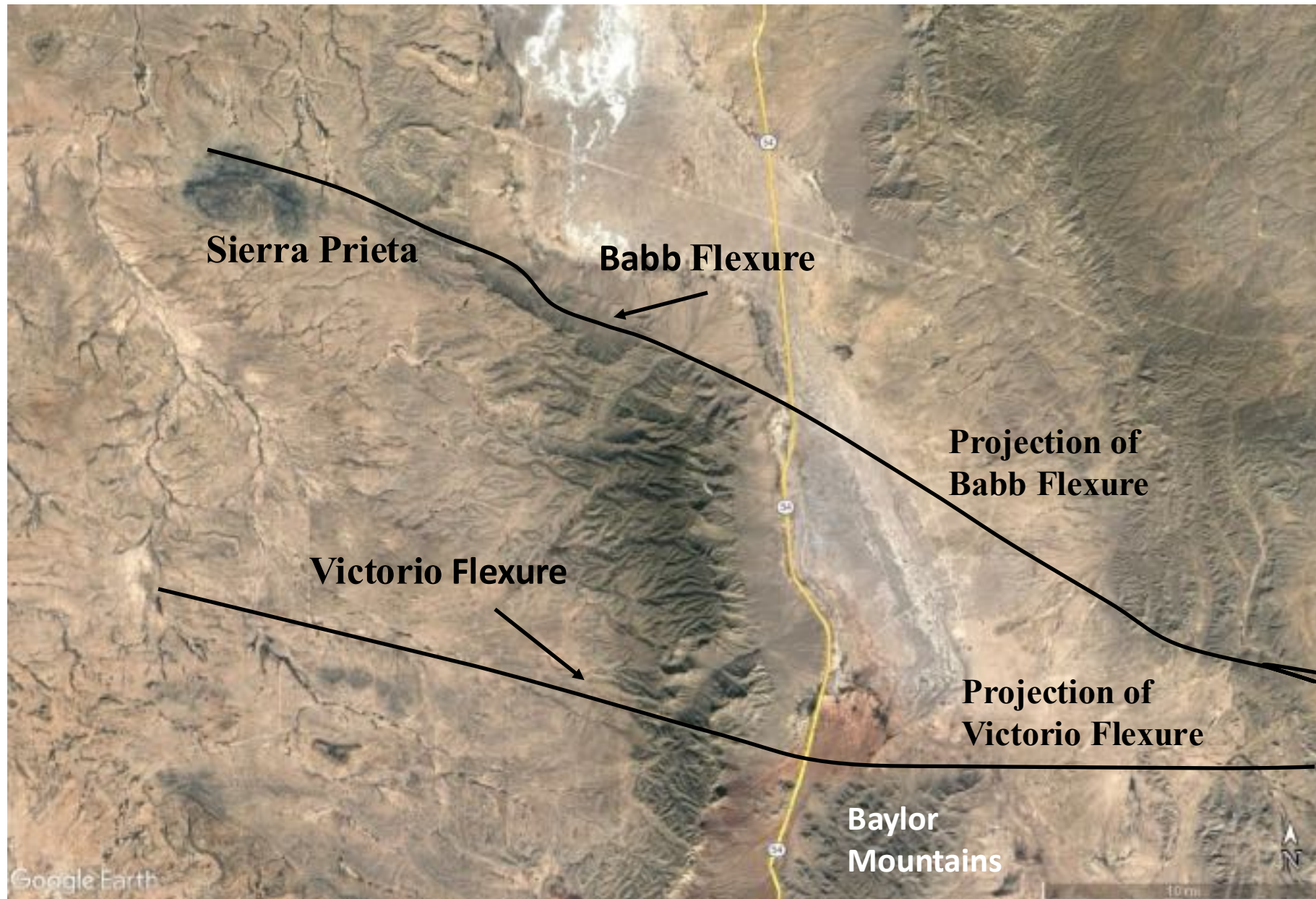
Figure 3.04 – Projection of Victorio and Babb flexures southeast across Salt Basin. The projection is based on King (1965) and Goetz (1977).
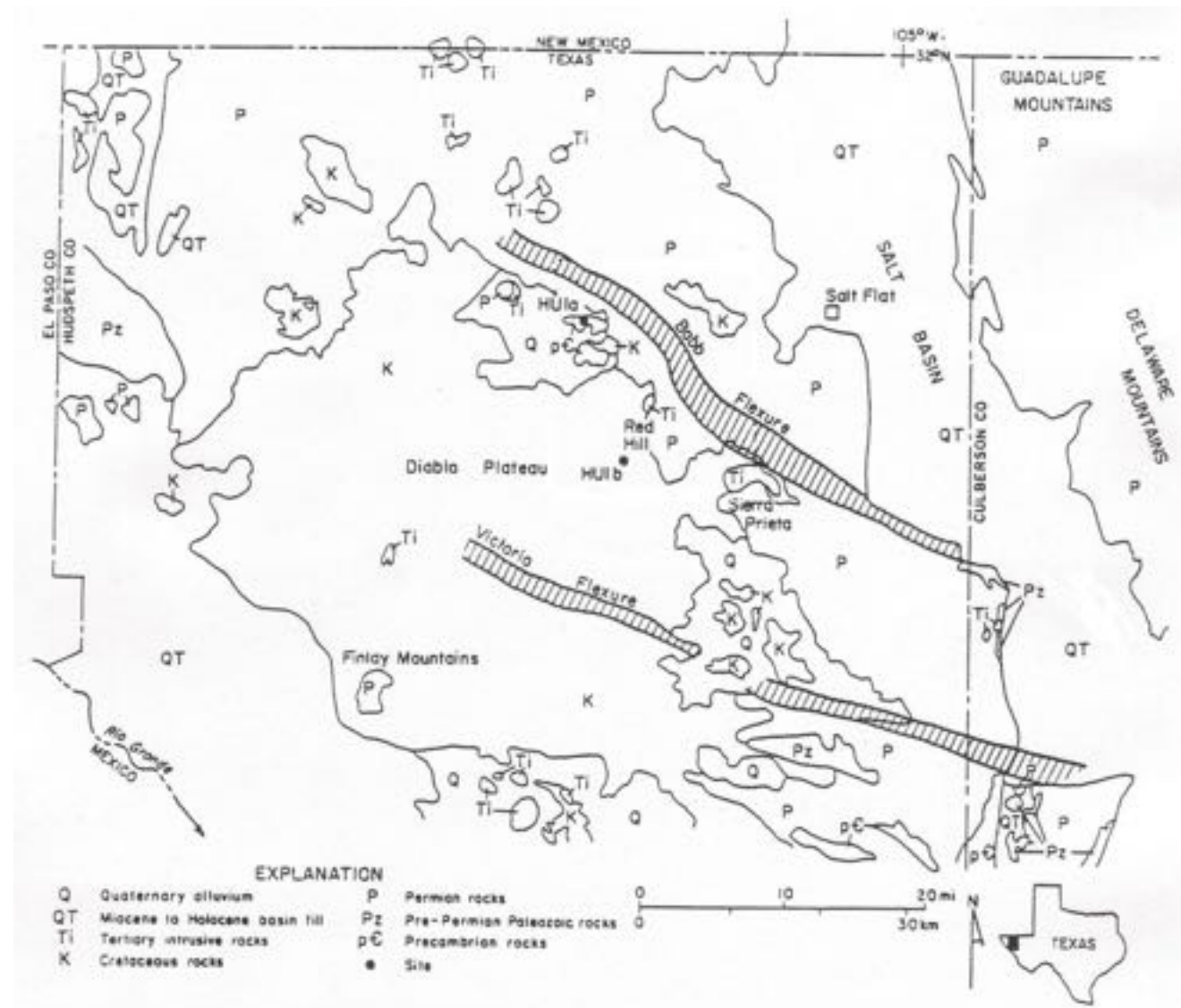
174

Figure 3.05 – Victorio and Babb flexures. Source: Mullican and Mace (20

175

Northward dipping beds
of Victorio Flexure

Figure 3.06 – Victorio Flexure as seen from Highway 54. Photo by BK Darling.

Figure 3.07 – Babb Flexure as seen from Highway 54. Photo by BK Darling.

Figure 3.08 – Sign at entrance to Blue Origin's Culberson County Launch site. Photo by BK Darling.
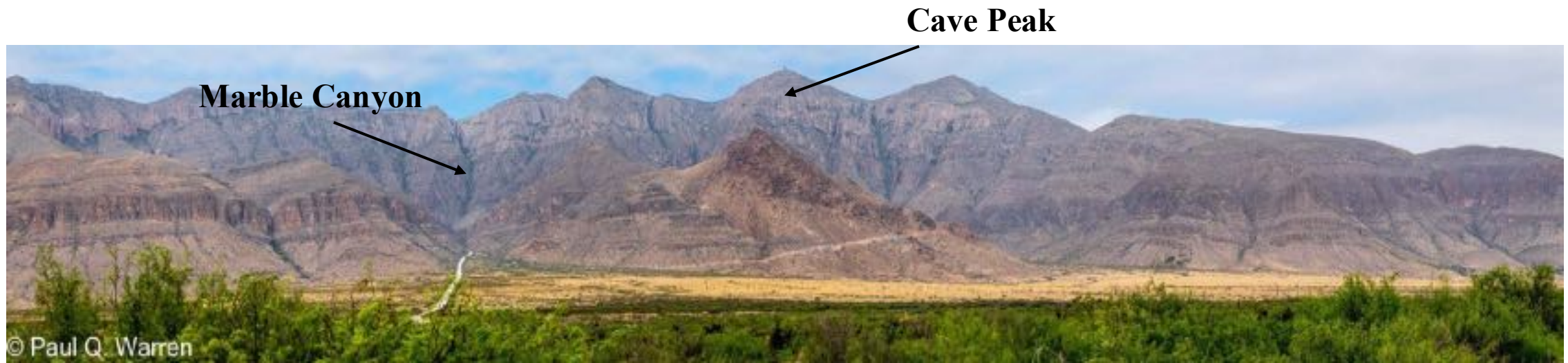
Figure 3.09 – Panoramic view of Marble Canyon and Cave Peak as seen from Stop 4. Photo by Paul Warren.

Figure 3.10 – Rich Kyle leads discussion of Marble Canyon and Cave Peak systems.
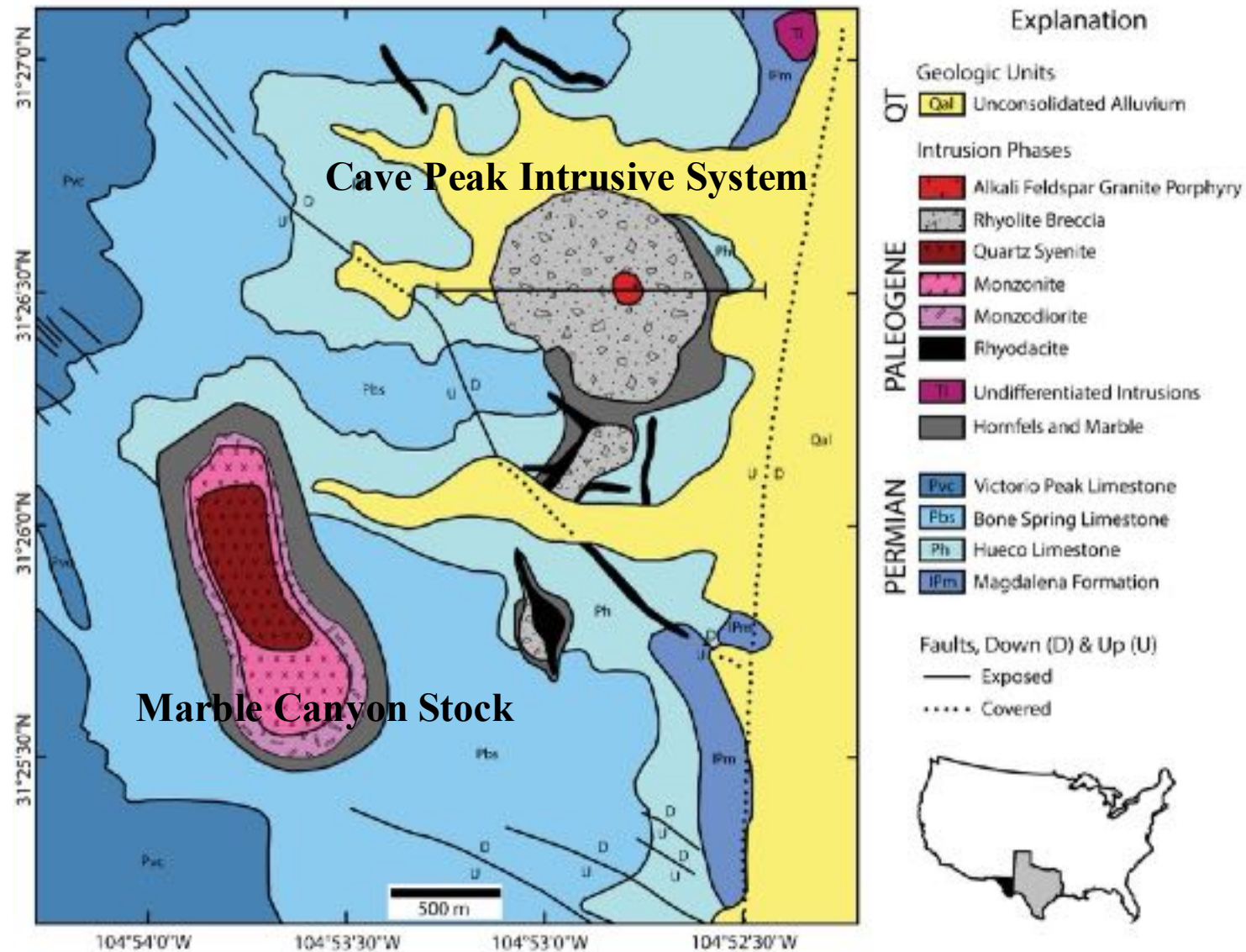
Figure 3.11 - Generalized geological map of Cave Peak and Marble Canyon area. Map
by Ugurhan and Kyle (2023), modified from Sharp (1979), Audetat (2010) and TNRIS geologic atlas of Texas.
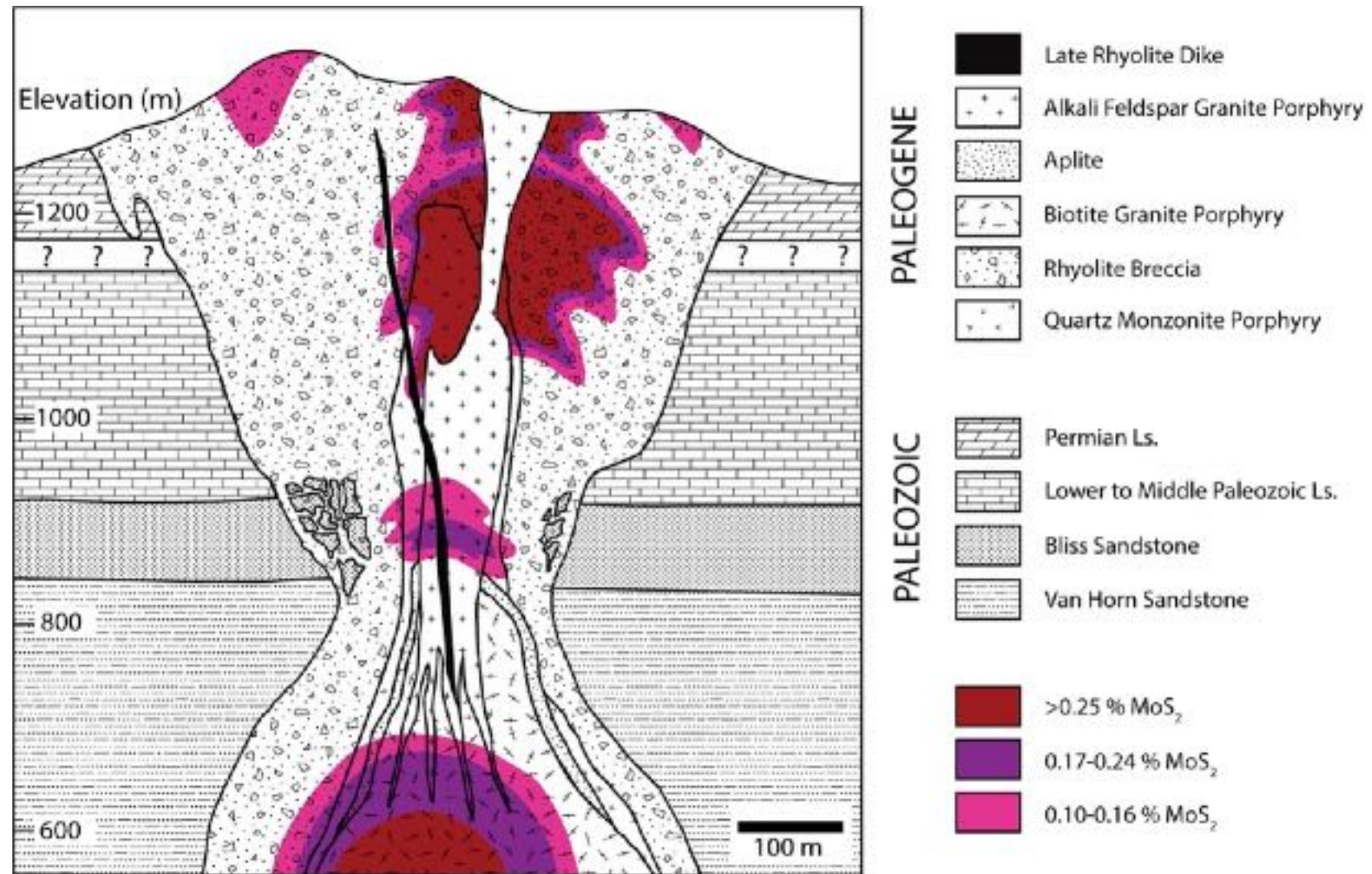
Figure 3.12 – Generalized cross-section of the Cave Peak deposit showing the spatial relationship among intrusive phases and mineralized zones. Source: Ugurhan and Kyle (2023), modified after Sharp (1979).

.

182

Figure 3.13 – Sign at entrance to Figure 2 Ranch, Highway 54. Photo by BK Darling.
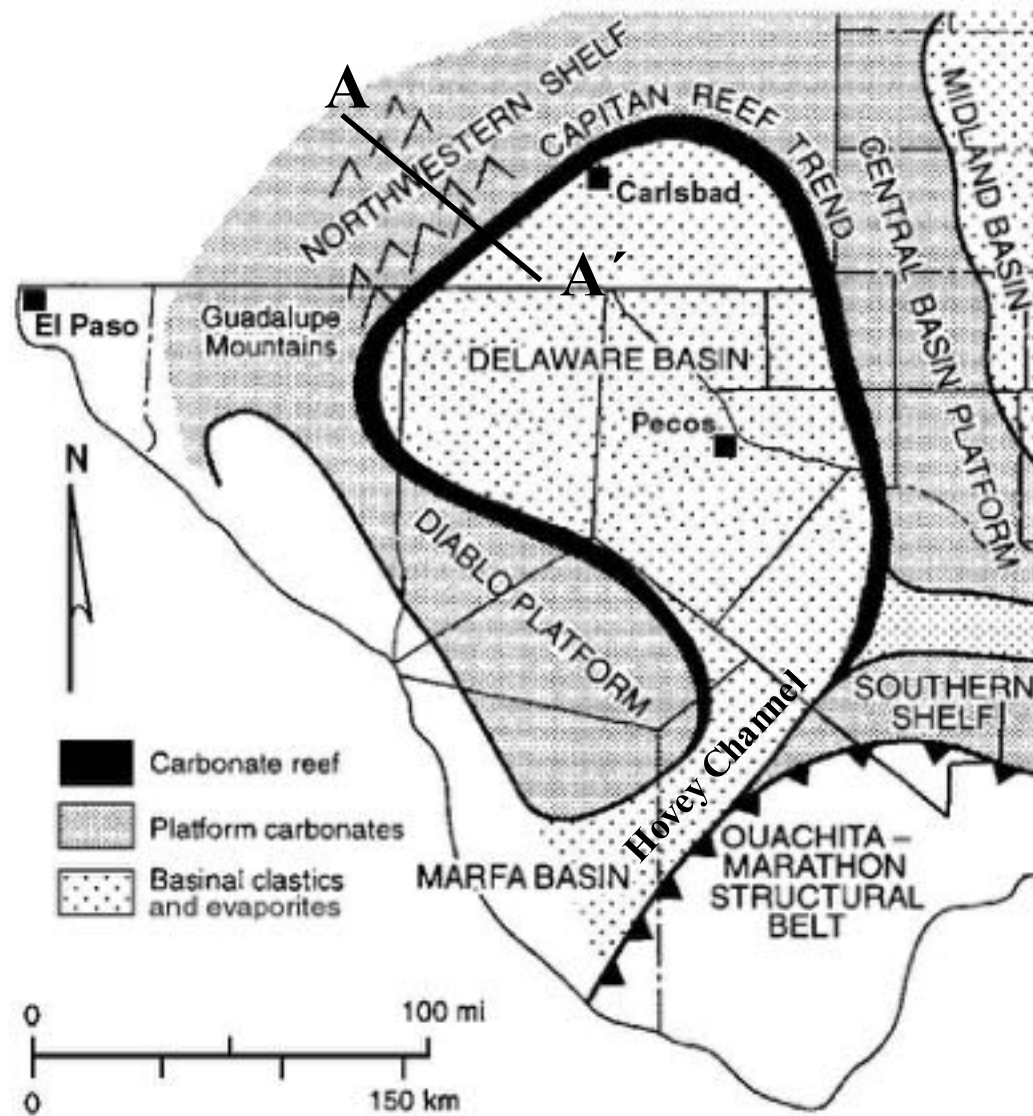
Figure 3.14 – Generalized map of Delaware Basin (Middle to Late Permian) and platforms bounding the basin on northeast (Central Basin Platform), southwest (Diablo Platform), and northwest (Northwestern Shelf). From Uliana (2000).
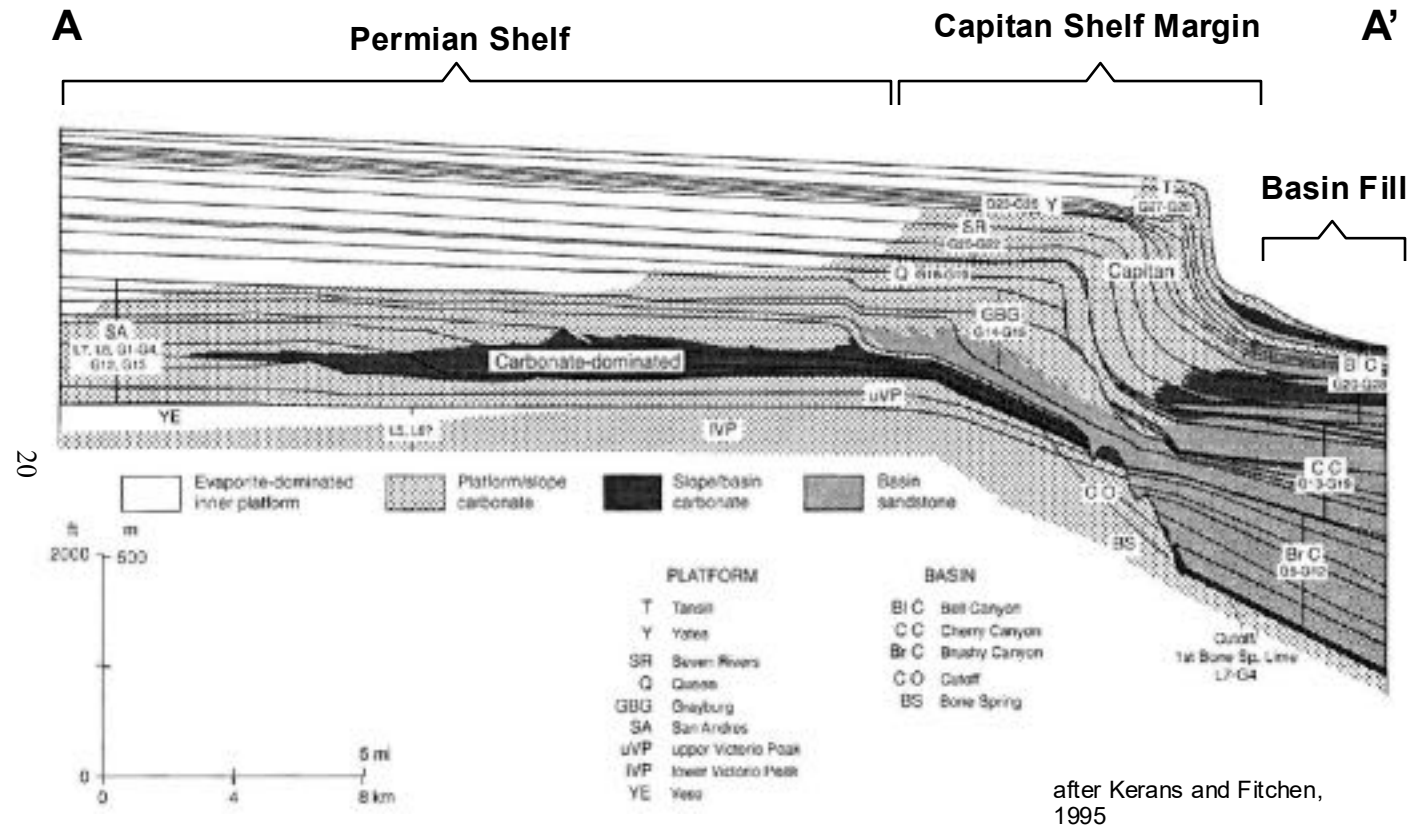
184

A   **Permian Shelf**   **Capitan Shelf Margin**   **A'**

Basin Fill

after Kerans and Fitchen, 1995

Figure 3.15 – Cross section illustrating (Middle Permian – Guadalupian) shelf, shelf-edge, and deep-water deposits of Delaware Basin (see **Figure 3.14**). Formations of the Delaware Mountain Group (Brushy Canyon, Cherry Canyon and Bell Canyon) are the off-shelf deep-water deposits exposed the Delaware Mountains of Culberson County, Texas. Figure modified from Uliana (2000).

Figure 3.16 – Guadalupe Mountains in background, and Bell Canyon Formation, uppermost member of the Delaware Mountain Group.   Photo by BK Darling.

Figure 3.17 -   Capitan Formation (shelf edge carbonate complex) overlying beds of Bell Canyon Formation (Delaware Mountains Group). Note the prominent dip of the Bell Canyon Formation. The Brushy Canyon, Cherry Canyon, and Bell Canyon formations are deep-water deposits. The Capitan Formation and coeval equivalent formations of the shelf are shallow-water deposits. Some of the best exposures of the series of shelf formations are along the western face (escarpment) of the Guadalupe Mountains as seen from the northern Salt Flat.

Figure 3.18 – Guadalupe Mountains as seen from northern Salt Flat (Gypsum Playa).
Photo by BK Darling.

Figure 3.19 – Guadalupe Mountains as seen from flooded Salt Flat (Gypsum Playa). This photo was shot during a reconnaissance of the field trip area in October 2022. Heavy precipitation had inundated the flat, leaving much of the area under 6 inches to 1 foot of water. Photo by Diane Darling.

Figure 3.20 – Gypsum crust accumulating on surface of Salt Flat. Photo by Paul Warren.

Figure 3.21 – Hills formed by igneous rocks of Sierra Tinaja Pinta. This photo was taken during a reconnaissance trip to the field trip area in October 2022. Photo by Diane Darling.
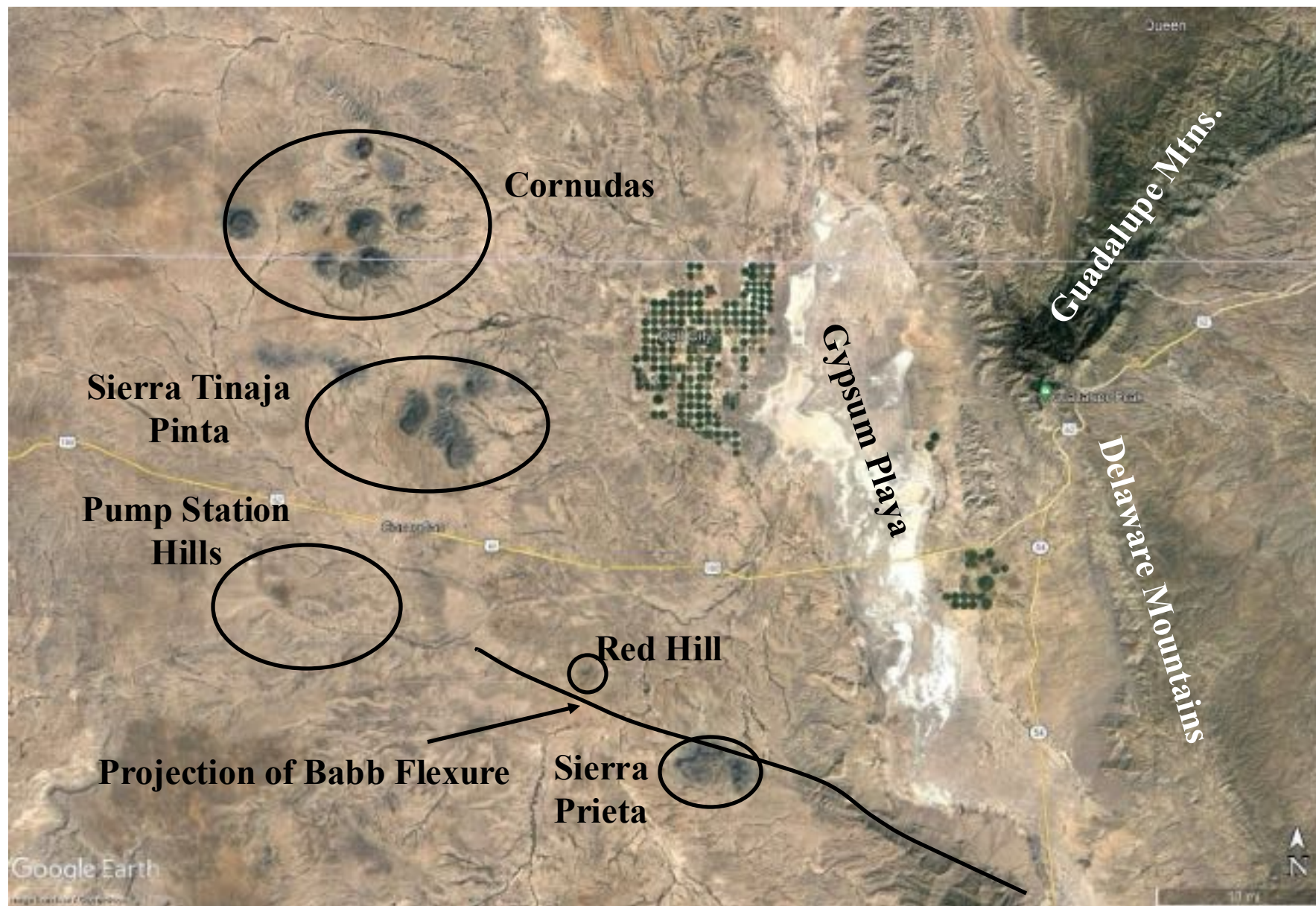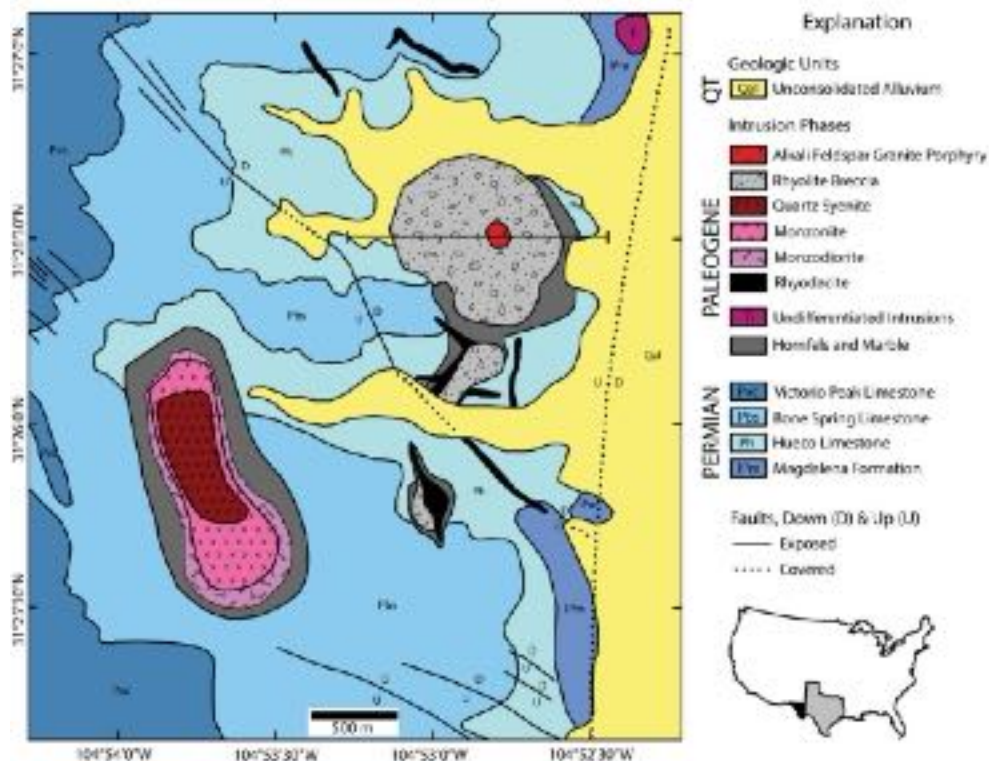
Figure 3.22 – Google Earth image showing prominent geological features of northern Diablo Plateau.

Figure 3.23 – Sierra Blanca Mountain and Triple Hill as seen from FM 1111, near base of Diablo Plateau escarpment. Photo by Paul Warren.

GEOLOGY OF HUDSPETH COUNTY, TEXAS

GUIDEBOOK OF AIPG-TEXAS
SPRING FIELD TRIP

APRIL 21 – 23, 2023

SUPPLEMENTAL MATERIAL

Ugurhan, M. and Kyle, J.R., 2023, Geology of the Cave Peak porphyry Mo deposit, Trans-Pecos Texas: University of Texas at Austin – Bureau of Economic Geology paper prepared for AIPG-Texas 2023 Spring field trip guidebook.

Geology of the Cave Peak porphyry Mo deposit, Trans-Pecos Texas

Mert Ugurhan and J. Richard Kyle

Bureau of Economic Geology, Jackson School of Geosciences,

University of Texas at Austin, Austin, Texas

Introduction

The Cave Peak porphyry molybdenum deposit is located in Culberson County, Texas, approximately 35 miles north of Van Horn, along the eastern boundary of the Sierra Diablo adjacent to the Salt Basin. Porphyry ore deposits are the differentiated products of magmatic and tectonic events that created economic metal sources (Carten et al., 1993). These systems can produce large-scale mineralized zones, commonly as stockwork veinlets in large volumes of hydrothermally altered rock. Classification of porphyry systems usually focuses on differences in tectonic setting, timing, and metallic concentrations of Cu, Mo, Au, W, and Sn.

The Cave Peak deposit is a Paleogene porphyry Mo system that formed by multiple magmatic and hydrothermal events (Sharp, 1979). Cave Peak is a breccia-hosted, fluorine-rich porphyry Mo system that is enriched in Nb, REE, and other critical minerals. The system is genetically linked to the nearby Marble Canyon Stock and is considered to be the highly differentiated felsic endmember of this magmatic system (Price and Henry, 1986; Audetat, 2010; Ugurhan, 2018). Episodic magmatic activity formed a complex intrusive interior, and recurrent fluid exsolution associated with these events created at least three distinct mineralization zones, producing high grade ore and wide variety of mineralogical assemblages (Sharp, 1979).

According to its magma series chemistry (F, Nb, Rb, and Sr contents), tectonic origin and timing, the Cave Peak system can be classified as a Climax-type porphyry Mo system (Ugurhan, 2018). These molybdenum ore deposits are rare, mostly as Late Cretaceous and Paleogene magmatic systms in western North America (Ludington and Plumlee, 2009).

Mineralization associated with the Cave Peak intrusive system was recognized by the early 20th century, initially by the presence of wolframite (Richardson, 1914). Numerous adits and shafts were developed in the early 1940s (King, 1965). Localized occurrences of Be (+Nb) along shear zones at Cave Peak were documented by Holser (1959).

The presence of oxidized Mo minerals at Cave Peak was recognized by Union Carbide geologists in the 1960s. An exploration program was started in 1965 and 26 diamond drill holes were completed. The property was sold to the Draco Mines in 1975 which continued drilling operations (Sharp, 1979). Other companies have held exploration license since. A total of 34 diamond drill cores have been documented for the area, totaling more than 40,000 feet.

Cave Peak currently is considered to be a known resource for Mo, Nb, W, and Cu (Schultz et al., 2017). Elevated REE + Y concentrations documented in limited sampling at both Cave Peak and Marble Canyon (Ugurhan, 2018) suggest additional REE resources in this region.

1

Geologic Setting

The Cave Peak and Marble Canyon magmatic system is located within the Trans-Pecos Magmatic Province. Trans-Pecos magmatism is bimodal, from mafic to highly evolved silicic magmas that were emplaced in two distinct tectonic environments (Price et al., 1987). The Magmatic Province is divided into two geochemical affinities, a calc-alkaline suite to the west and an alkaline suite to the east (Barker, 1977). Cave Peak and Marble Canyon intrusive systems are part of the alkalic belt.

The Cenozoic period in Trans-Pecos is characterized by three major tectonic stages. Magmatic activity started in a compressional regime that occurred as a result of subduction of the Farallon plate beneath the North American plate from 75 to 58 Ma (Shepard and Walper, 1982; Price et al., 1987). Crustal shortening caused thrust faulting and folding, and warping of Cretaceous and older rocks (Price et al., 1985). Residual NNW-oriented compression from the Laramide Orogeny triggered widespread magmatism from 48 to 32 Ma, which is divided into two phases (Price et al., 1987). The early phase (48–38 Ma) is characterized by minor intrusions, mafic lava flows, and two minor caldera eruptions (Henry and McDowell, 1986; Price et al., 1990). The most voluminous magmatism in the region occurred during the late phase (38–32 Ma) which is characterized by numerous intrusions and large-volume caldera-sourced ash flows that extend throughout the Trans-Pecos province (Henry and McDowell, 1986; Price et al., 1990).

Transition to Basin and Range extension shifted the regional stress orientations from east-northeast to north-northwest around 31 Ma (Henry et al., 1991). This shift is recorded by the orientations of small-volume basaltic dikes, which are products of the youngest magmatism in Trans-Pecos Texas (Price and Henry, 1984; Price et al., 1987). The youngest tectonic event, Basin and Range extension, resulted in normal faulting starting ~24 Ma and continuing to the present (Price et al., 1985; Price et al., 1990).

Marble Canyon Stock

The Marble Canyon Stock is an unmineralized, compositionally zoned alkalic pluton with a silica-undersaturated rim of monzodiorite, a transition phase of monzonite, and a silica-oversaturated core of quartz syenite, located approximately one mile southwest of Cave Peak. Silica content progressively increases from a silica-undersaturated periphery to the silica-oversaturated core, changing from 49 to 71% SiO_2 (Price et al., 1986). Nepheline-bearing dikes, quartz trachyte dikes, pegmatite, and aplite dikes are present throughout the stock (Price et al., 1986). Metamorphism of Hueco Limestone and Bone Spring Limestone units developed a contact aureole of marble and hornfels around the stock (Bridge, 1986; Price and Henry, 1986). Currently, calcite-brucite marble is being mined around the Marble Canyon intrusion perimeter.

Cave Peak Intrusive System

The Cave Peak intrusive system consists of an outer rhyolite breccia with a hypabyssal rhyolitic core that has been overprinted by multiple magmatic and hydrothermal events. The breccia pipe has a diameter of approximately 2500-ft at the surface; drilling suggests the complex is hour-glass in shape and narrows to ~800-ft in diameter at approximately 1300-ft depth before expanding at depth (Sharp, 1979; Figure 1B). The core consists of older quartz monzonite and quartz latite porphyries. These older phases have been cut by an alkali feldspar

granite porphyry, biotite granite porphyry, aplite and late rhyolite dikes (Figure 1). Two smaller breccia pipes crop out to the south of the main deposit (Figure 1A).

Recurrent fluid exsolution from the successive magmatic activity appears to have formed distinct mineralized zones within the Cave Peak system. At least three spatially and temporally distinct mineralization zones were interpreted by Sharp (1979) (Figure 1B). Assay evaluations of historic drilling confirm high-grade molybdenum occurrences within these zones.

Molybdenite is the primary Mo-bearing mineral and typically occurs in stockwork veinlets commonly with quartz, biotite and fluorite. Additionally, spherules of molybdenite (sizes up to few hundred microns) are also present, and are judged to be what was referred to as molybdenite "disseminations" by Sharp (1979). Mo spherules are hosted by concentrations of Na-Ca-Al fluorides (Ugurhan, 2018). Cu, Zn, and Pb are concentrated locally, as well as enrichment of F, Nb, W, and Sn. Secondary Mo-bearing minerals, such as powellite, wulfenite and ferrimolybdite, are present in the oxidized zones.

Sharp (1979) characterized the intrusive phases, mineralogy and alteration patterns of Cave Peak, and presented K-Ar ages of intrusions and mineralization. Price and Henry (1986) studied the geology of Marble Canyon and determined K-Ar ages of Marble Canyon and Cave Peak intrusions. Ugurhan (2018) provided zircon U-Pb ages for Marble Canyon (~36 Ma) and for the youngest major intrusion at Cave Peak (~35 Ma).

Price et al. (1986) presented geochemical data for Marble Canyon rocks and discussed the magma differentiation between silica-undersaturated and silica-oversaturated rocks. Audetat (2010) used fluid and melt inclusion data to suggest a genetic link between the Cave Peak and Marble Canyon deposits, including within-plate geochemical signatures. Additionally, the Mo content of Cave Peak was suggested to have been derived by fractional crystallization of mafic magmas.
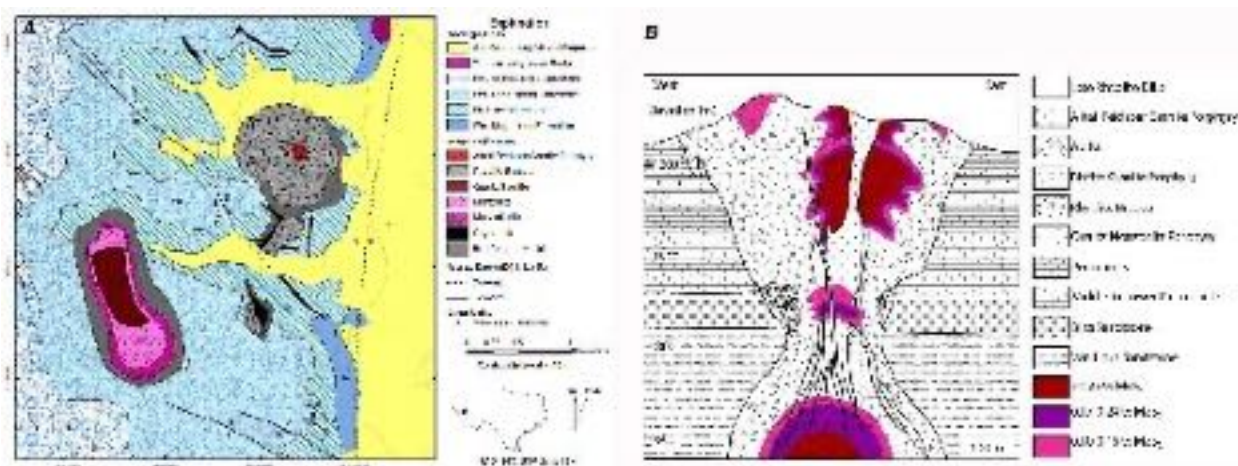

Fig. 1A. Generalized geological map of Cave Peak and Marble Canyon area. Map modified from Sharp (1979), Audetat (2010) and TNRIS geologic atlas of Texas.
1B. Generalized cross-section of the Cave Peak deposit showing the spatial relationship among intrusive phases and mineralized zones. Modified after Sharp (1979).

3

References

Audétat, A., 2010, Source and evolution of molybdenum in the porphyry Mo (–Nb) deposit at Cave Peak, Texas. Journal of Petrology, 51, p. 1739-1760.

Barker, D.S., 1977, Northern Trans-Pecos magmatic province: Introduction and comparison with the Kenya rift. Geological Society of America Bulletin, 88, p. 1421-1427.

Bridge, T.E., 1986, Contact metamorphism around the Marble Canyon stock. Igneous Geology of Trans-Pecos, Texas: Field Trip Guide and Research Articles, Bureau of Economic Geology, Guidebook 23, The University of Texas at Austin, p. 26-30.

Carten, R.B., White, W.H., and Stein, H.J., 1993, High-grade granite-related molybdenum systems: Classification and origin, *in* Kirkham, R.V., et al., eds., Mineral deposit modeling. Geological Association of Canada, Special Paper, 40, p. 521–554.

Henry, C.D. and McDowell, F.W., 1986, Geochronology of magmatism in the Tertiary volcanic field, Trans-Pecos Texas. Igneous geology of Trans-Pecos Texas. Bureau of Economic Geology, The University of Texas at Austin, Guidebook no 23, p. 99-122.

Henry, C.D., Price, J.G. and James, E.W., 1991, Mid-Cenozoic stress evolution and magmatism in the southern Cordillera, Texas and Mexico: transition from continental arc to intraplate extension. Journal of Geophysical Research: Solid Earth, 96, p. 13545-13560.

Holser, W.T., 1959, Trans-Pecos region, Texas and New Mexico - Cave Peak area, *in* Warner, L.A., et al., eds., Occurrence of nonpegmatite beryllium in the United States. US Geological Survey, Professional Paper 318, p. 140-143.

King, P.B., 1965, Geology of the Sierra Diablo region, Texas. US Geological Survey, Professional Paper 480, 185 p.

Ludington, S. and Plumlee, G.S., 2009, Climax-type porphyry molybdenum deposits. US Geological Survey, Open-file report 2009-1215. 16 p.

Price, J.G. and Henry, C.D., 1984, Stress orientations during Oligocene volcanism in Trans-Pecos Texas: Timing the transition from Laramide compression to Basin and Range tension. Geology, 12, p. 238-241.

Price, J.G. and Henry, C.D., 1986, Geology of Marble Canyon Field Trip Guide and Research Articles, Bureau of Economic Geology, Guidebook 23, The University of Texas at Austin, p. 17-26.

Price, J.G., Henry, C.D., Barker, D.S. and Parker, D.F., 1987, Alkalic rocks of contrasting tectonic settings in Trans- Pecos Texas. Geological Society of America Special Paper, 215, p. 335-346.

Price, J.G., Henry, C.D., Barker, D.S. and Rubin, J.N., 1986, Petrology of the Marble Canyon stock, Culberson County, Texas. Igneous Geology of Trans-Pecos, Texas: Field Trip Guide and Research Articles, Bureau of Economic Geology, Guidebook 23, The University of Texas at Austin, p. 303-319.

Price, J.G., Henry, C.D., Dickerson, P.W. and Muehlberger, W.R., 1985, Summary of Tertiary stress orientations and tectonic history of Trans-Pecos Texas, *in* Structure and tectonics of Trans-Pecos Texas: West Texas Geological Society Field Conference, p. 149-151.

Price, J.G., Rubin, J.N., Henry, C.D., Pinkston, T.L., Tweedy, S.W., and Koppenaal, D.W., 1990, Rare-metal enriched peraluminous rhyolites in a continental arc, Sierra Blanca area, Trans-Pecos Texas; chemical modification by vapor-phase crystallization: Geological Society of America, Special Paper, 246, p. 103-120.

4

Richardson, G.B., 1914, Description of the Van Horn quadrangle. US Geological Survey, Geol. Atlas, Folio 194, 9 p.

Schulz, K.J., Piatak, N.M., and Papp, J.F., 2017, Niobium and tantalum, chap. M of Schulz, K.J., DeYoung, J.H., Jr., Seal, R.R., II, and Bradley, D.C., eds., Critical mineral resources of the United States - Economic and environmental geology and prospects for future supply. U.S. Geological Survey, Professional Paper 1802, p. M1–M34.

Sharp, J.E., 1979, Cave Peak, a molybdenum-mineralized breccia pipe complex in Culberson County, Texas. Economic Geology, 74, p. 517-534.

Ugurhan, M., 2018, Characterization and timing of the Cave Peak porphyry molybdenum system, Culberson County, Texas. Master's thesis, The University of Texas at Austin, 171 p.

5